

**Report on key comparison CCAUV.A-K5: Pressure calibration of
laboratory standard microphones in the frequency range 2 Hz to
10 kHz**

**JANINE AVISON
RICHARD BARHAM**

SEPTEMBER 2014

Report on key comparison CCAUV.A-K5: pressure calibration of laboratory standard microphones in the frequency range 2 Hz to 10 kHz

Janine Avison and Richard Barham
Acoustics & Ionising Radiation

ABSTRACT

This document and the accompanying spreadsheets constitute the final report for key comparison CCAUV.A-K5 on the pressure calibration of laboratory standard microphones in the frequency range from 2 Hz to 10 kHz. Twelve national measurement institutes took part in the key comparison and the National Physical Laboratory piloted the project. Two laboratory standard microphones IEC type LS1P were circulated to the participants and results in the form of regular calibration certificates were collected throughout the project. One of the microphones was subsequently deemed to have compromised stability for the purpose of deriving a reference value. Consequently the key comparison reference value (KCRV) has been made based on the weighted mean results for sensitivity level and for sensitivity phase from just one of the microphones. Corresponding degrees of equivalence (DoEs) have also been calculated and are presented.

© Queen's Printer and Controller of HMSO, 2014

ISSN 1754-2936

National Physical Laboratory
Hampton Road, Teddington, Middlesex, TW11 0LW

Extracts from this report may be reproduced provided the source is acknowledged
and the extract is not taken out of context.

Approved on behalf of NPLML by Giuseppe Schettino (Knowledge Leader).

CONTENTS

1	INTRODUCTION	1
2	PROTOCOL	2
3	DESCRIPTIONS OF PARTICIPANTS' MEASUREMENT SYSTEMS	3
	3.1 NPL.....	3
	3.2 DPLA.....	4
	3.3 GUM.....	5
	3.4 NIM	6
	3.5 INMETRO.....	6
	3.6 CENAM.....	8
	3.7 INRiM.....	9
	3.8 NMISA	9
	3.9 KRISS	10
	3.10 NRC.....	11
	3.11 VNIIFTRI.....	12
	3.12 NMIJ.....	13
4	UNCERTAINTIES.....	13
5	STABILITY OF TRAVELLING STANDARDS.....	14
6	PRELIMINARY ANALYSIS OF RESULTS AND IDENTIFICATION OF OUTLIERS ...	16
7	KEY COMPARISON REFERENCE VALUES	23
8	DEGREES OF EQUIVALENCE.....	25
9	RESULTS FOR 4160 2652754.....	37
10	CONCLUSIONS.....	55
11	ACKNOWLEDGMENTS.....	55
12	REFERENCES	55
	ANNEX A: DETAILED STABILITY ANALYSIS.....	56

1 INTRODUCTION

This document and the accompanying Microsoft Excel spreadsheets '[CCAUV.A-K5 Final Report Tables of Data.xls](#)' and '[CCAUV.A-K5 Uncertainty Budgets Final Report.xlsx](#)', together form the final report for key comparison CCAUV.A-K5. The key comparison was organized by the Consultative Committee for Acoustics, Ultrasound and Vibration in support of the Mutual Recognition Arrangement and Calibration and Measurement Capabilities (CMCs) for primary measurement standards for sound pressure in air. The basis of the key comparison was the calibration of laboratory standard microphones upon which such primary measurement standards are founded. The accompanying spreadsheet contains tables of declared results and uncertainties for the travelling standard microphones.

Twelve national measurement institutes took part and the National Physical Laboratory in the UK, piloted the project. The participants are listed in Table 1.

Table 1 List of participating institutes

Participant (in order of participation)	Acronym	Country/ Economy	Code
National Physical Laboratory	NPL	United Kingdom	UK
Danish Primary Laboratory for Acoustics	DPLA	Denmark	DK
Central Office of Measures	GUM	Poland	PL
National Institute of Metrology	NIM	China	CN
Instituto Nacional de Metrologia, Qualidade e Tecnologia (in English: National Institute of Metrology, Quality and Technology)	INMETRO	Brazil	BR
Centro Nacional de Metrología	CENAM	Mexico	MX
Istituto Nazionale di Ricerca Metrologica	INRIM	Italy	IT
National Metrology Institute of South Africa	NMISA	South Africa	ZA
Korea Research Institute of Science and Standards	KRISS	Republic of Korea	KR
National Research Council	NRC	Canada	CA
All-Russian Scientific and Research Institute for Physical-Technical and Radiotechnical Measurements	VNIIFTRI	Russian Federation	RU
National Metrology Institute of Japan	NMIJ	Japan	JP

2 PROTOCOL

The protocol [1] specified the determination of the pressure sensitivity of two IEC type LS1P microphones, according to the requirements specified in IEC 61094-2:2009 [2], at the reference environmental conditions specified therein. The microphones were circulated as travelling standards to each participant in turn, returning to NPL for interim calibration after every second participant. Each participant was asked to calibrate the microphones by their normal method (as might be offered to a customer) and report the results in their usual calibration certificate format. In addition, information was requested on the microphone parameters used to determine the sensitivity, any variation from the requirements of IEC 61094-2 together with an estimate of its likely effect on the results, and a breakdown of the declared uncertainty showing the components considered.

Table 2 Scope of key comparison

Frequency range	Sensitivity level	Sensitivity phase
2 Hz - 20 Hz (1/3-octave)	Optional	Optional
20 Hz – 10 kHz (1/12-octave)	Mandatory	Optional

Table 2 shows the measurands and frequency ranges within the scope of this key comparison. Participants were asked to complete the mandatory elements and at least one optional element of the scope, unless agreed in advance with the pilot laboratory. Each participant was asked to determine the pressure sensitivity level of each reference microphone, and optionally the pressure sensitivity phase.

The first participant received the microphones in January 2011 and the final participant completed their measurements in July 2012.

3 DESCRIPTIONS OF PARTICIPANTS' MEASUREMENT SYSTEMS

Participants were asked to provide details of their methods including any aspects that deviate from IEC 61094-2. Since there are aspects of the standard that can be applied in differing ways, participants were also asked to clarify which approach has been used.

3.1 NPL

3.1.1 Method

Traceability for the electrical transfer impedance in the NPL system comes from a set of calibrated resistors and one calibrated capacitor, which was used for measurements at frequencies below 19.95 Hz. A single coupler of length 7.5020 mm and radius 9.30135 mm was used for all measurements. The coupler was fitted with a capillary tube, but this was blocked using a wire. Sealing of the microphones in the coupler was achieved by a constant applied force and without sealant.

The measurement process was controlled using NPL's own in-house designed software. The same software also implements the calculation of acoustic transfer impedance.

3.1.2 Deviations from standard

None declared.

3.1.3 Declared parameters

The effective volume of the microphone's front cavity was measured using an acoustical technique and the cavity depth was measured using a depth measuring microscope. Nominal values were assumed for the acoustical impedance parameters.

3.1.4 Calculations

The effects of non-radial motion inside the coupler have been accounted for using a model that assumes a Bessel-shaped diaphragm profile leading the determination of a correction for sensitivity level. However, this has not been applied for the sensitivity phase, nor has an uncertainty component been determined for the effect on phase. The effect of heat conduction in the coupler on sensitivity level and phase has been accounted for by using the "Broad-band" model of IEC 61094-2:2009 clause A.3.

The models for the temperature and pressure coefficients given in IEC 61094-2:2009 were used to correct the results to reference environment conditions. The required microphone diaphragm resonance frequency was calculated from the acoustical compliance and mass parameters.

3.2 DPLA

3.2.1 Method

The calibrations were performed at BKS-V-DPLA following IEC 61094-2:2009. Four different plane wave couplers were used. During the measurements the venting tubes of the couplers were closed with a needle, leaving only very small leakage around the needle and at the microphones' front surfaces.

The electrical transfer impedances are measured with Microphone Reciprocity Calibration System, Brüel & Kjær Type 9699 with a Brüel & Kjær PULSE analyser and the associated measurement program PRMP.EXE.

The current in the transmitter microphone is determined by measuring the voltage across a series capacitor built into the transmitter unit and directly coupled to the preamplifier. The open circuit voltage of the receiver microphone is measured by the normal insert voltage technique. The gain of the transmitter preamplifier is measured by coupling the signal in series with the series capacitor and connecting the microphone housing to the output of the preamplifier. With this method the polarization resistor is changed from being in parallel to being in series with the series capacitance. This is compensated for in the measurement software.

The output from the two channels are measured simultaneously using two channels in a Brüel & Kjær PULSE analyser so that the complex ratio between the output signals are determined first with current in the transmitter and subsequently with the same signal applied for reference measurement in both channels. The measurements are made using Brüel & Kjær's so-called SSR algorithm, which is an adaptive filtering method.

3.2.2 Deviations from standard

The shield is driven (having virtually the same potential as the center terminal of the microphones) on the transmitter as well as on the receiver. This is a deliberate deviation from the procedure in the standard. With the driven shield the input capacitances of the transmitter and receiver preamplifiers are considerably smaller than they are with a grounded shield. This reduces the influence of tolerances in the geometry on the input capacitances and it also reduces the influence of missing or approximate correction for the input capacitances.

3.2.3 Declared parameters

The front cavity volume and the lumped microphone impedance parameters, resonance frequency, equivalent volume and loss factor are determined using the third method mentioned in clause E.4 of IEC 61094-2. The resonance frequency is determined as the 90° phase shift frequency, and the total volume, the equivalent volume and loss factor are determined by minimising the difference between the results from four different couplers.

The additional surface area due to the thread in 4160 811012, used in the heat conduction correction, as mentioned above, is calculated by using simple geometrical considerations.

The low frequency value of the static pressure coefficient of the microphones is determined from the pressure sensitivity at 250 Hz.

3.2.4 Calculations

The calculations were performed using a dedicated version of DFM microphone pressure sensitivity calibration calculation program, MP.EXE. The dedicated version implements the differences in the methods described here from those implemented in the standard version 4.00 of the program.

The acoustic transfer impedances of the couplers are calculated with the transmission line formulation in equation (4) of IEC 61094-2.

Heat conduction losses were calculated as a combination of the low frequency (Gerber) solution at low and medium frequencies, and the broad-band (Navier-Stokes) solution at higher frequencies. In order to minimise (unrealistic) fluctuations on the microphone responses, a gradual transition between the two methods was made in the frequency range from 1/7 to 2/7 of the lowest length resonance frequency in the coupler. At very low frequencies where (A.2) of IEC 61094-2 does not match the full frequency domain solution, the latter was used as proposed in the standard. The low frequency solution is applied as a complex factor to the cross sectional area of the coupler and considering the propagation coefficient, γ , as purely imaginary.

Radial wave motion in the couplers is calculated as described in ref. [C.2] of the standard, assuming a Bessel shaped diaphragm excursion.

3.3 GUM

3.3.1 Method

A single acoustic coupler of diameter 18.5939 mm and length 5.7642 mm, without capillary tubes, was used for the measurements.

The total volume of each microphone was measured using an acoustical technique.

GUM uses a customised version of NPL's reciprocity measurement system and software.

3.3.2 Deviations from standard

None declared.

3.3.3 Declared parameters

The acoustic impedance parameters were determined for each microphone individually. The method is based on the optimization of the results of four sensitivity magnitude and phase determinations obtained for four couplers of different length.

3.3.4 Calculations

Sensitivity level and phase values at frequencies close to power line frequency and its harmonics (47.3 Hz, 50.1 Hz, 53.1 Hz, 100 Hz, 149.6 Hz, 199.5 Hz and 251 Hz), have been calculated by interpolation.

Heat conduction losses were calculated using the full Gerber (low frequency) solution, without simplification.

No radial corrections were applied.

3.4 NIM

3.4.1 Method

The calibration is based on the pressure reciprocity calibration technique according to IEC 61094-2:2009. Four plane-wave couplers of different length, with nominal lengths 5.7 mm, 7.5 mm, 10 mm and 15 mm were used to determine the parameters of the microphones. The B&K type 5998 reciprocity apparatus with low frequency option was used. The transmitter microphone was connected to B&K transmitter unit ZE 0796 and the receiver microphone to a preamplifier B&K type 2673. The transfer function was measured using B&K 3560C with the Steady State Response (SSR) algorithm.

3.4.2 Deviations from standard

None declared.

3.4.3 Declared parameters

The front cavity depth was measured by an optical method, using TESA Visio 300. The total of front cavity volume and the equivalent volume was determined by data fitting from the results of different couplers between 250 Hz to 2 kHz. The resonance frequency was determined by the phase response at the 90° shift relative to low frequency. The loss factor was determined by the ratio of the sensitivity at the resonance frequency to 250 Hz.

3.4.4 Calculations

The sensitivity was calculated using the software MP.EXE 4.0 in 'Standard mode'.

3.5 INMETRO

3.5.1 Method

The microphone's front cavity depths were measured with a microscope equipped with meter scale and the coupler lengths determined by means of a Carl Zeiss UMM-500 precision coordinate measurement system.

A broadband signal in conjunction with synchronous AD/DA conversion, FFT and deconvolution techniques were used to determine the complex electrical transfer functions between the transmitting and receiving microphones with high spectral resolution.

The measurements of the electrical transfer impedances were accomplished with four different couplers (Brüel & Kjaer CPL2848, CPL2844, CPL201 and CPL202). The nominal volumes of the couplers are: CPL2848 is 5cc, CPL2844 is 3cc, CPL202 is 1.6cc and CPL201 is 1.2cc. The capillary tubes were sealed.

3.5.2 Deviations from standard

None declared.

3.5.3 Declared parameters

Nominal values for the resonance frequency, the equivalent volume and the loss factor were used to yield the lumped elements (acoustic mass, compliance and resistance, connected in series in the equivalent electric circuit) according to the three equations given in Annex E of the standard.

3.5.4 Calculations

The microphone sensitivity (magnitude and phase) was calculated according to equation (7) of IEC61094-2:2009.

The measuring system (Aurelio CMF22) used to measure the electrical transfer impedance ($Z_{e,xy}$) was conceived at the Acoustic and Vibration Division (DIAMI) of INMETRO. The software *Monkey Forest* controls the Aurelio CMF22 and also performs the complete calculation of the sensitivities of microphones.

The acoustic impedance of each coupler was estimated by taking into account isothermal and viscous losses according to the broadband solution.

3.6 CENAM

3.6.1 Method

The calibrations were carried out according to IEC 61094-2. Five plane wave couplers were used. They had nominal lengths of 15 mm, 10 mm, 7.5 mm, 5.7 mm and 4.3 mm. Measurements at frequencies below 40 Hz were made using the three longest couplers. Measurements at frequencies from 20 Hz and above were measured using the three shortest couplers.

Measurements are performed using a Brüel & Kjær 5998 Reciprocity Apparatus, without modifications.

The electrical transfer impedance was determined by the measurement of the transfer function between the transmitter and receiver channels, using a two channel signal analyser B&K Pulse 3560D. Measurements were carried out using the FFT function in three different frequency ranges in order to adjust the frequency resolution as close as possible to the set of frequencies required for the CCAUV.A-K5 Key Comparison. Furthermore, additional frequencies were included, in order to measure more closely above and below of 1/12-octave band centre frequencies. Final sensitivity levels and sensitivity phase, for the set of frequencies required, were obtained by linear interpolation from the modified frequency set used to perform measurements.

3.6.2 Deviations from standard

None declared.

3.6.3 Declared parameters

The resonance frequency was estimated using the measured sensitivity phase. The microphone impedance parameters (equivalent volume, frontal cavity volume and loss factor) were obtained by the curve fitting method, using data obtained from the different sized couplers.

3.6.4 Calculations

Calculations of pressure sensitivity levels are carried out using the version 4.00 of the MP.EXE program, which takes into account additional heat conduction losses.

3.7 INRiM

3.7.1 Method

INRiM uses a Brüel & Kjær reciprocity calibration unit, type 5998.

Four plane wave couplers were used in the measurements in the frequency range 20 Hz to 10 kHz. They had a nominal radius of 18.6 mm and lengths of 4.3 mm, 5.7 mm, 7.5 mm and 10 mm. For low frequency measurements, only the coupler of length 5.7 mm was used.

3.7.2 Deviations from standard

None declared.

3.7.3 Declared parameters

The microphone parameters were estimated indirectly by data fitting. The resonance frequency was calculated from the 90 ° phase response, the equivalent volume by minimizing the differences in the 200-2000 frequency range in the sensitivity, the damping factor by minimizing the differences in the upper frequency range.

The cavity depth was measured by means of an optical microscope with a linear encoder, 8 points at 45° were measured.

3.7.4 Calculations

The calculation program has been realized at INRiM using the Matlab© programming language. It follows IEC 61094-2:2009. The heat conduction correction has been calculated using the broadband solution outlined in the Annex A of the standard.

3.8 NMISA

3.8.1 Method

The NMISA calibration system is fully compliant with IEC 61094-2: 2009.

The microphones are coupled in pairs using four ceramic plane-wave couplers, filled with air at all frequencies. The four couplers are of nominal lengths; 9.5 mm, 7.5 mm, 5.5 mm and 3.5 mm respectively. The couplers do not employ any facility to accommodate capillary tubes.

The automated system for this measurement has been developed by the NMISA. The electrical transfer impedance of the coupled microphone pair is determined using two Stanford Research SR810 phase sensitive detectors to measure the complex electrical transfer impedance. A custom made transmitter/pre-amplifier with built-in series capacitor is used to determine the current.

3.8.2 Deviations from standard

None declared.

3.8.3 Calculations/ Declared parameters

The acoustical transfer impedance is calculated by software developed at the NMISA to implement the transmission line analysis and associated models given in IEC 61094-2: 2009.

Corrections of ambient pressure and temperature use the coefficients reported in [3]. No correction for humidity variation is applied.

Heat conduction and viscous losses are accounted for using the broadband solution given in IEC 61094-2, Annex A.

The physical properties of air are calculated as per IEC 61094-2, Annex F.

The front cavity depth of the microphone is measured using a μ CMM with an optical probe. The front cavity volume and equivalent volume are determined using the data fitting of the measurement results obtained using four couplers of different lengths.

The resonant frequency is taken as the frequency where the phase difference between sound pressure acting on the diaphragm and the open-circuit voltage is 90° . This value is “refined” using the data fitting technique.

3.9 KRIS

3.9.1 Method

The calibration is performed by a reciprocity calibration according to IEC 61094-2 using a Brüel & Kjær reciprocity calibration unit, type 5998.

The microphones are coupled in pairs with two plane-wave couplers with nominal length of 7.5 mm and 15 mm, filled with air at all frequencies.

3.9.2 Deviations from standard

None declared.

3.9.3 Declared parameters

The front cavity depths of the microphones are measured by the Video Measuring Scope, Nikon, VMH-300N. The equivalent volume is determined by fitting the final results for the two couplers at the frequency of about 250 Hz. The resonance frequency and the loss factor of the microphone diaphragm are determined by fitting the frequency response of the sensitivity to the single-degree-of-freedom vibration model.

3.9.4 Calculations

The microphone pressure sensitivities are calculated by using the Brüel & Kjær Sensitivity Calculation Program MP.EXE, Ver. 4.00.

3.10 NRC

3.10.1 Method

The magnitude and phase of the pressure sensitivity levels of the microphones were determined using the reciprocity technique described in IEC 61094-2:2009.

The measurements of acoustic transfer impedance were performed on a triad of microphones (the two circulated microphones plus one owned by NRC) in a set of four plane-wave couplers of various lengths. The couplers were Brüel & Kjær models WA0834, WA0835, UA1429, and WA0836; no capillary tubes are fitted to the plane-wave couplers in order to equalize the static pressure inside and outside the couplers; the effect of this deviation is estimated to be negligibly small.

A Brüel & Kjær Type 5998 reciprocity apparatus, fitted with low-frequency modification WH-3432, was used. Voltages and phase differences were measured sequentially using a voltmeter (Datron 1271) and a phasemeter (Krohn-Hite 6620).

The front cavity depths of the microphones were measured using a custom translation stage and a homodyne interferometer. A Mirau 10X interferometry objective was used to locate the microphone surfaces by simply varying the surface height until maximum fringe contrast was observed.

3.10.2 Deviations from standard

The length-to-diameter ratios of the plane-wave couplers B&K WA0834 and B&K WA0835 are outside the recommended range given in C.2 of the standard; the effects of these deviations are estimated to be negligibly small. The length of the plane-wave coupler B&K WA0836 is outside the recommended range given in C.2 of the standard; the effect of this deviation is estimated to be negligibly small.

3.10.3 Calculations

The magnitude and phase of the pressure sensitivity levels were determined using NRC-written software which implements the calculations described IEC 61094-2:2009. The calculations used the broadband solution for heat conduction and viscous losses (clause A.3 of the standard) and the suggested equations for the physical properties of air (Annex F of the standard).

3.10.4 Declared parameters

The temperature and static pressure coefficients of the microphones used in the calculations were determined using the equations developed by Rasmussen [4]. The low frequency values of the static pressure (magnitude) coefficients of the microphones were calculated from the measured magnitude of the pressure sensitivity level of each individual microphone at 251.1 Hz. The normalized frequencies were calculated from the measured resonance frequency of each individual microphone, determined by a change of phase response of 90° from the phase at low frequencies.

The values of front cavity volume, diaphragm equivalent volume, and loss factor for each microphone were iteratively adjusted until the best agreement was achieved between the resulting values of magnitude of pressure sensitivity levels from the four couplers.

The reported results are arithmetic averages of the results from the four couplers after the adjustment process.

3.11 VNIIFTRI

3.11.1 Method

The calibration is performed by a reciprocity calibration according to IEC 61094-2, using a Brüel & Kjær reciprocity calibration systems type 9699, PULSE Multi-analyser and PULSE based reciprocity measurement software type WT 9708 Version 1.009.

The microphones are coupled in pairs with two plane-wave couplers with nominal length of 7.5 mm (UA 1429) and 15 mm (UA 1413), filled with air at all frequencies. The couplers had one capillary tube, but this was blocked using a wire. Sealing of the microphones in the coupler was achieved by a constant applied force and without sealant. The current in the transmitter microphone is determined by measuring the voltage across a series capacitor. The series capacitor is built into the transmitter unit and directly coupled to the preamplifier.

3.11.2 Deviations from standard

None declared.

3.11.3 Declared parameters

The resonance frequency and loss factor were taken from Brüel & Kjær's nominal values. Front cavity depth was measured using a microscope calibrated by a block gauge.

The low frequency value of the static pressure coefficient of the microphones is determined from the pressure sensitivity at 250 Hz.

3.11.4 Calculations

Calculations of pressure sensitivity levels are carried out using the version 4.00 of the MP.EXE program, which takes into account additional heat conduction losses. The additional surface area due to the thread in 4160 811012 is calculated by using simple geometrical considerations and taken into account.

3.12 NMIJ

3.12.1 Method

The pressure sensitivity was determined in compliance with IEC 61094-2:2009, using a reciprocity calibration system developed by NMIJ. In this system, the signal generation was made by a frequency generator, HP 33120A of Agilent Technology and the signal processing were executed by a dual-channel FFT analyser, model CF-5220 of ONO SOKKI Co. Signal-to-noise ratio was improved by the synchronous waveform averaging method. The insert voltage technique was used to cancel the effect of the gain and impedance of an electrical circuit. The calibration was performed using software developed at NMIJ.

Brüel & Kjær type UA1429 plane-wave (short) coupler was used for the reciprocity calibration and a long coupler type UA1413 was also used for determining the equivalent volume of the microphones under test. Both couplers were filled with air and no grease was used to the contacting surfaces between the microphones and the coupler. Capillary tube correction was considered to be unnecessary because a capillary tube was blocked by a needle bung DA5563 so that both equalization of static pressure and an acoustic seal could be ensured.

3.12.2 Deviations from standard

None declared.

3.12.3 Declared parameters

Microphone parameters were determined as follows: The resonance frequency and loss factor were taken from Brüel & Kjær's nominal values. Front depth was measured using a microscope calibrated by a block gauge. Equivalent volume was calculated as averaged value from 125 Hz to 2 kHz.

3.12.4 Calculations

Modulus and phase of pressure sensitivity was corrected to reference environmental conditions by based on [3]. The low frequency static pressure coefficients were determined from the modulus of pressure sensitivity below 250 Hz according to [5]. Below 80 Hz, pressure and temperature dependency of the phase was not corrected because there were no reliable pressure and temperature coefficients.

4 UNCERTAINTIES

The uncertainty budgets submitted by the participants are provided in accompanying Excel spreadsheet "*CCAUV_A-K5 Uncertainty Budgets Final Report.xlsx*".

5 STABILITY OF TRAVELLING STANDARDS

Two Brüel and Kjær type 4160 microphones were selected for this project. One was a new microphone, provided by Brüel and Kjær, and the other was a 30 year old microphone with a history of stability. The microphones are slightly different in design: the older microphone (serial number 811012) has a screw-thread, inside the front cavity, designed for attaching a protective grid. The newer microphone (serial number 2652754) has no such screw-thread. Both microphones were part of a larger group of microphones that were calibrated regularly at NPL prior to circulation, to establish their suitability for the key comparison. The two microphones used were selected as having the best stability of those in the group. The results declared by NPL are derived from a discrete set of measurements performed at the end of these pre-circulation measurements.

The stability of the microphones was monitored throughout the project through interim calibration by the pilot laboratory. A full calibration of each microphone was conducted, before and after circulation to groups of two participants. The spread in these NPL results is shown in Figures 1 and 2, and gives an initial impression of the stability of each microphone.

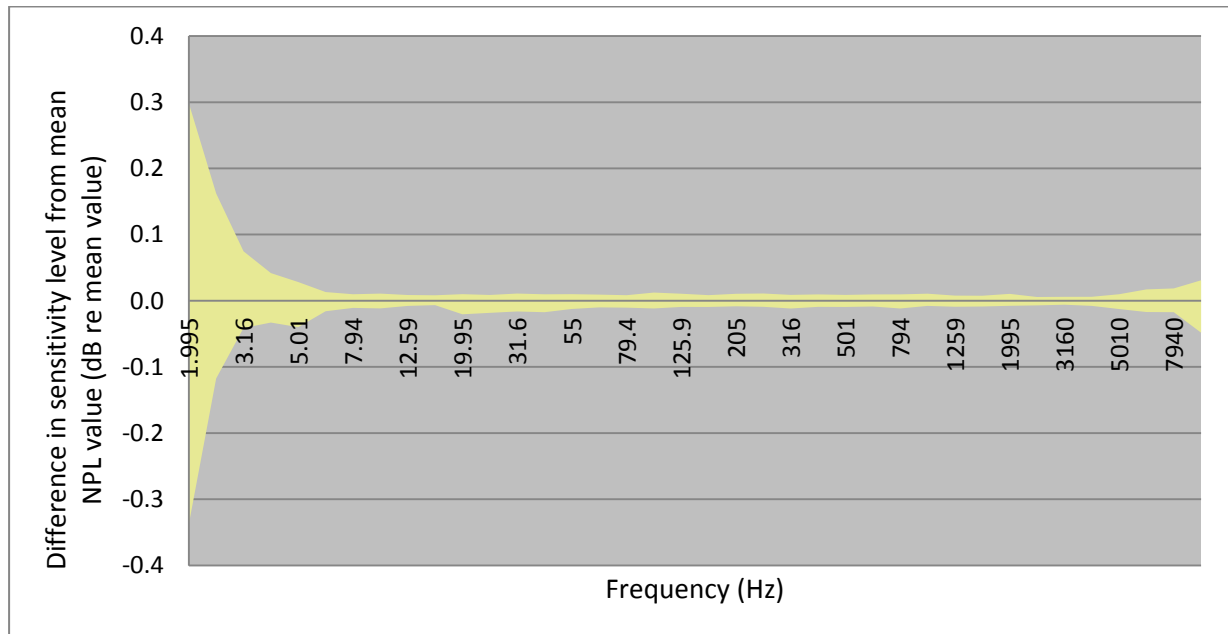


Figure 1 Stability of 4160 811012 in terms of the maximum positive and negative differences from the mean value of NPL measurements throughout the key comparison.

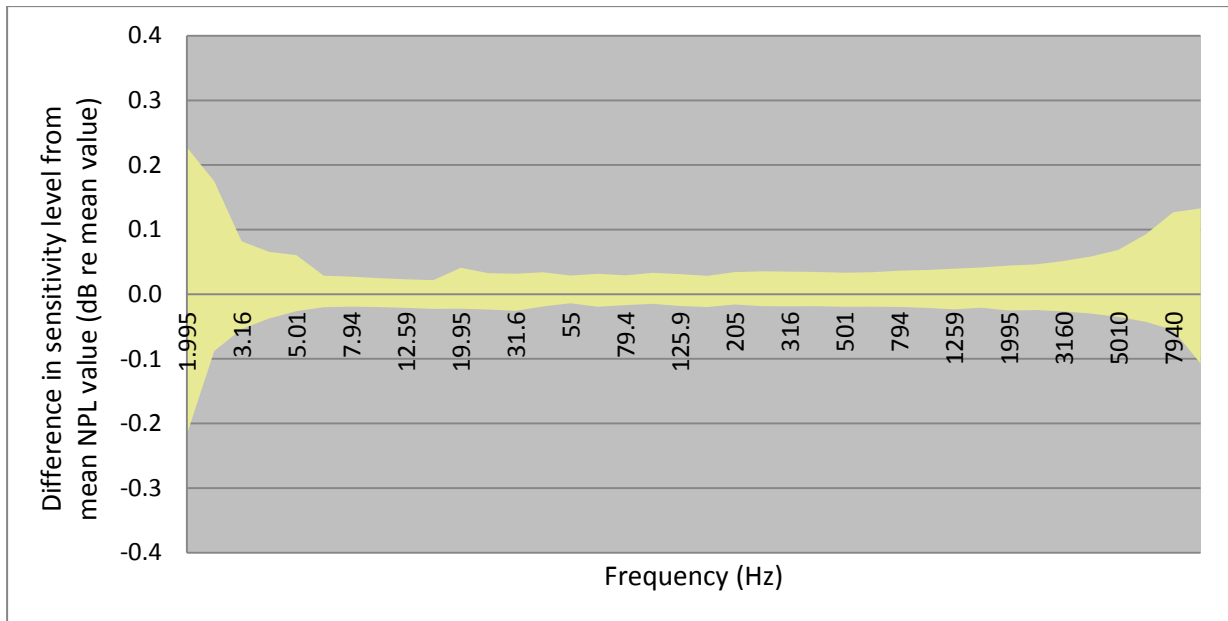


Figure 2 Stability of 4160 2652754 in terms of the maximum positive and negative differences from the mean value of NPL measurements throughout the key comparison.

For microphone 4160 811012, the absolute value of the difference in magnitude sensitivity level from the NPL mean value is no more than 0.02 dB at frequencies from 6.31 Hz to 7940 Hz. The standard deviation of these NPL results is less than the short-term variation allowed for in the NPL uncertainty analysis, thus indicating that the microphone had an acceptable level of stability over the full duration of these measurements.

It is clear from comparing Figures 1 and 2 above, that the measurements of microphone 4160 2652754 indicate a less stable behaviour. Both microphones were therefore subjected to a detailed stability analysis, which is fully described in Annex A of this report to which the reader is referred.

Here we need only consider the conclusions of the analysis, which are:

- microphone 4160 811012 has an acceptable stability performance,
- microphone 4160 2652754 does not have an acceptable level of stability and requires a correction to be applied in order to make use of its data,
- for frequencies below 5 kHz, the sensitivity of microphone 4160 2652754 was found to have a linear dependence with time, enabling a correction to be applied with good reliability,
- for frequencies above 5 kHz, the sensitivity of microphone 4160 2652754 was found to have a more complex dependence with time, making correction less reliable and unsuitable for the purpose of this key comparison,
- for frequencies above 1 kHz, the magnitude of the drift with time, in sensitivity of microphone 4160 2652754 was found to increase rapidly with frequency.

It was therefore recommended and agreed with the participants in the key comparison that:

- microphone 4160 811012 be used as the sole basis for the calculation of KCRVs at all measurement frequencies,
- the results for microphone 4160 2652754 up to and including 1 kHz provide useful information about measurement consistency and have been retained for this purpose. Results for this microphone above 1 kHz are presented in this report, but are not analysed further.

6 PRELIMINARY ANALYSIS OF RESULTS AND IDENTIFICATION OF OUTLIERS

Tables of declared results and uncertainties for both microphones are provided in ‘CCAUV-A-K5 Final Report Tables of Data.xls’.

As pilot laboratory, NPL was tasked with identifying anomalous results and providing the participants concerned with the opportunity to review their data. CIPM Guidelines state that:

“If, on examination of the complete set of results, the pilot institute finds results that appear to be anomalous, the corresponding institutes are invited to check their results for numerical errors but without being informed as to the magnitude or sign of the apparent anomaly. If no numerical error is found the result stands and the complete set of results is sent to all participants. Note that once all participants have been informed of the results, individual values and uncertainties may be changed or removed, or the complete comparison abandoned, only with agreement of all participants and on the basis of a clear failure of the travelling standard or some other phenomenon that renders the comparison or part of it invalid.”

Following the proposal to exclude results from microphone 4160 2652754, the analysis of outliers was based on results from 4160 811012 only.

The approach taken was applied independently for each frequency, and was as follows:

- 1) Using the data from all the institutes, the weighted mean and its associated standard uncertainty were evaluated (allowing for the actual number of data elements where some institutes did not submit data at all frequencies). The weighted mean y was evaluated using the following equation:

$$y = (x_1/u^2(x_1) + \dots + x_N/u^2(x_N)) / (1/u^2(x_1) + \dots + 1/u^2(x_N))$$

Where x_i represents the participants’ result and $u(x_i)$ is the declared uncertainty associated with the result;

- 2) A chi-squared test was applied to test the consistency of the data with the weighted mean (see Annex A);
- 3) If the test was passed, the weighted mean was accepted and Degrees of Equivalence (DoEs) were evaluated for each frequency. Each DoE was the difference between the value reported by a participant and the key comparison reference value (KCRV):

$$d = x - y,$$

where d is the DoE, x is the value reported by a participant and y is the KCRV ;

- 4) If the test did not pass, outlying values were removed until all the remaining participants’ data was found consistent with the weighted mean of this remaining data. This new weighted mean was then accepted as the KCRV and DoEs evaluated. The calculation of the uncertainties of each participant’s DoE was different according to whether or not the participant’s data was used in the evaluation of the KCRV.

The calculation of the uncertainty component of a DoE for a participant included in the calculation of the KCRV was:

$$U(d) = 2 u(d), \text{ where } u^2(d) = u^2(x) - u^2(y),$$

For a participant not included in the calculation of the KCRV the calculation of the uncertainty component of a DoE was:

$$U(d) = 2 u(d), \text{ where } u^2(d) = u^2(x) + u^2(y),$$

where $u(x)$ denotes the standard uncertainty associated with the participant's measured value and $u(y)$ the standard uncertainty associated with the KCRV. The reason for the different calculations is that, in the first case, x and y are correlated (because y is evaluated in terms of x) whereas, in the second case, x and y are uncorrelated. The second case applies in only a very small number of cases.

Note: for most participants' data, expanded uncertainties were divided by a coverage factor before use in the above calculations. The NRC standard uncertainties, however, were used directly as reported in the calibration report, because they used the Monte Carlo approach to uncertainty analysis and coverage factors do not apply.

For sensitivity level (magnitude), the consistency test was passed for the complete data set at all the frequencies.

For sensitivity phase, however, the test was not passed for the complete data set for low frequencies, and for some high frequencies. It was necessary that KRIS (for frequencies between 1.9953 Hz and 19.9526 Hz), NMISA (for frequencies between 19.9526 Hz and 84.1395 Hz), NRC (for frequencies between 6683.4392 Hz and 8912.5094 Hz) and NMIJ (at 6309.5734 Hz) were excluded from the calculation of the weighted mean for the chi-squared test to pass.

KRIS and NMISA, each having a significant number of excluded frequencies, were contacted and given the opportunity to check their results for numerical errors. KRIS requested that their phase results below 20 Hz be withdrawn and NMISA submitted a revised set of results.

It was found to be necessary to exclude some of the revised NMISA results (this time for frequencies between 3349.6544 Hz and 4731.5126 Hz) for the chi-squared test to pass. NMISA was informed and they requested that all their phase results be withdrawn. These results have not therefore been included in the calculation of the weighted mean. A comparison of the original data, and the revised data for NMISA, can be found in the accompanying Microsoft Excel spreadsheet '*CCAUV-A-K5 Final Report Tables of Data.xls*' on tab '*NMISA-Revisions*'.

In addition, GUM submitted revised data for their phase measurement (during the measurement stage of the key comparison and before the publication of the Draft A report). The original data, alongside revisions, can be found in '*CCAUV-A-K5 Final Report Tables of Data.xls*' on tab '*GUM-Revisions*'.

Tables of calculated weighted means and DoEs for each participant are provided in '*CCAUV-A-K5 Final Report Tables of Data.xls*'. Withdrawn and excluded data is marked as such within the tables.

Figures 3(a) to 3(e) show the difference from the weighted mean for each participant. Please note that withdrawn results are shown but were not included in the calculation of the weighted mean. For microphone 2652754 all results above 1 kHz are excluded from the figures because it was difficult to compensate for the microphone's instability.

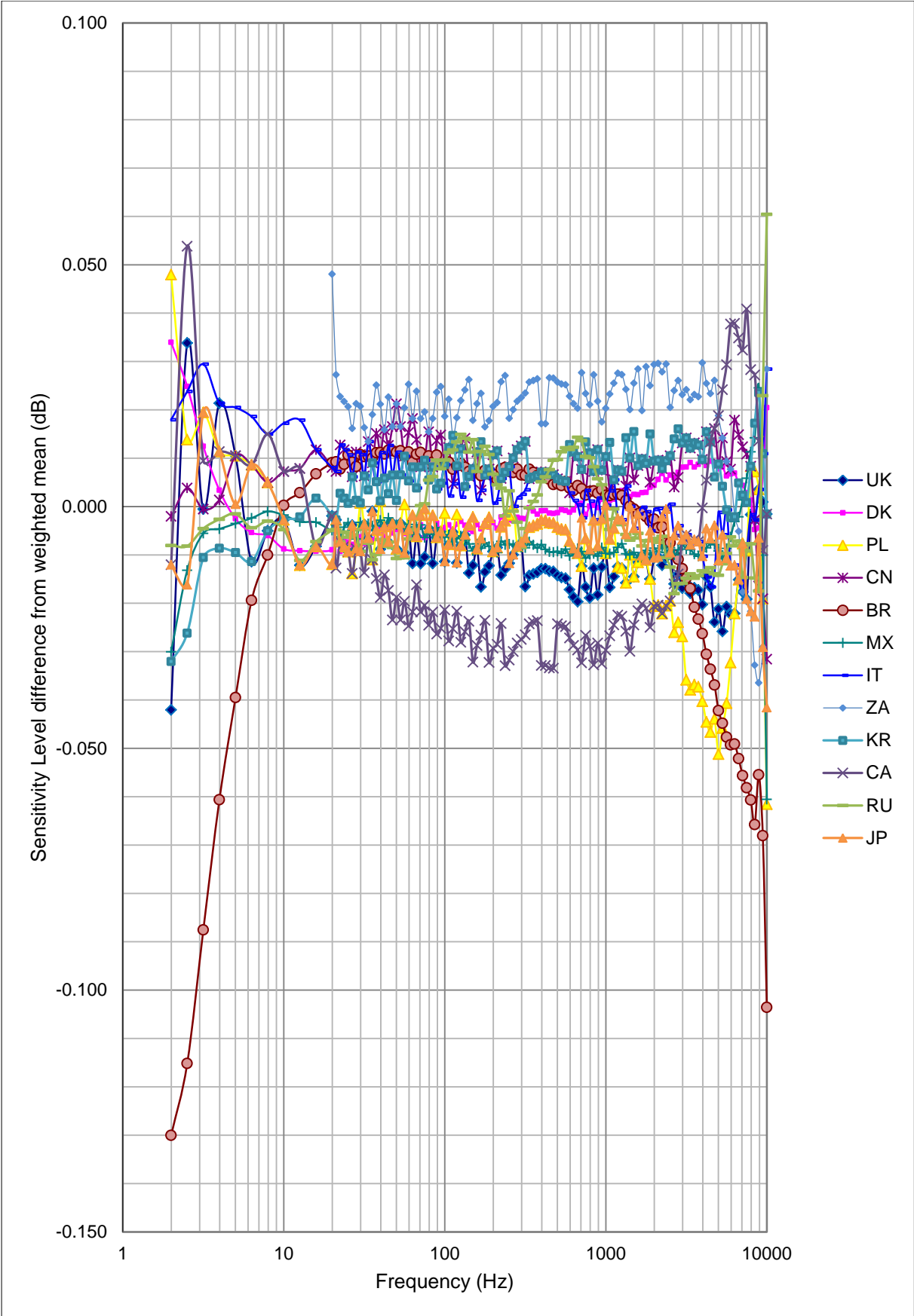


Figure 3(a) Difference from weighted mean sensitivity level for 4160 811012 for each participant.

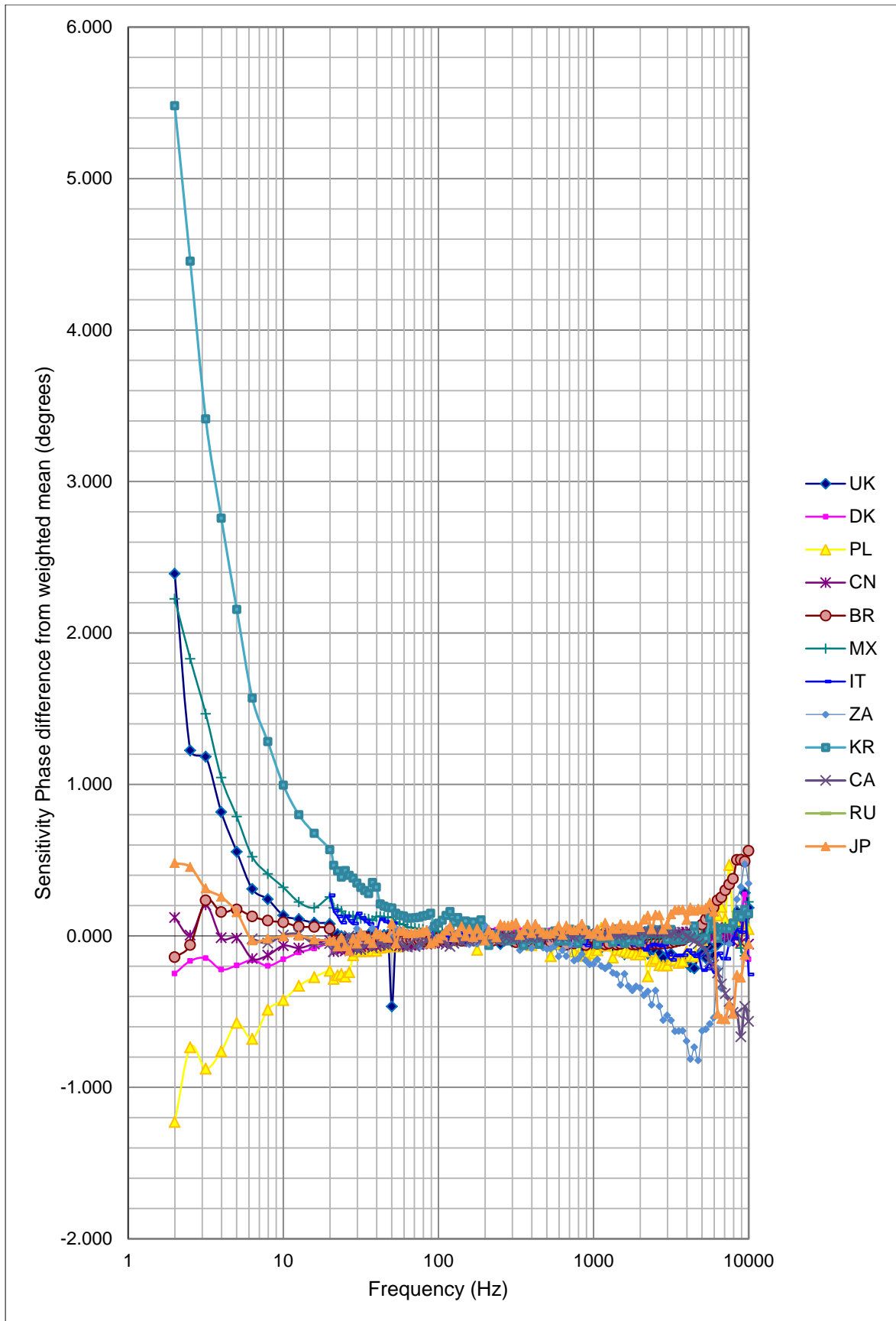


Figure 3(b) Difference from weighted mean sensitivity phase for 4160 811012 for each participant.

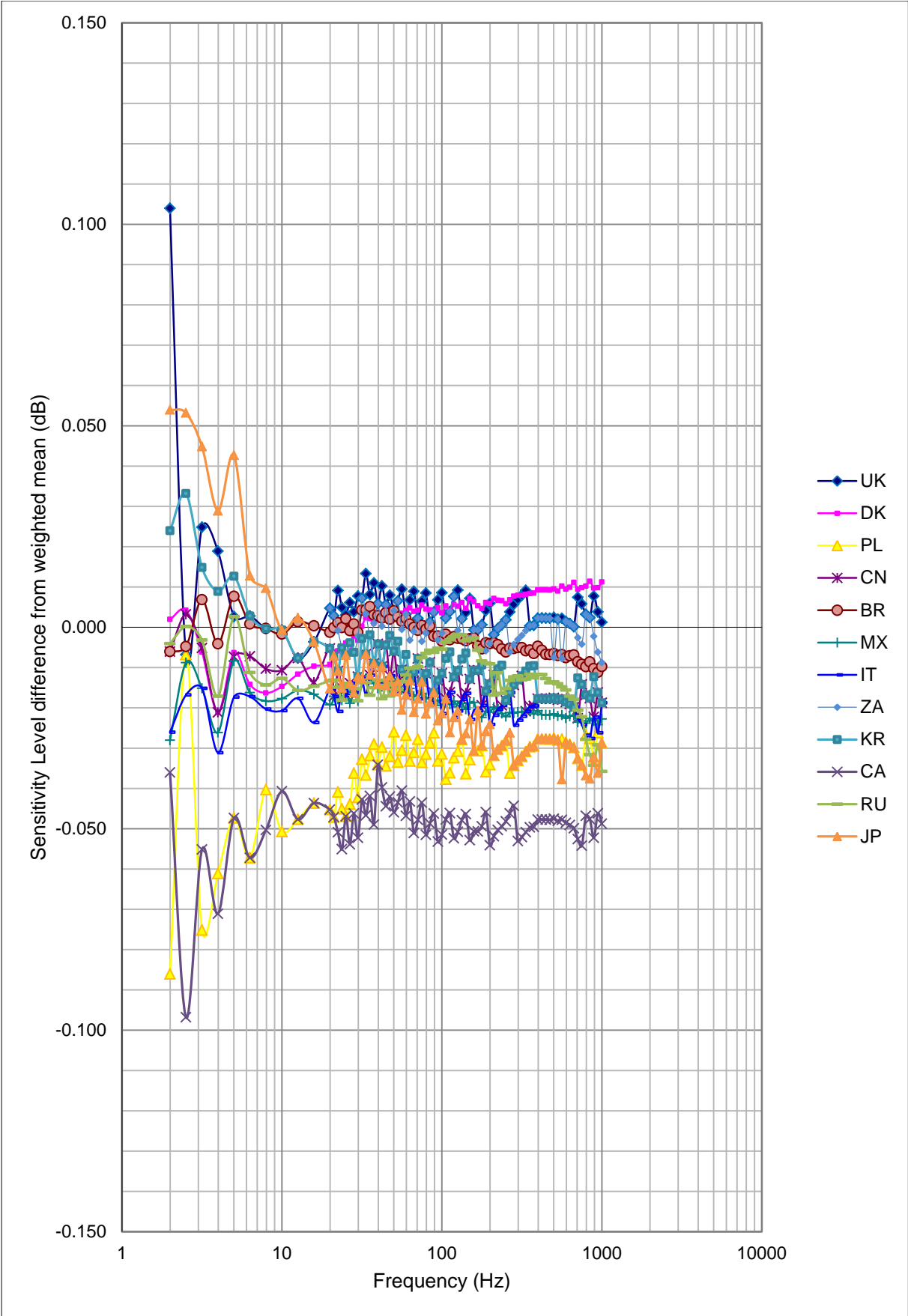


Figure 3(c) Difference from weighted mean sensitivity level for 4160 2652754 for each participant.

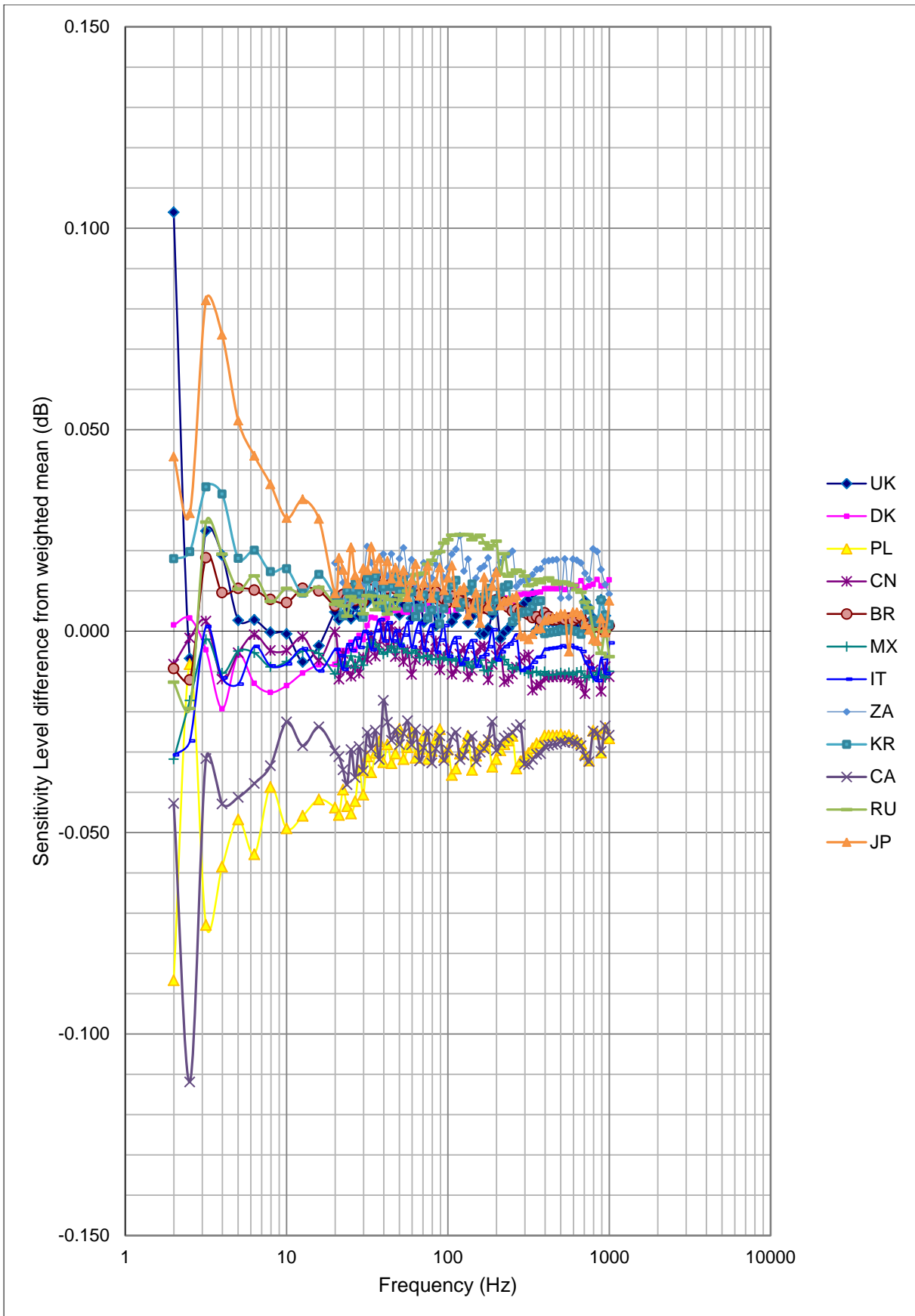


Figure 3(d) Difference from weighted mean sensitivity level for 4160 2652754 for each participant after the results were adjusted to compensate for microphone sensitivity level drift.

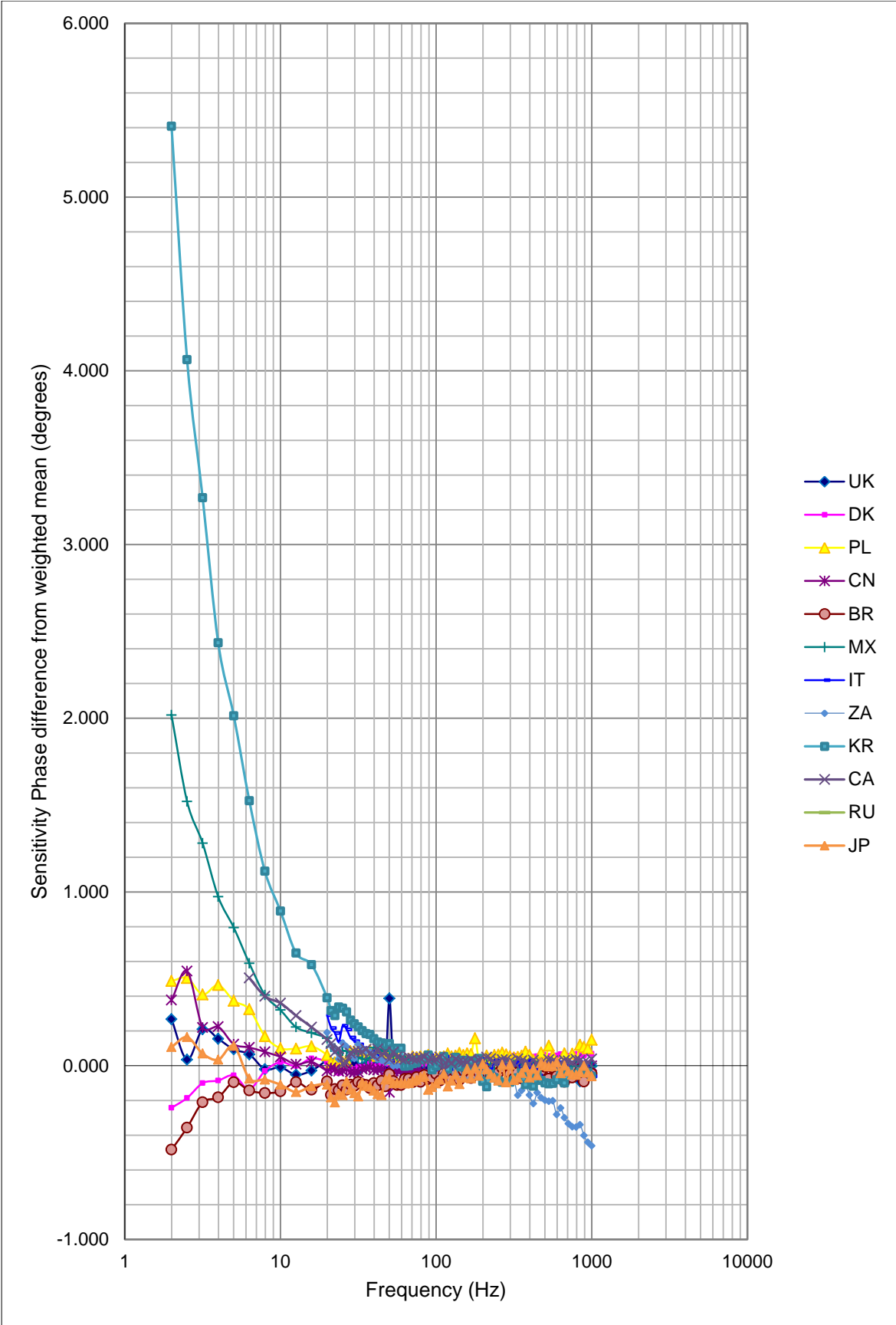


Figure 3(e) Difference from weighted mean sensitivity phase for 4160 2652754 for each participant.

7 KEY COMPARISON REFERENCE VALUES

Following the preliminary analysis of results and uncertainties, and the proposal to use only data from microphone 4160 811012, it was agreed that the KCRVs for CCAUV.A-K5 be calculated using the weighted mean of results for the sensitivity level and sensitivity phase respectively. This approach is consistent with the recommendations made in [6]. The weighting was based on the declared expanded uncertainties of the participating institutes. The method is described in greater detail in the ‘Preliminary analysis of results and identification of outliers’ section.

The following graphs show the KCRVs for sensitivity level and phase as calculated by the method described above. Please note: the appearance of quantisation on these graphs is due to the resolution of the plotting. The values are provided to 3 decimal places in ‘CCAUV-A-K5 Final Report Tables of Data.xls’.

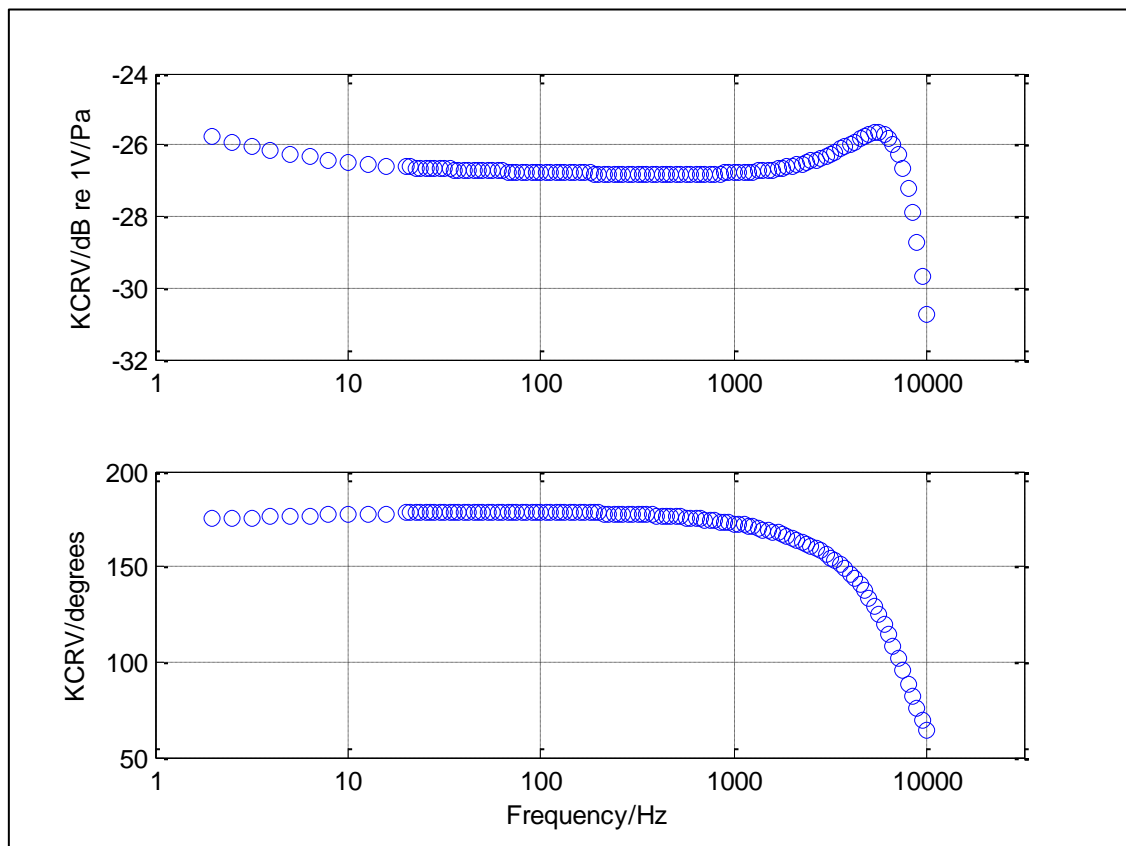


Figure 4 The KCRV for sensitivity level and phase based on the weighted mean results of all participating institutes, for microphone 4160 811012.

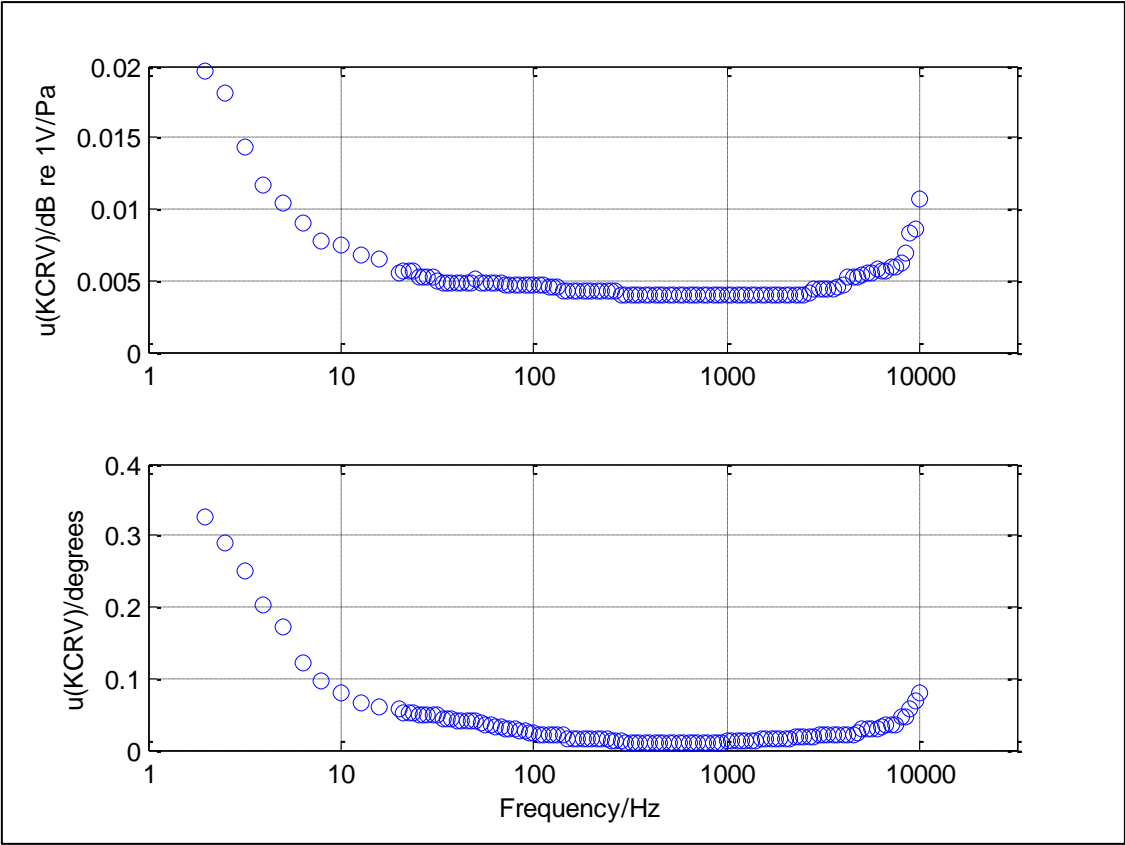


Figure 5 The uncertainty in the calculation of KCRV for sensitivity level and phase based on the weighted mean results of all participating institutes, for microphone 4160 811012.

8 DEGREES OF EQUIVALENCE

The graphs of results shown below, for each participant, display the Degrees of Equivalence for each frequency with uncertainty bars corresponding to coverage factor $k=2$. For convenience, the graphs for each participant have been drawn on the same scales. The frequency range has also been split, to enable results at very low frequencies to be separated from other results, thus allowing an expanded vertical scale to be used for the latter.

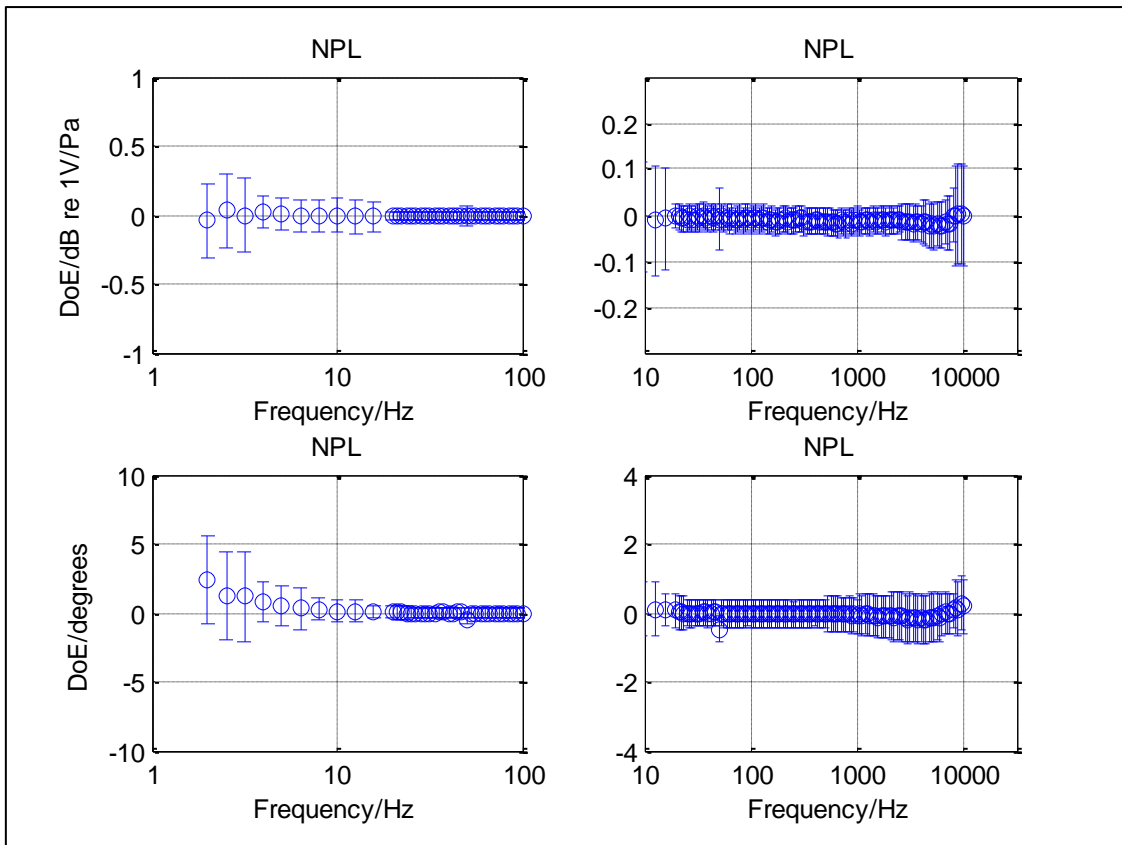


Figure 6(a) Degrees of Equivalence for NPL sensitivity level and phase measurements with uncertainty bars corresponding to coverage factor $k=2$ based on microphone 4160 811012.

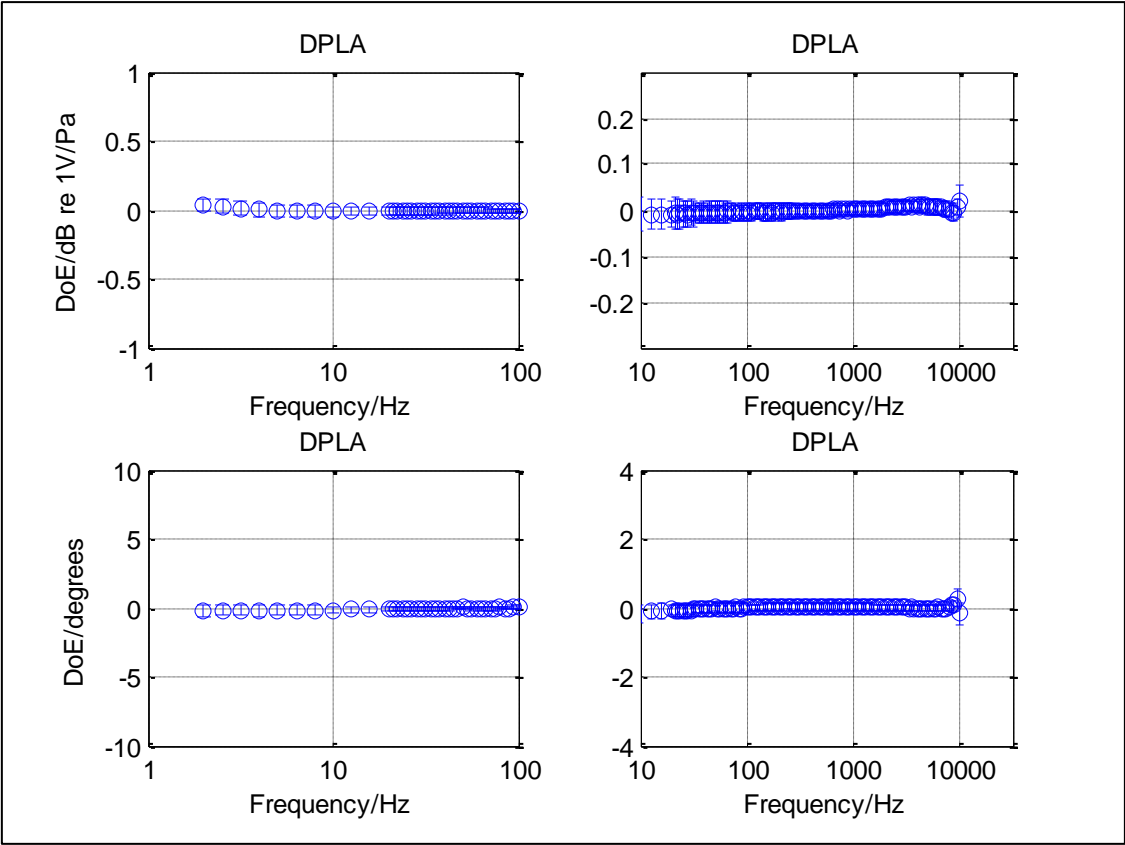


Figure 6(b) Degrees of Equivalence for DPLA sensitivity level and phase measurements with uncertainty bars corresponding to coverage factor $k=2$ based on microphone 4160 811012.

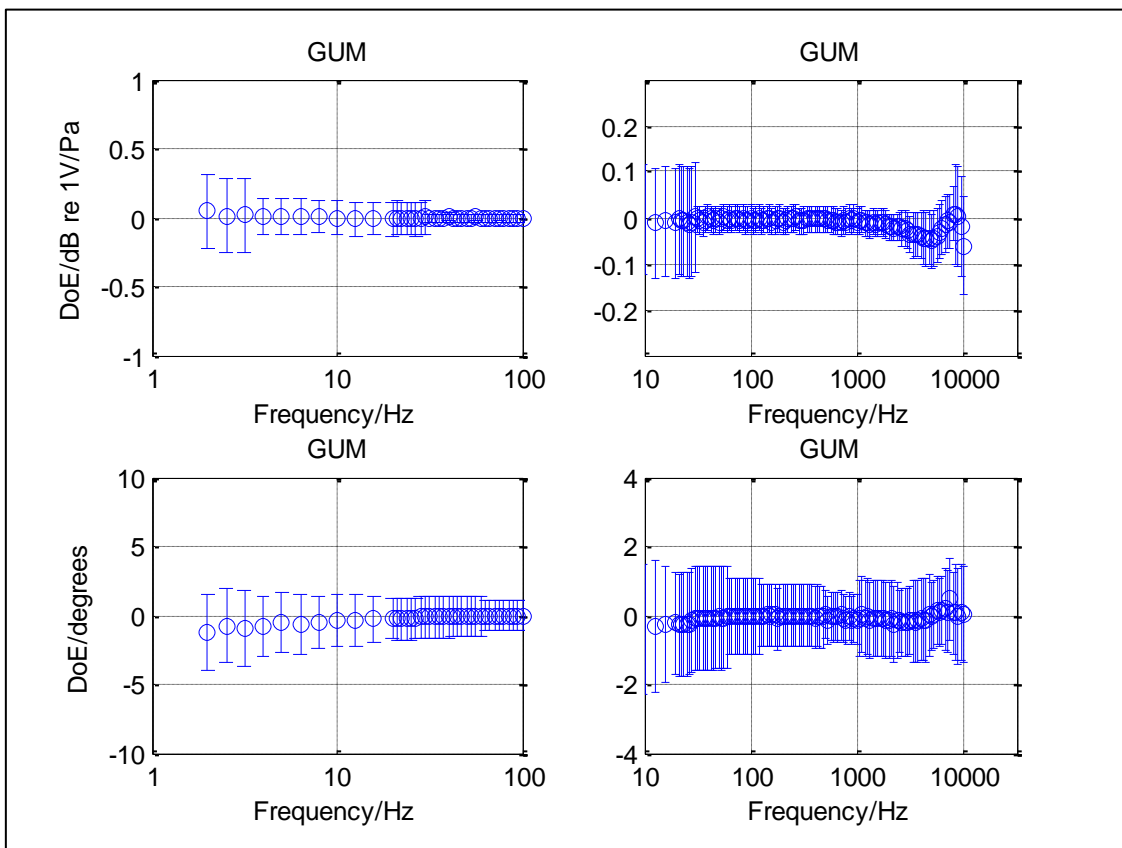


Figure 6(c) Degrees of Equivalence for GUM sensitivity level and phase measurements with uncertainty bars corresponding to coverage factor $k=2$ based on microphone 4160 811012.

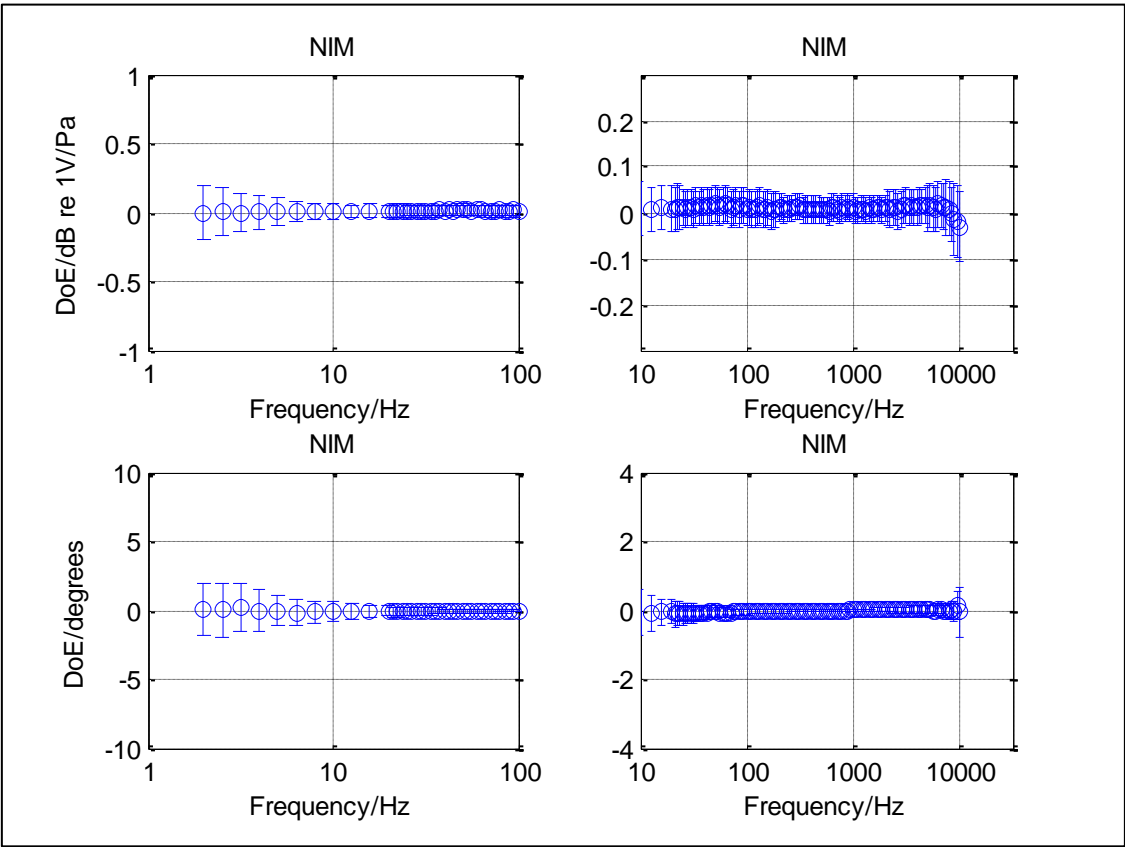


Figure 6(d) Degrees of Equivalence for NIM sensitivity level and phase measurements with uncertainty bars corresponding to coverage factor $k=2$ based on microphone 4160 811012.

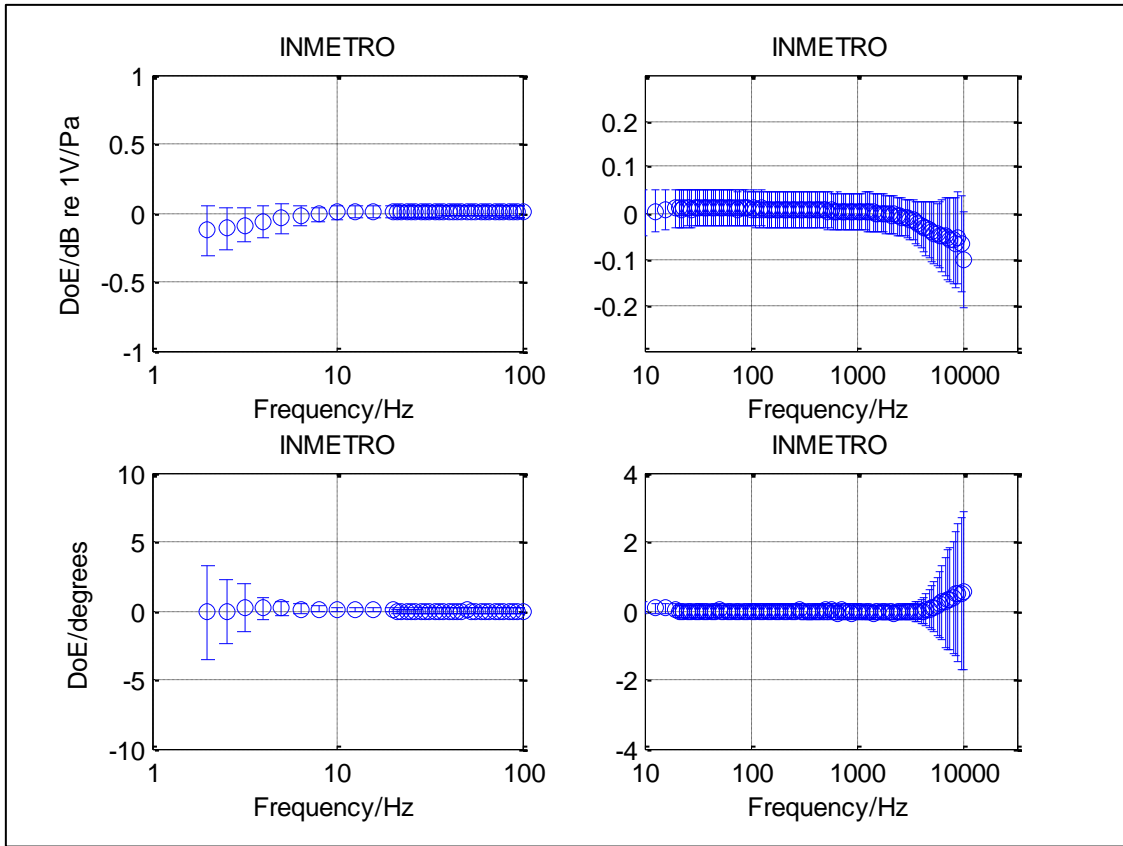


Figure 6(e) Degrees of Equivalence for INMETRO sensitivity level and phase measurements with uncertainty bars corresponding to coverage factor $k=2$ based on microphone 4160 811012.

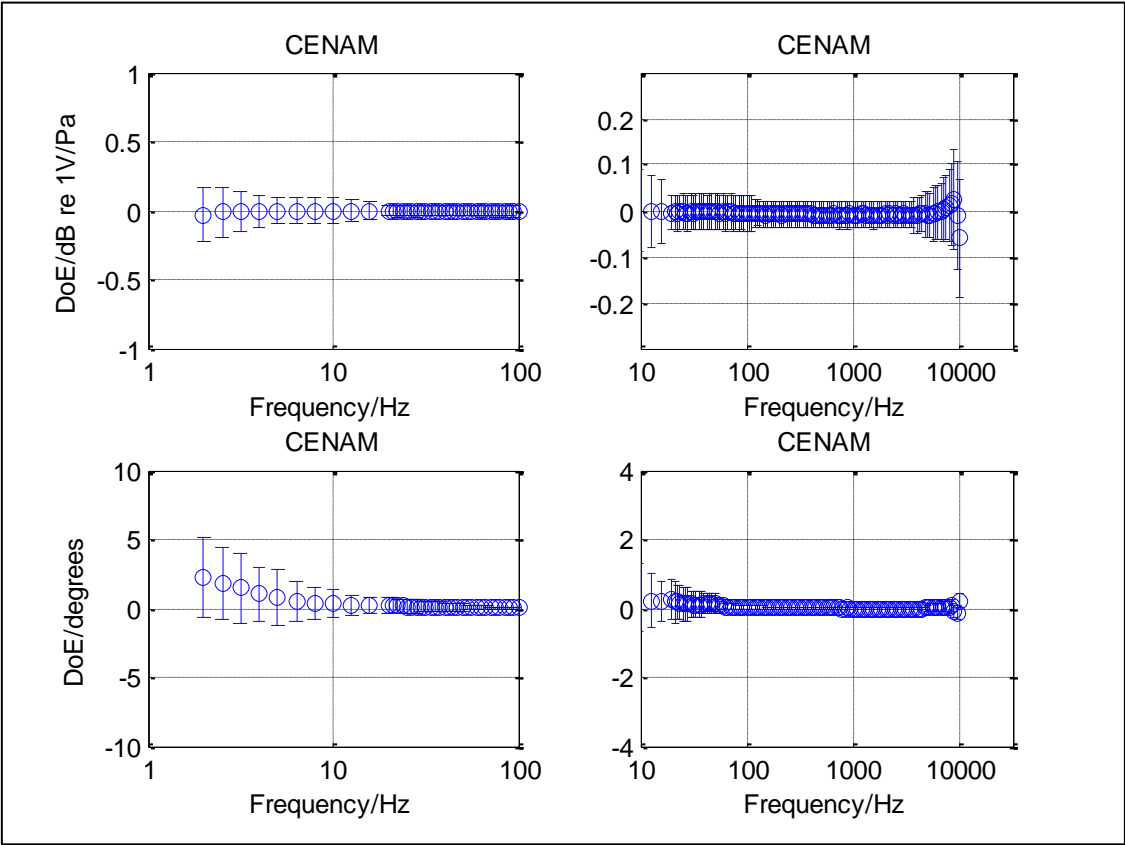


Figure 6(f) Degrees of Equivalence for CENAM sensitivity level and phase measurements with uncertainty bars corresponding to coverage factor $k=2$ based on microphone 4160 811012.

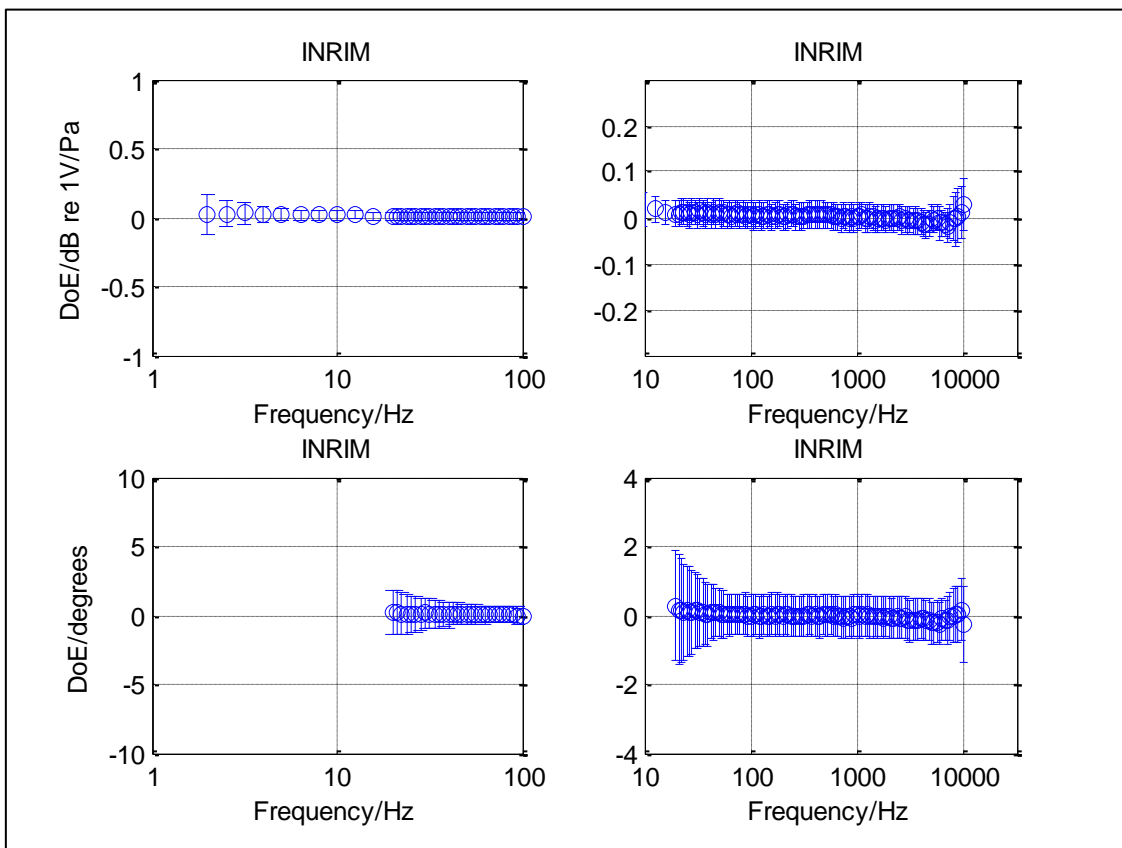


Figure 6(g) Degrees of Equivalence for INRIM sensitivity level and phase measurements with uncertainty bars corresponding to coverage factor $k=2$ based on microphone 4160 811012.

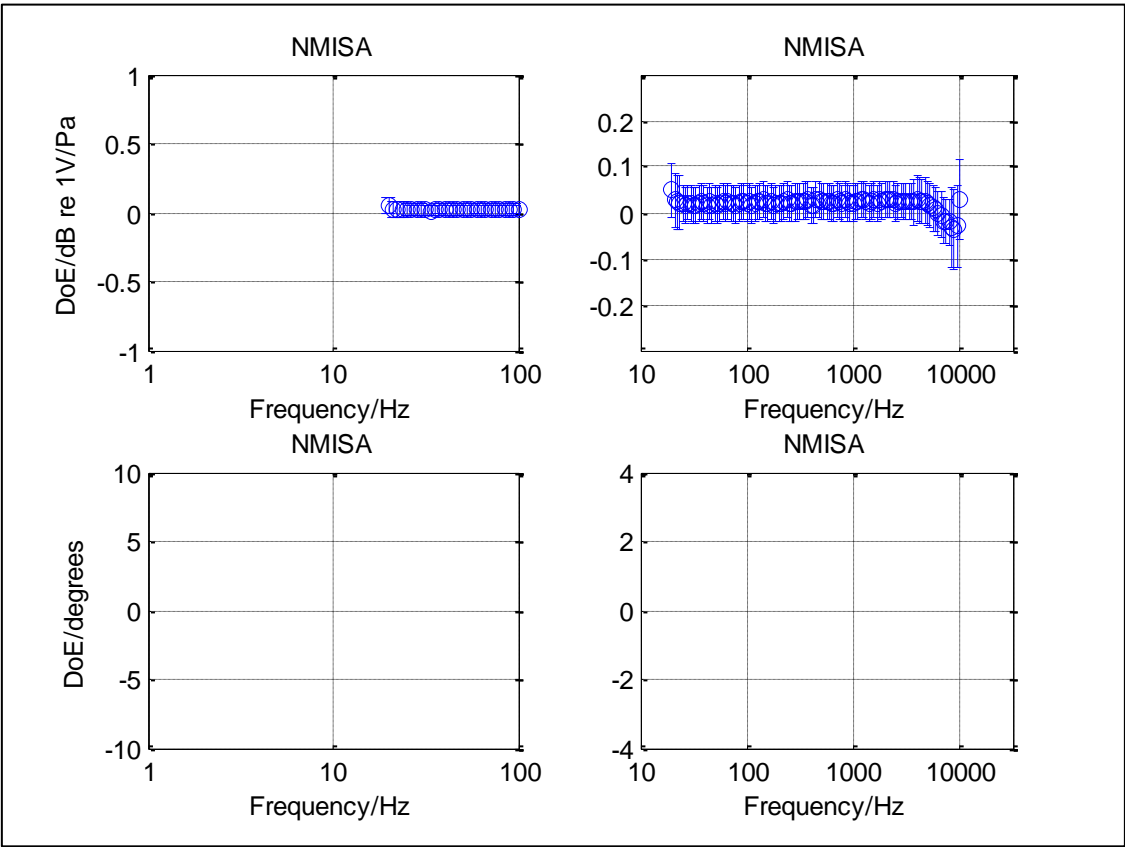


Figure 6(h) Degrees of Equivalence for NMISA sensitivity level and phase measurements with uncertainty bars corresponding to coverage factor $k=2$ based on microphone 4160 811012 (phase measurement results were withdrawn).

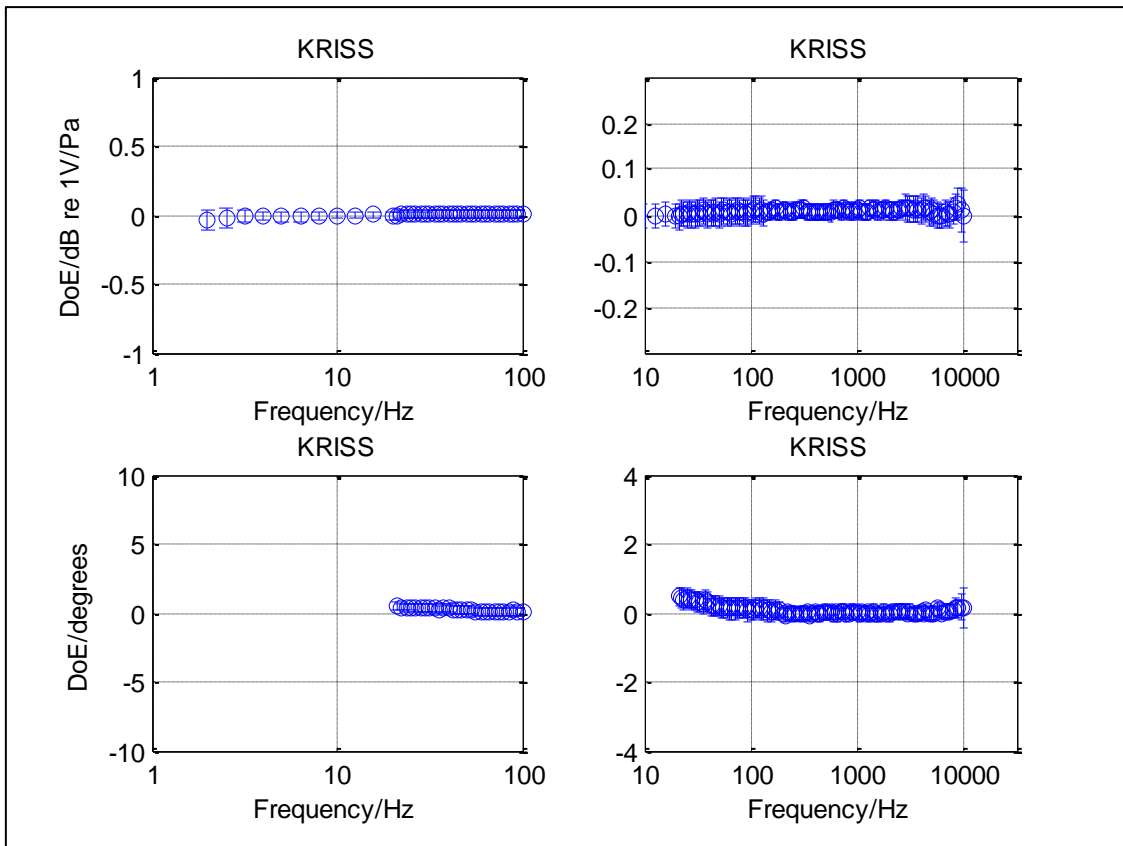


Figure 6(i) Degrees of Equivalence for KRISS sensitivity level and phase measurements with uncertainty bars corresponding to coverage factor $k=2$ based on microphone 4160 811012.

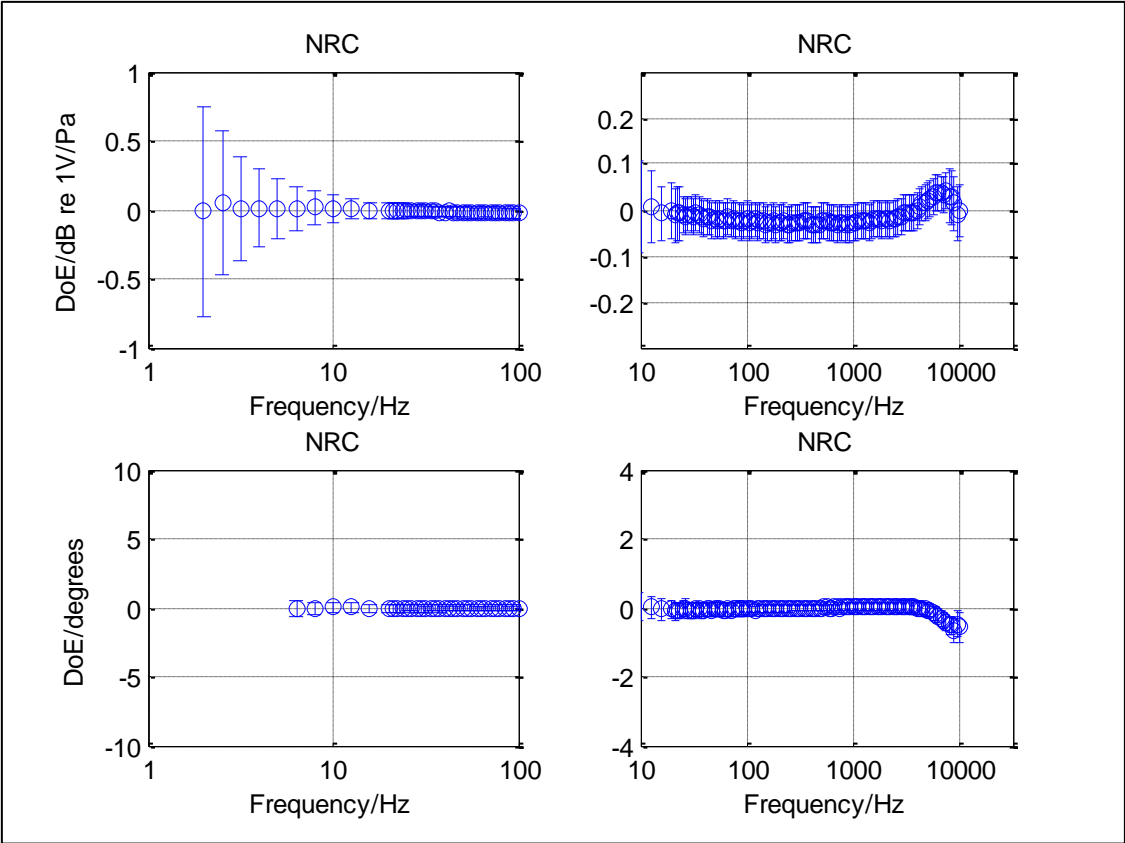


Figure 6(j) Degrees of Equivalence for NRC sensitivity level and phase measurements with uncertainty bars corresponding to coverage factor $k=2$ based on microphone 4160 811012.

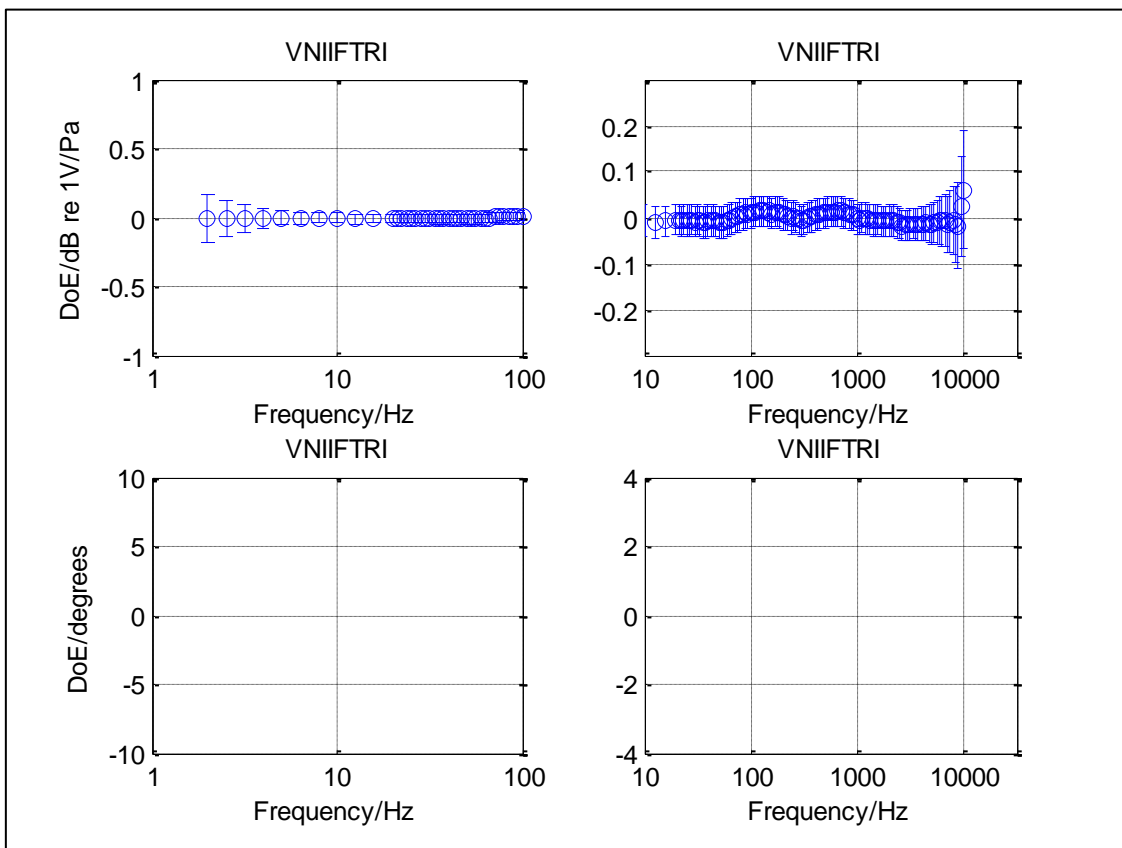


Figure 6(k) Degrees of Equivalence for VNIIFTRI sensitivity level measurements with uncertainty bars corresponding to coverage factor $k=2$ based on microphone 4160 811012 (no phase results were reported).

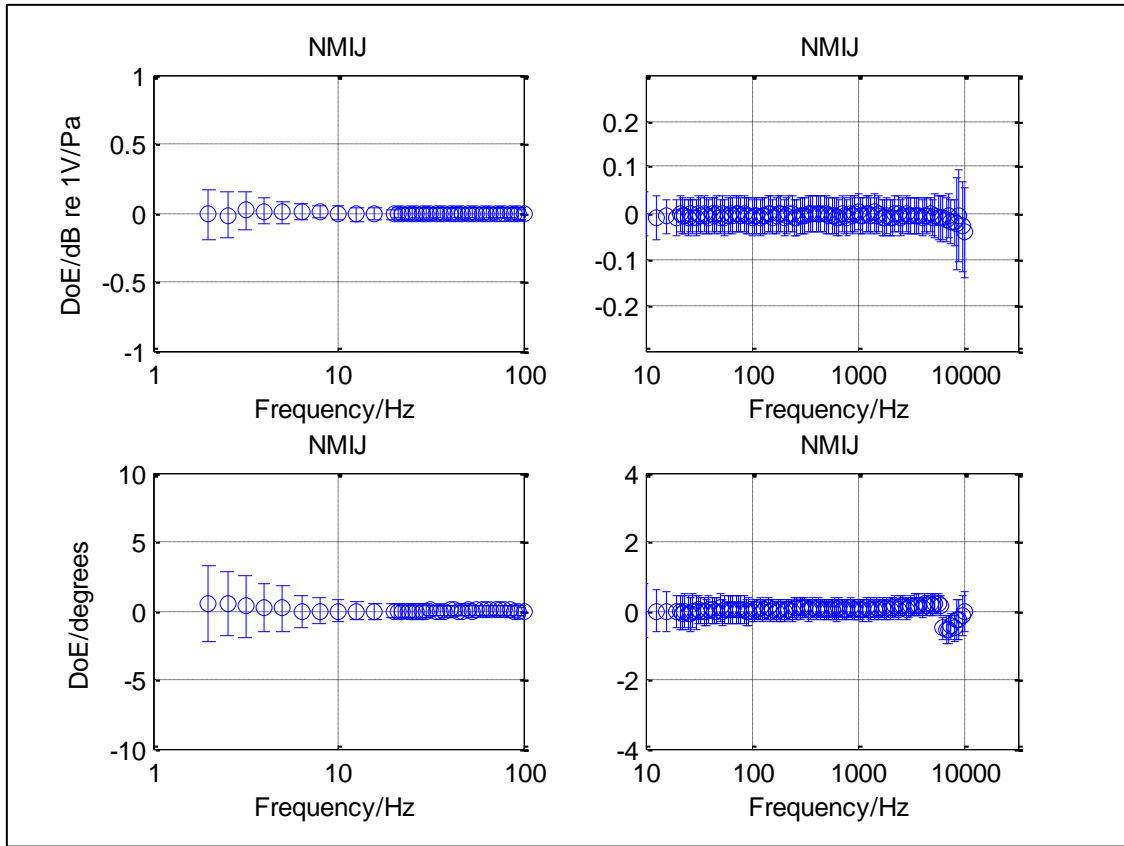


Figure 6(l) Degrees of Equivalence for NMIJ sensitivity level and phase measurements with uncertainty bars corresponding to coverage factor $k=2$ based on microphone 4160 811012.

9 RESULTS FOR 4160 2652754

Although the measurements for microphone 4160 2652754 have not been included in the KCRVs, it was possible to analyse the results up to and including 1 kHz by applying a correction for the drift in its sensitivity. The detailed stability analysis described in Annex A, revealed that for these frequencies the drift was well-characterised by a linear change with time making it possible to correct this dataset with good reliability, albeit with some additional associated uncertainties.

The calculated weighted means, uncertainties and DoEs for individual institutes based on data for microphone 4160 2652754 only are shown below.

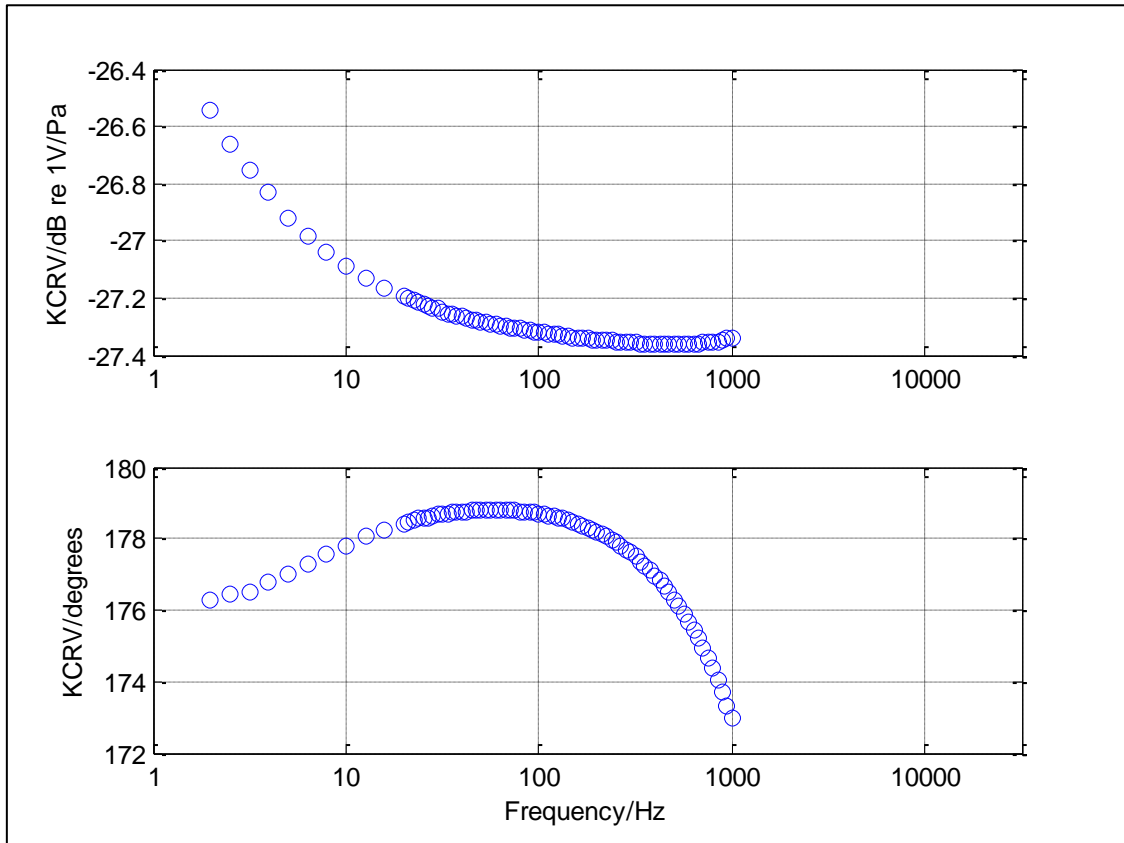


Figure 7 The calculated weighted mean values for sensitivity level and phase from the results up to 1 kHz of all participating institutes for microphone 4160 2652754.

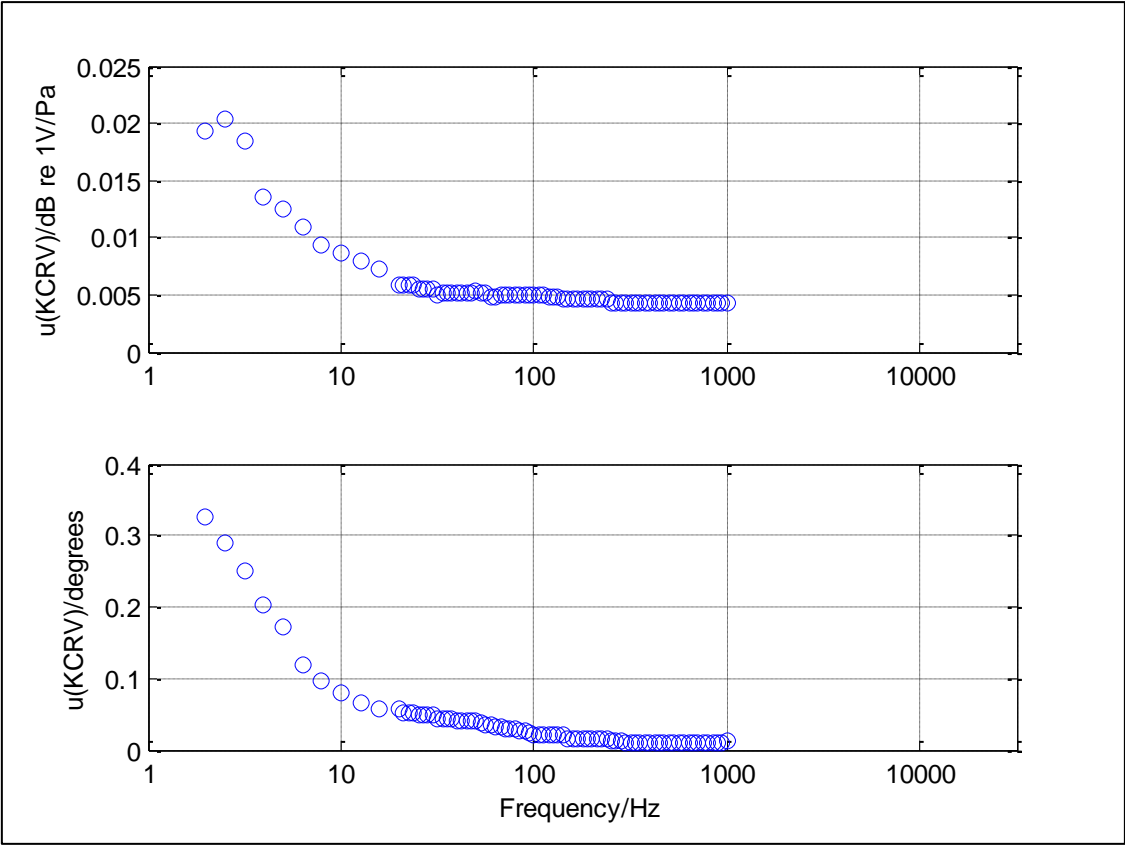


Figure 8 The uncertainty in the weighted mean calculations for sensitivity level and phase up to 1 kHz for microphone 4160 2652754.

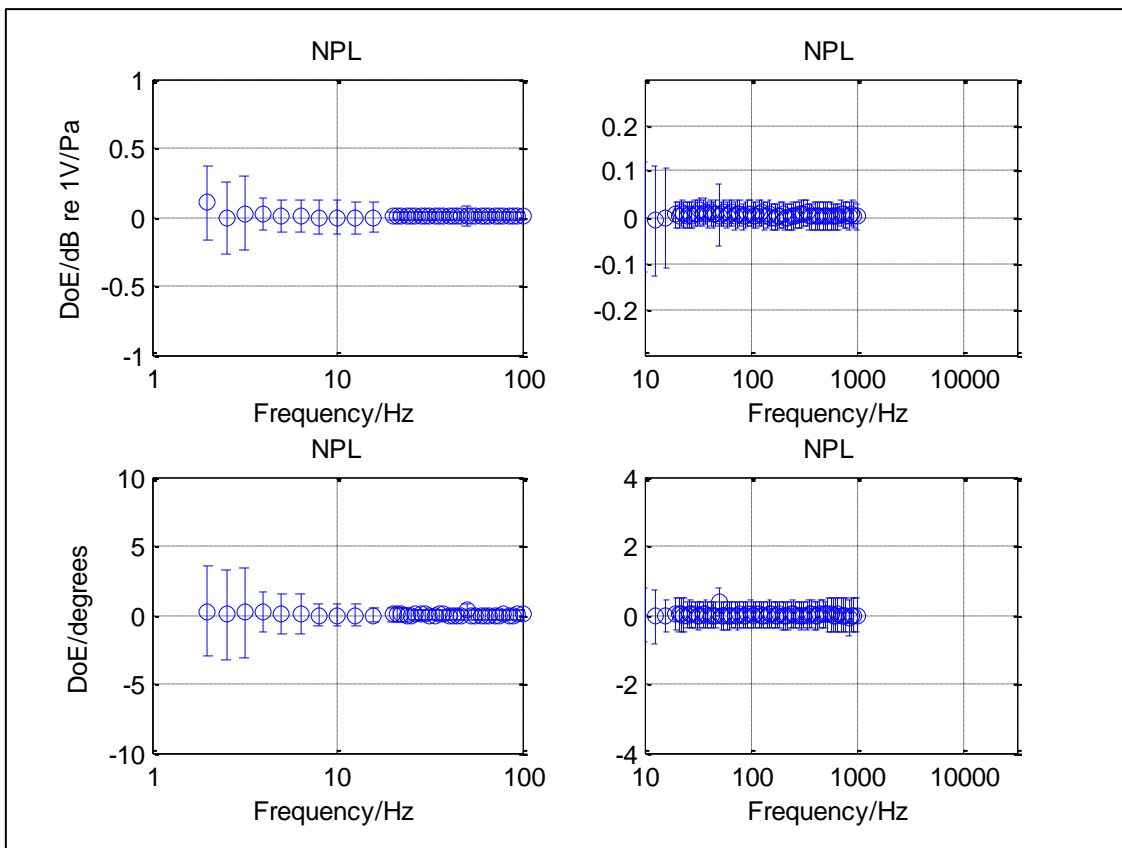


Figure 9(a) Degrees of Equivalence for NPL sensitivity level and phase measurements with uncertainty bars corresponding to coverage factor $k=2$ based on microphone 4160 2652754.

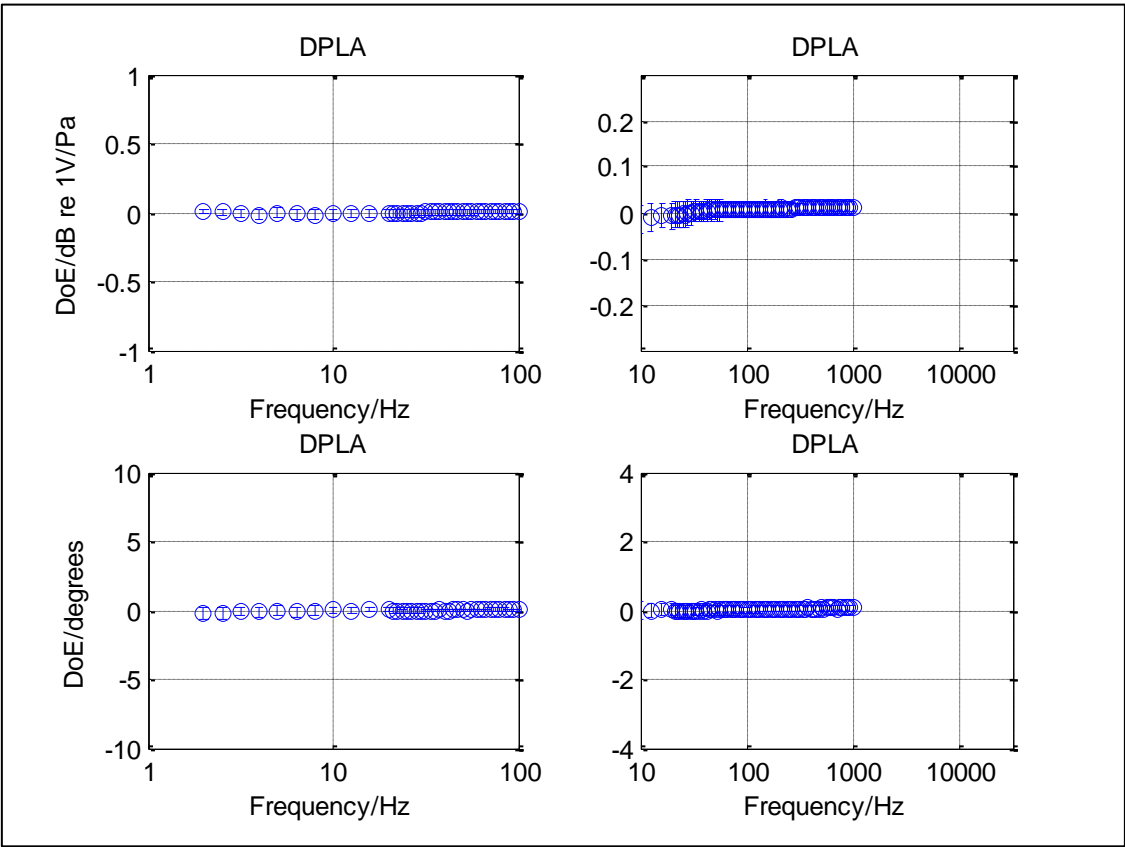


Figure 9(b) Degrees of Equivalence for DPLA sensitivity level and phase measurements with uncertainty bars corresponding to coverage factor $k=2$ based on microphone 4160 2652754.

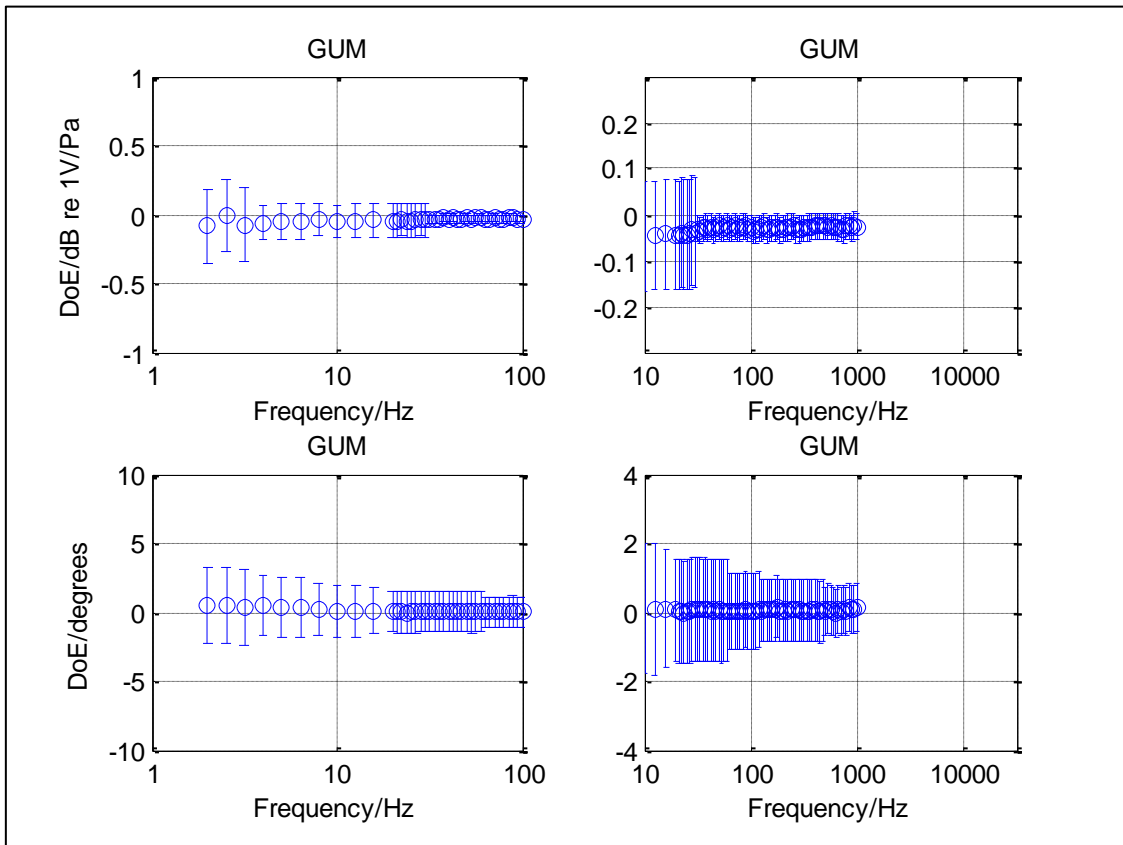


Figure 9(c) Degrees of Equivalence for GUM sensitivity level and phase measurements with uncertainty bars corresponding to coverage factor $k=2$ based on microphone 4160 2652754.

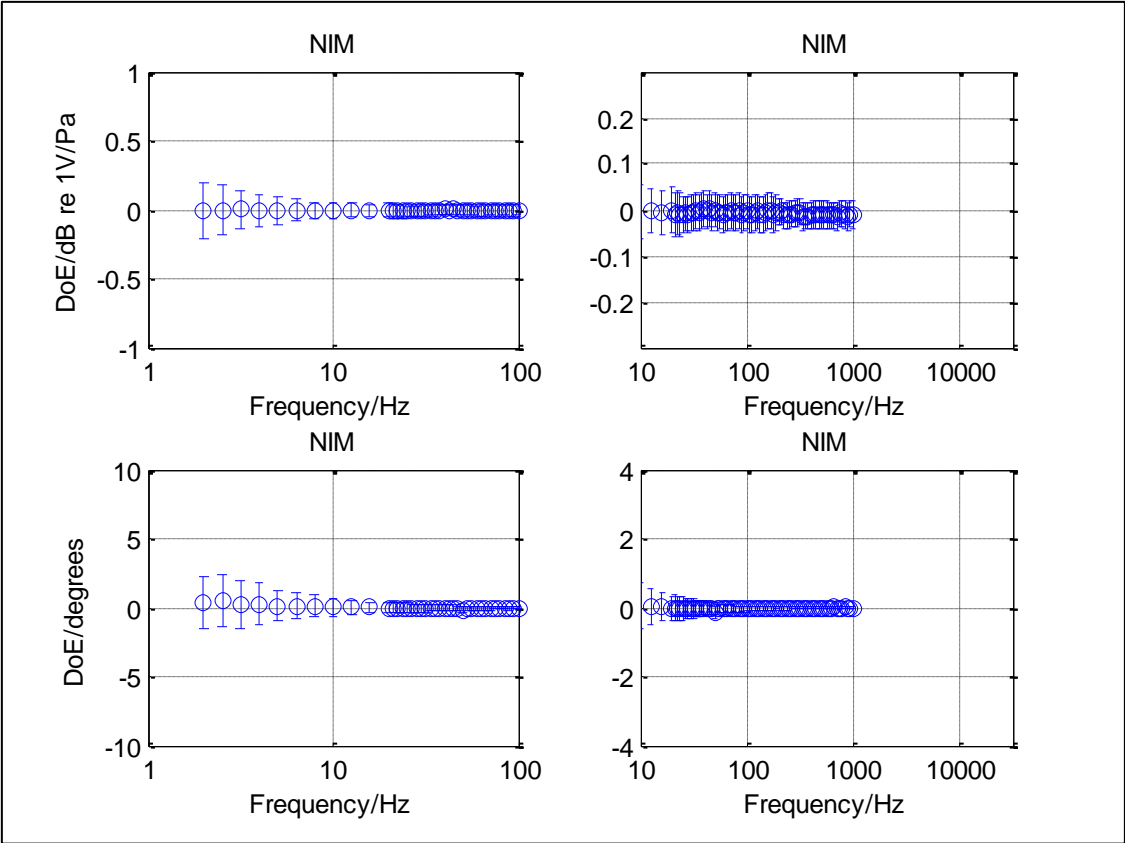


Figure 9(d) Degrees of Equivalence for NIM sensitivity level and phase measurements with uncertainty bars corresponding to coverage factor $k=2$ based on microphone 4160 2652754.

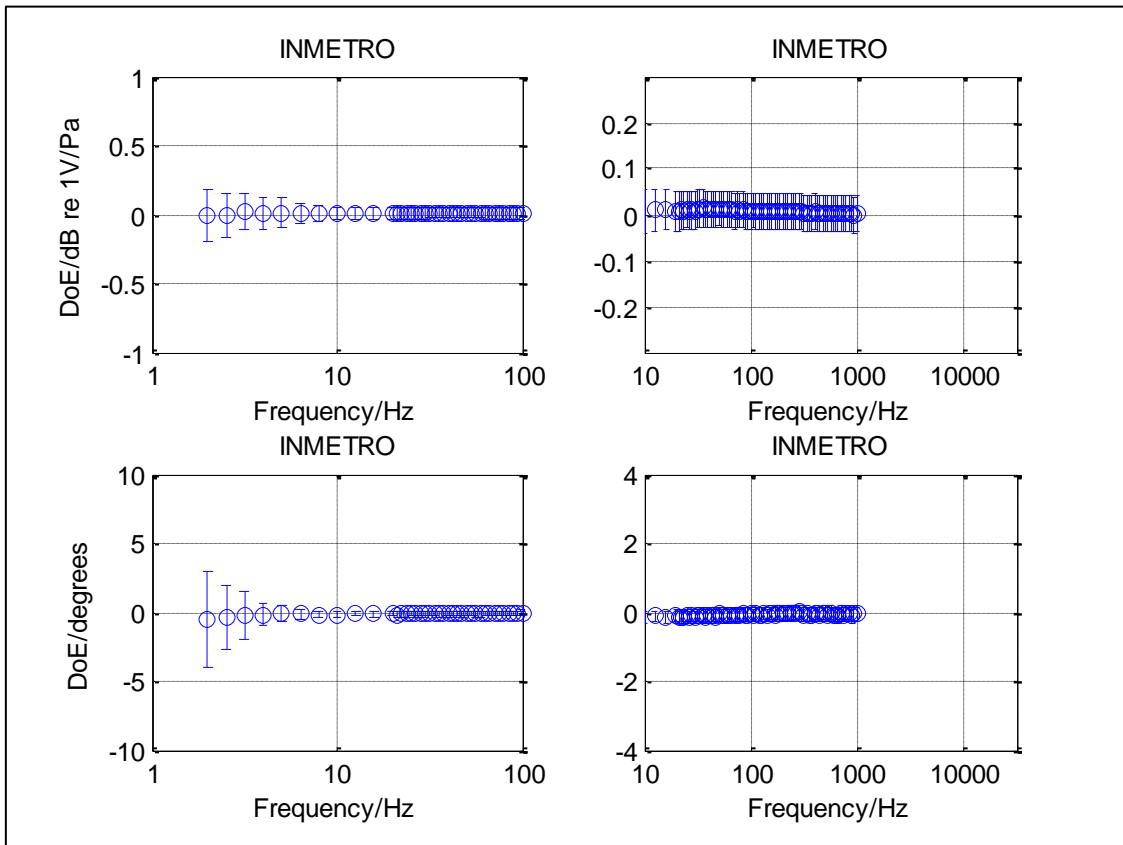


Figure 9(e) Degrees of Equivalence for INMETRO sensitivity level and phase measurements with uncertainty bars corresponding to coverage factor $k=2$ based on microphone 4160 2652754.

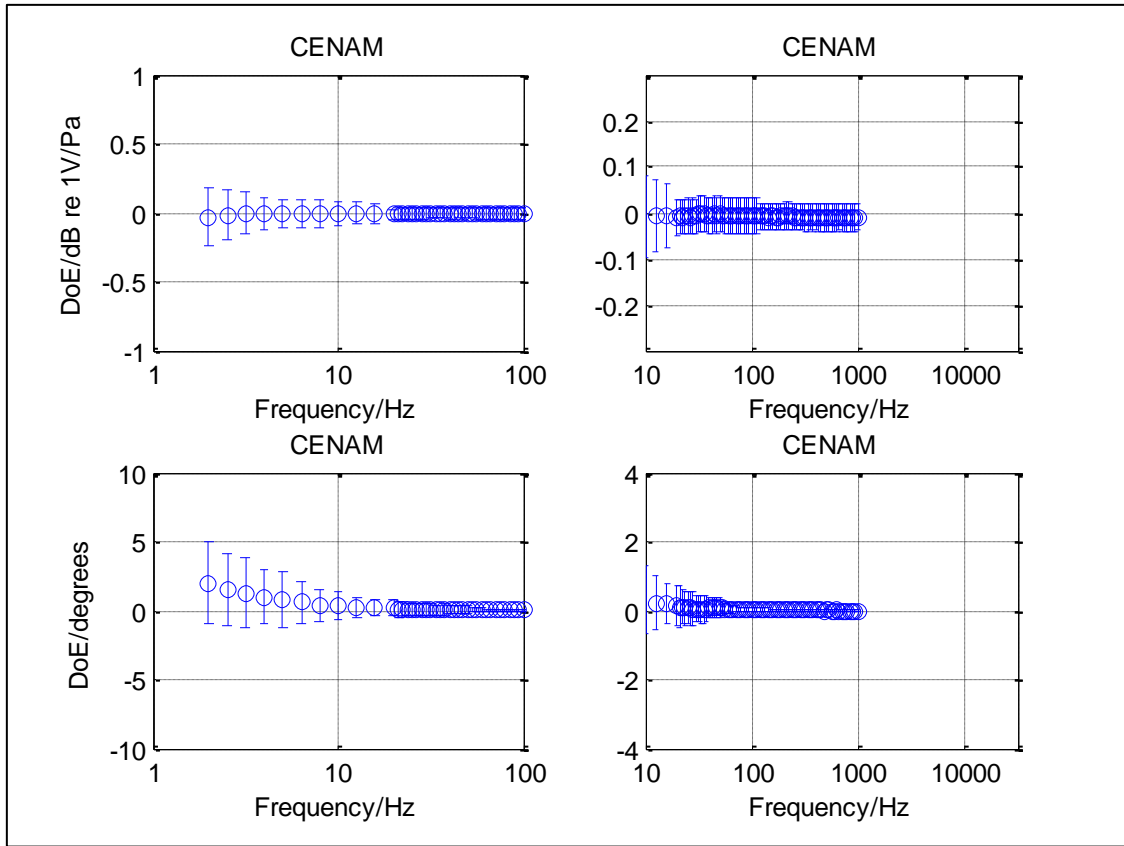


Figure 9(f) Degrees of Equivalence for CENAM sensitivity level and phase measurements with uncertainty bars corresponding to coverage factor $k=2$ based on microphone 4160 2652754.

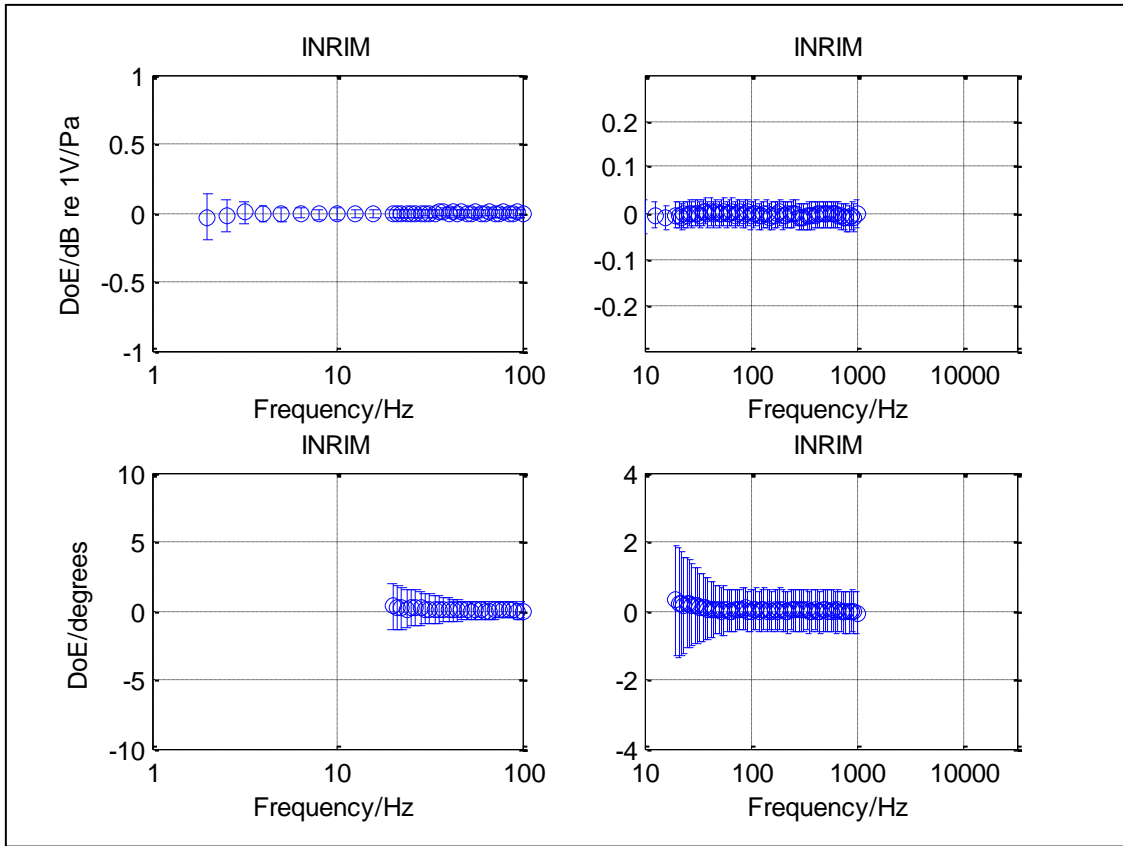


Figure 9(g) Degrees of Equivalence for INRIM sensitivity level and phase measurements with uncertainty bars corresponding to coverage factor $k=2$ based on microphone 4160 2652754.

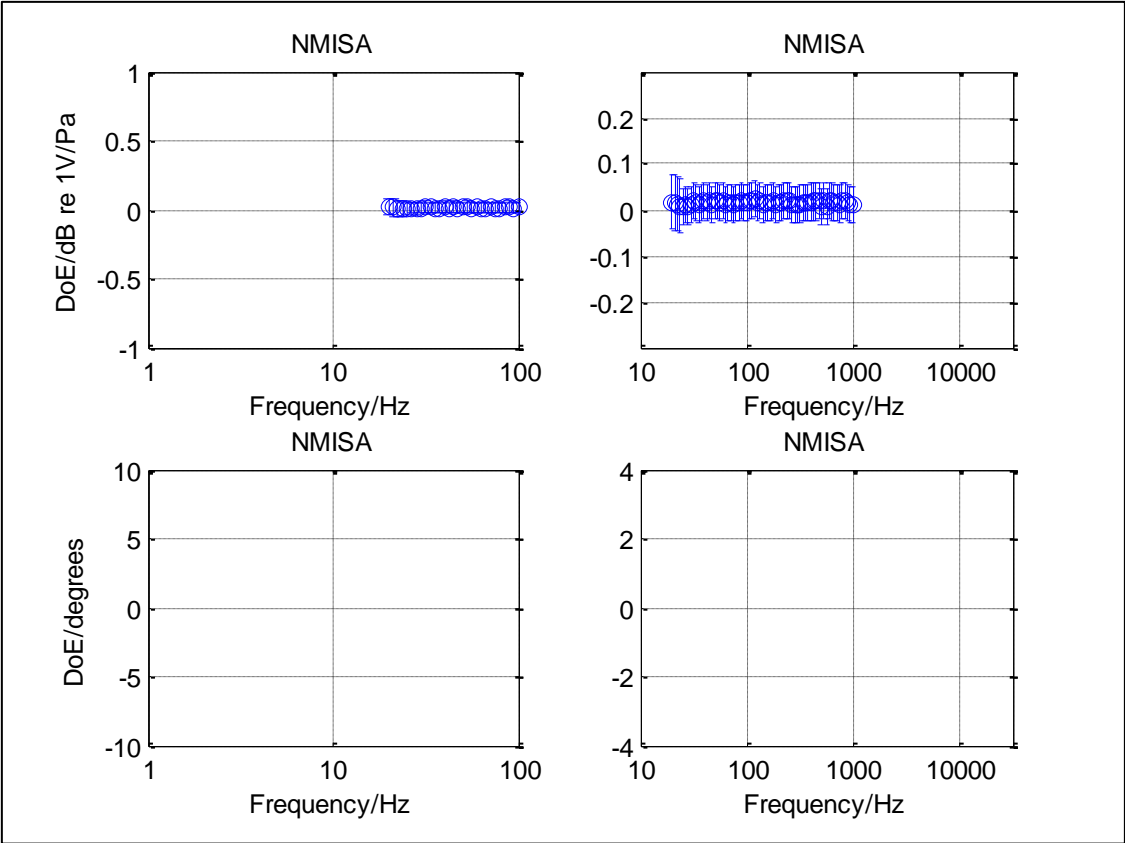


Figure 9(h) Degrees of Equivalence for NMISA sensitivity level measurements with uncertainty bars corresponding to coverage factor $k=2$ based on microphone 4160 2652754 (phase measurement results were withdrawn).

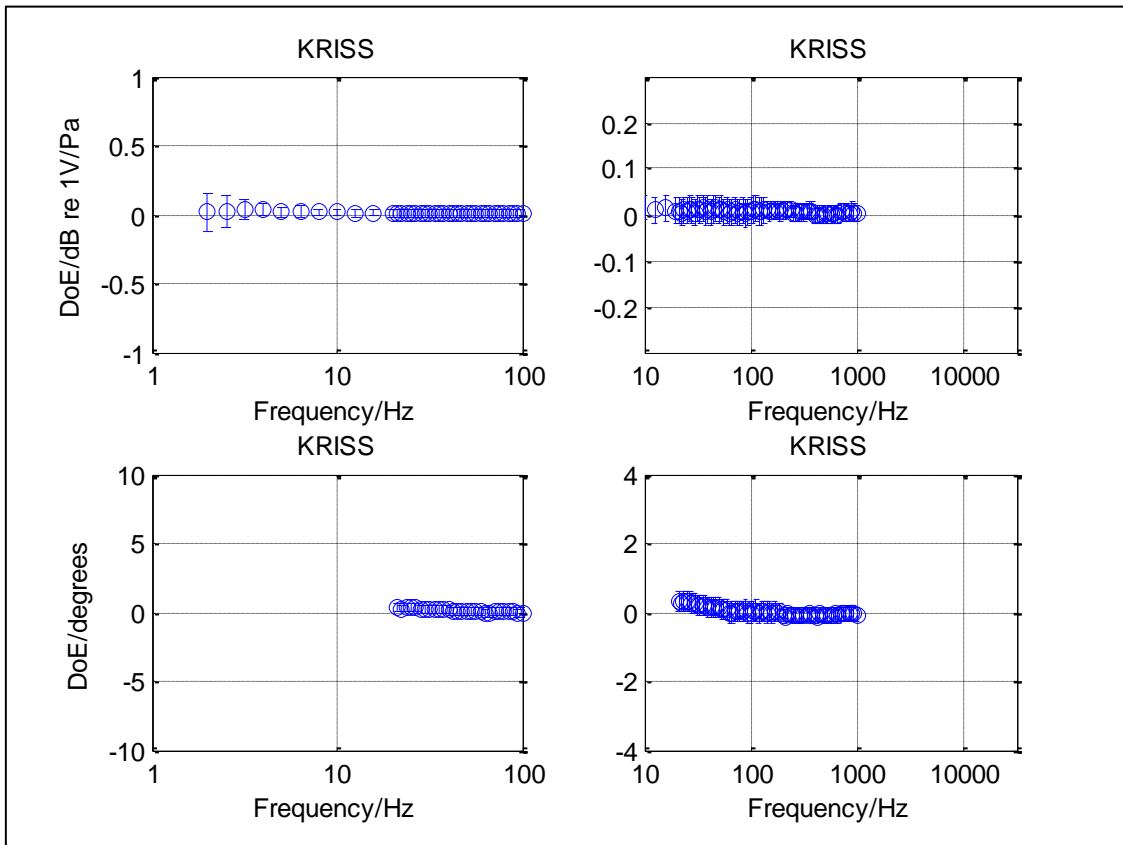


Figure 9(i) Degrees of Equivalence for KRISS sensitivity level and phase measurements with uncertainty bars corresponding to coverage factor $k=2$ based on microphone 4160 2652754.

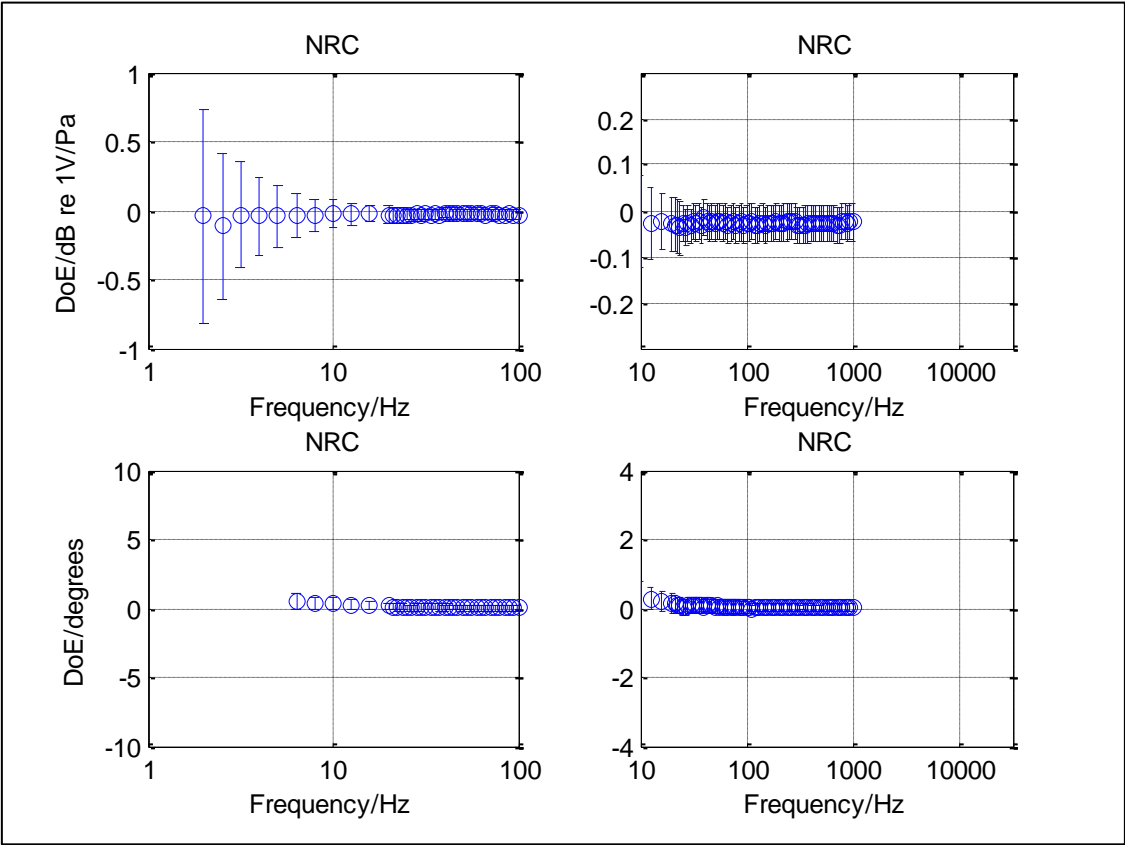


Figure 9(j) Degrees of Equivalence for NRC sensitivity level and phase measurements with uncertainty bars corresponding to coverage factor $k=2$ based on microphone 4160 2652754.

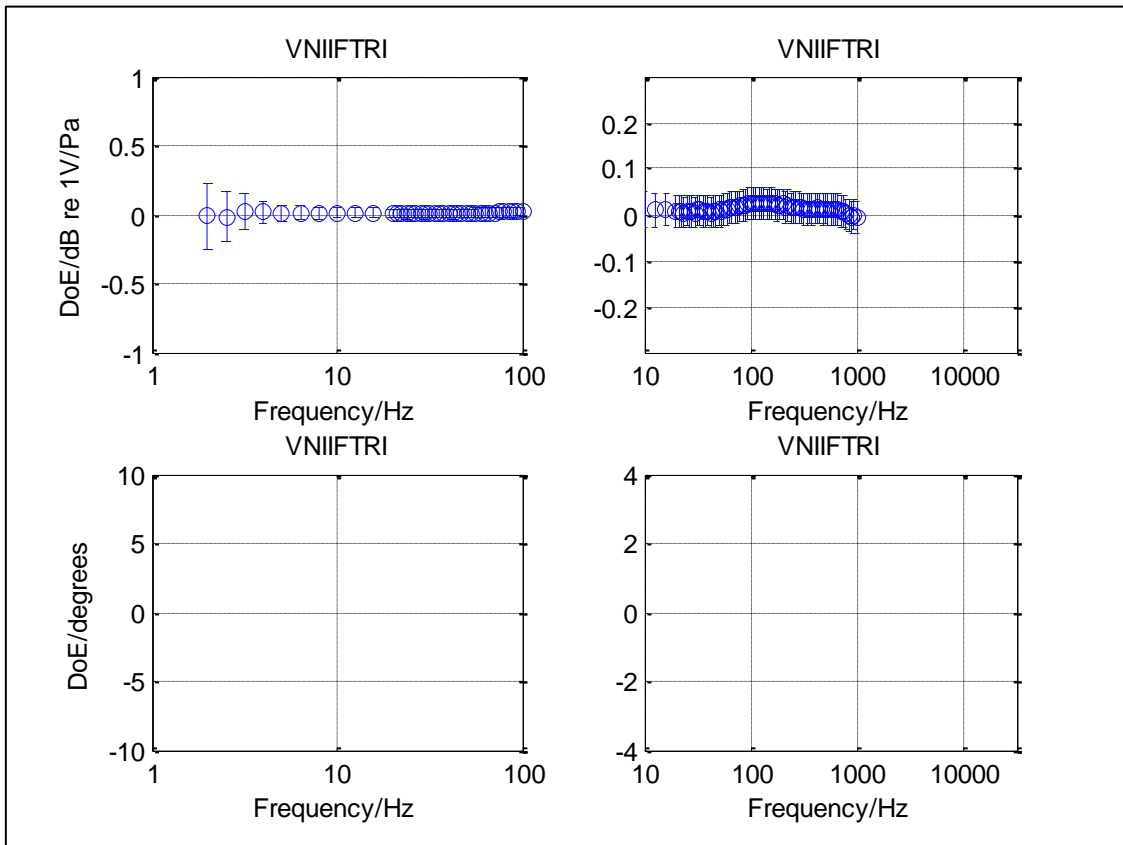


Figure 9(k) Degrees of Equivalence for VNIIFTRI sensitivity level measurements with uncertainty bars corresponding to coverage factor $k=2$ based on microphone 4160 2652754 (no phase results were reported).

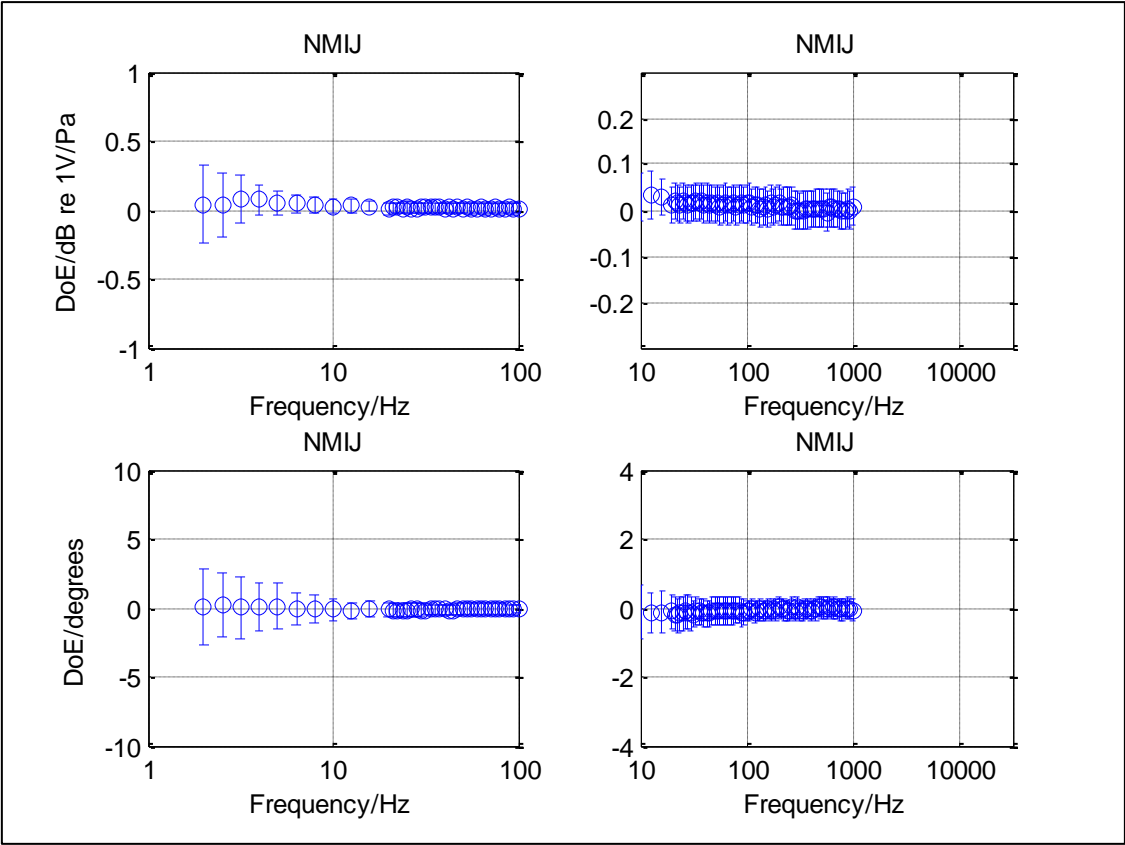


Figure 9(l) Degrees of Equivalence for NMIJ sensitivity level and phase measurements with uncertainty bars corresponding to coverage factor $k=2$ based on microphone 4160 2652754.

Microphone calibration typically requires many frequency points to be considered to fully characterise the microphone under test, and comparisons amongst participants at individual frequencies becomes cumbersome. However, as in past key comparisons, figure 10(a)-(h) presents the degrees of equivalence of all participant for 250 Hz and 1 kHz. These frequencies have been chosen for illustration purposes as they are often important in dissemination of primary calibrations. Since results for all frequencies can be found in the accompanying spreadsheet, the reader is able to produce similar representations for other frequencies as required.

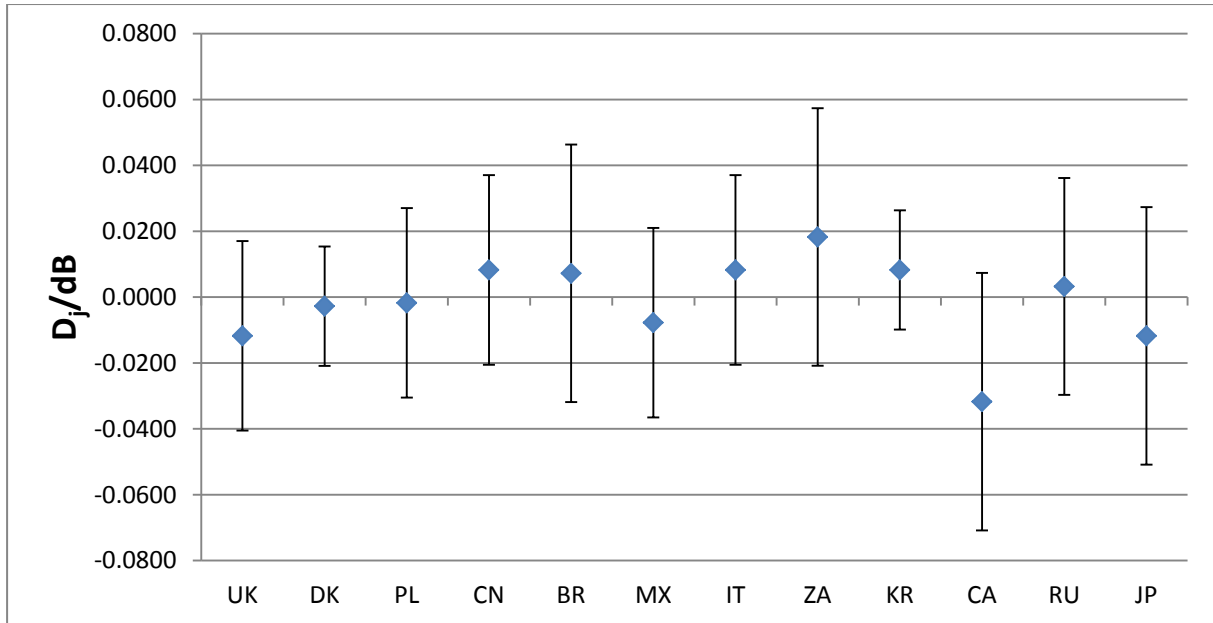


Figure 10(a) Degrees of equivalence for 4160 811012 sensitivity level at 251.189 Hz and their expanded uncertainties (k=2).

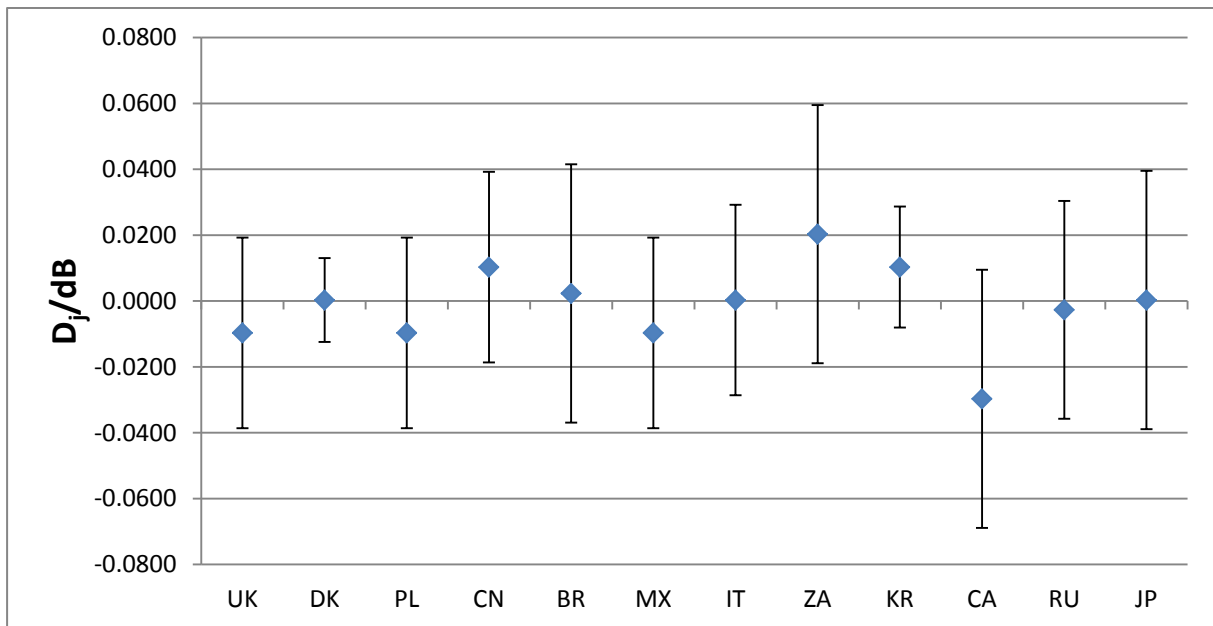


Figure 10(b) Degrees of equivalence for 4160 811012 sensitivity level at 1000 Hz and their expanded uncertainties (k=2).

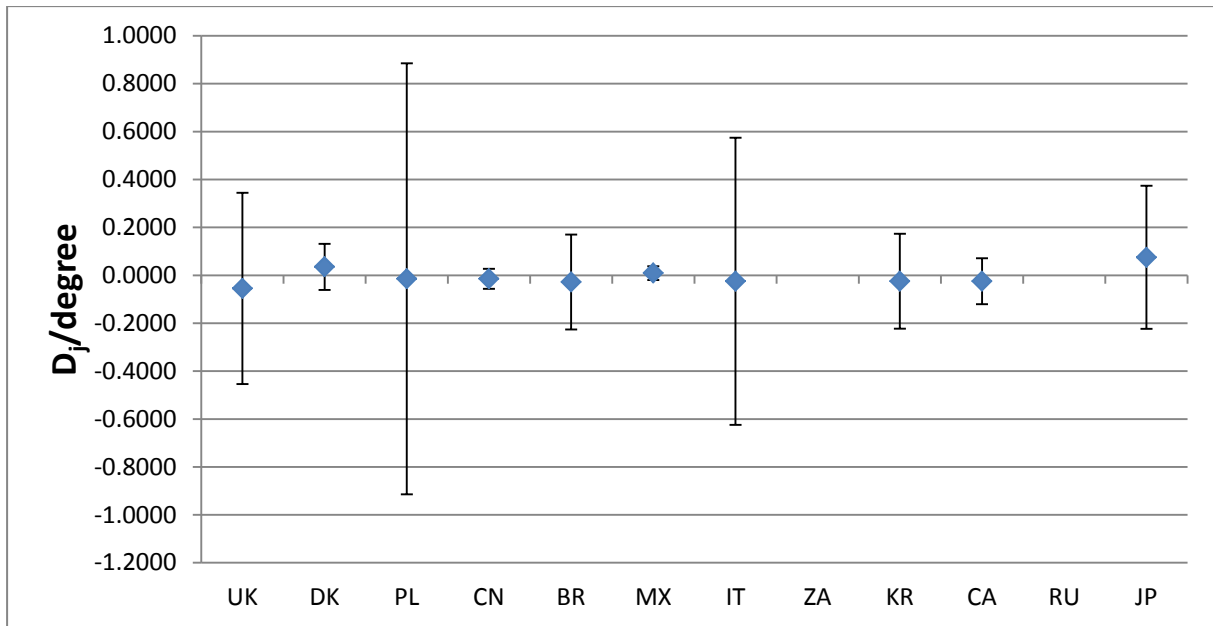


Figure 10(c) Degrees of equivalence for 4160 811012 sensitivity phase at 251.189 Hz and their expanded uncertainties (k=2).

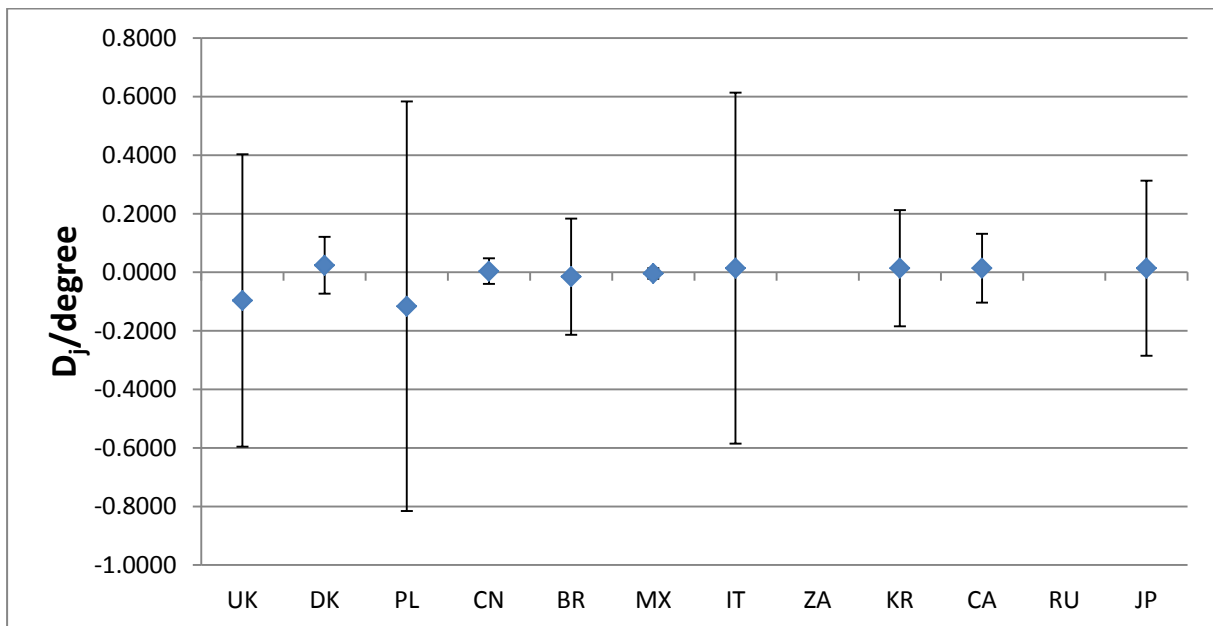


Figure 10(d) Degrees of equivalence for 4160 811012 sensitivity phase at 1000 Hz and their expanded uncertainties (k=2).

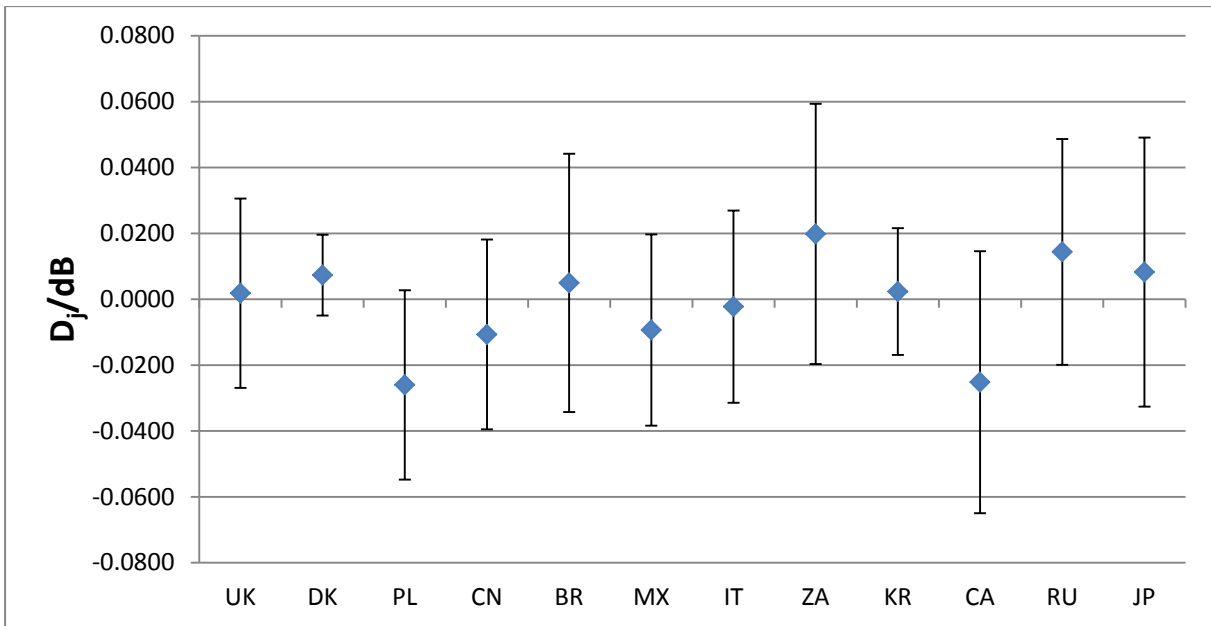


Figure 10(e) Degrees of equivalence for 4160 2652754 sensitivity level at 251.189 Hz and their expanded uncertainties (k=2).

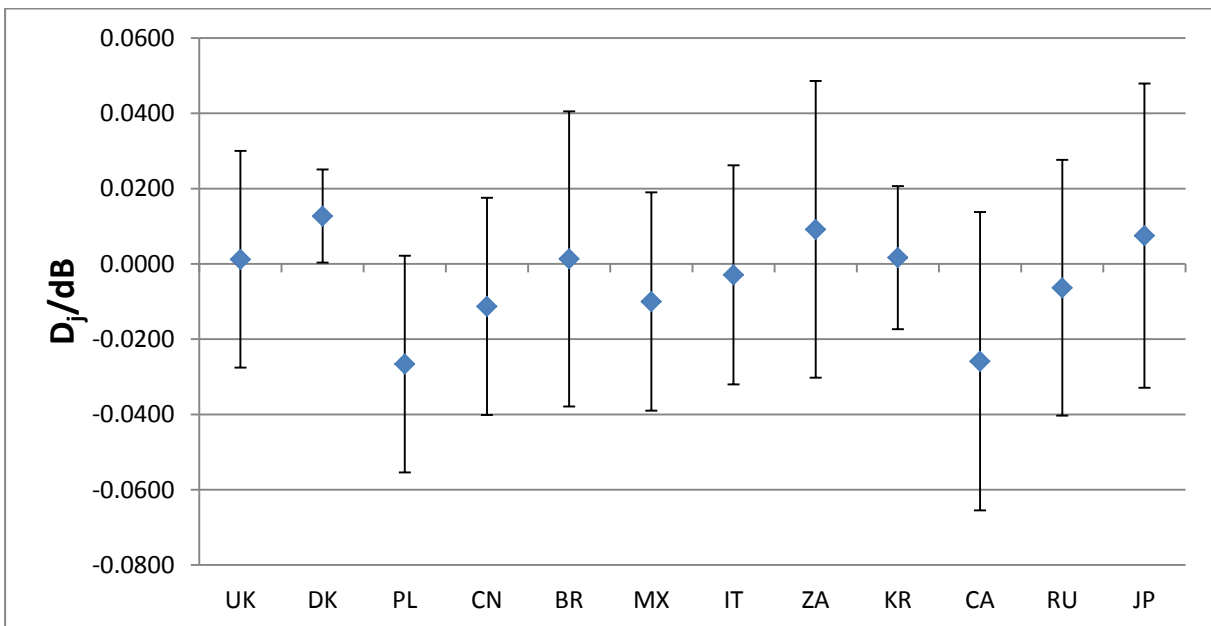


Figure 10(f) Degrees of equivalence for 4160 2652754 sensitivity level at 1000 Hz and their expanded uncertainties (k=2).

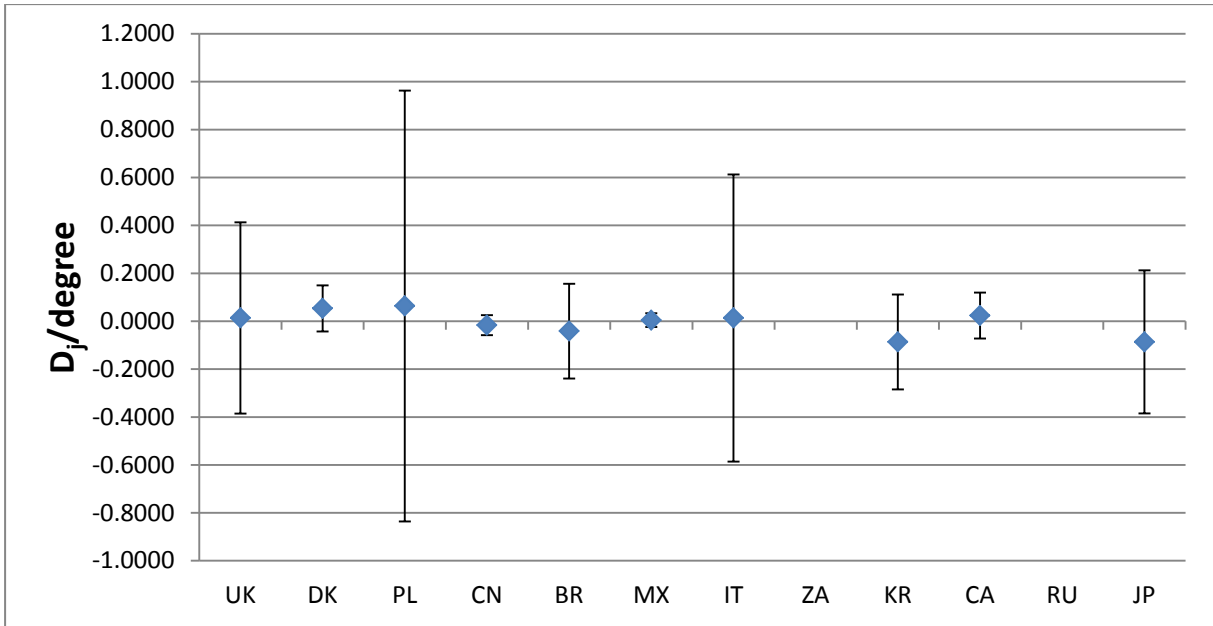


Figure 10(g) Degrees of equivalence for 4160 2652754 sensitivity phase at 251.189 Hz and their expanded uncertainties ($k=2$).

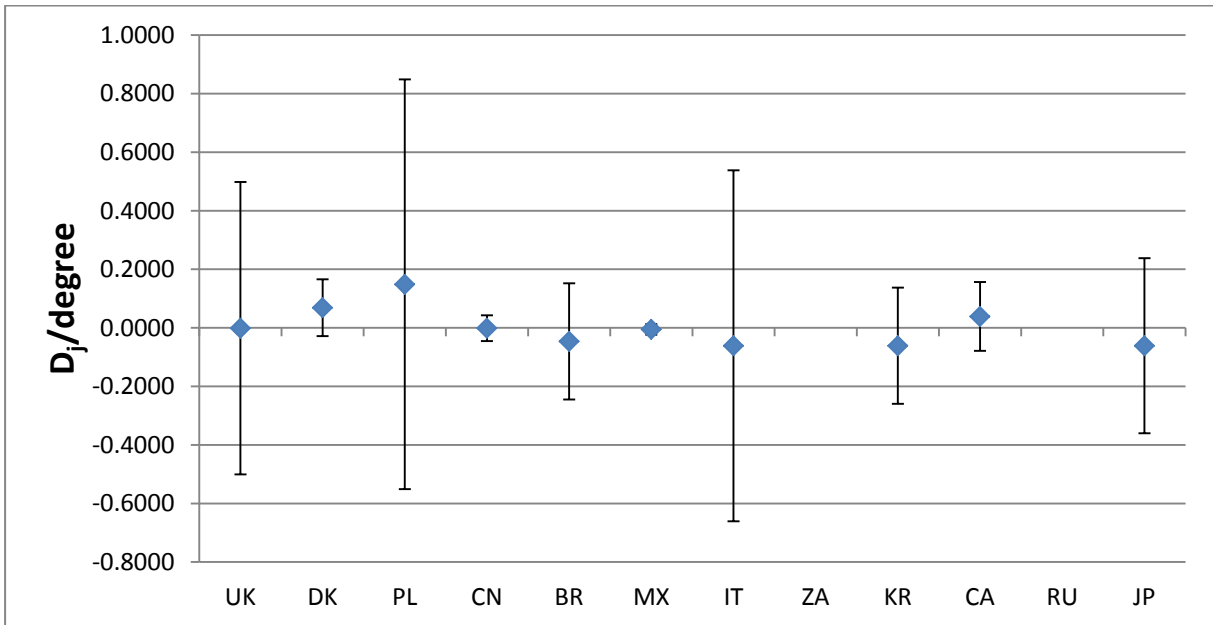


Figure 10(h) Degrees of equivalence for 4160 2652754 sensitivity phase at 1000 Hz and their expanded uncertainties ($k=2$).

10 CONCLUSIONS

Twelve institutes from five regional metrology organisations (RMOs) took part in a key comparison on the pressure sensitivity of laboratory standard microphones.

CCAUV.A-K5 covers and extends the scope of previous key comparisons CCAUV.A-K1 and CCAUV.A-K2.

CCAUV.A-K5 includes, for the first time, the phase of the pressure sensitivity within its scope.

Key comparison reference values have been determined based on the pressure sensitivity of a single microphone at a range of discrete frequencies, using a weighted mean estimate.

The consistency of each participant's results, with respect to the KCRVs, has been assessed using a chi-squared test. For measurements of the microphone's sensitivity level, the results were shown to be consistent with the KCRVs in all cases. For measurements of the microphone's sensitivity phase response, a small minority of the measurements were shown to be inconsistent with the KCRVs. These inconsistent results were withdrawn, revised or excluded from the final calculation of the KCRVs.

11 ACKNOWLEDGMENTS

The co-operation of all participants, enabling the measurement stage of this key comparison to progress smoothly, has been invaluable to the piloting of this key comparison. The authors gratefully acknowledge the contribution of Dr Peter Harris who carried out the detailed statistical analysis of the measurement results. The financial support of the National Measurement Office, part of the UK Government's Department of Business, Innovation and Skills, made it possible for NPL to pilot this project.

12 REFERENCES

- [1] Barham, Richard. Technical protocol for key comparison CCAUV.A-K5, Issue 1, December 2010. National Physical Laboratory, 2010.
- [2] IEC 61094-2:2009, Measurement microphones - Part 2: Primary method for pressure calibration of laboratory standard microphones by the reciprocity technique.
- [3] Rasmussen, K. The static pressure and temperature coefficients of laboratory standard microphones. *Metrologia* **36**, 265-273. 1999.
- [4] Rasmussen, K. The influence of environmental conditions on the pressure sensitivity of measurement microphones, B&K Technical Review, 1. 2001.
- [5] Kosobrodof, R. Static pressure coefficients of laboratory standard microphones in the frequency range 2-250 Hz. 11th ICSV, 1441-1448. 2004.
- [6] Cox, M.G. The evaluation of key comparison data. *Metrologia* **39**, 589-595. 2002.

ANNEX A: DETAILED STABILITY ANALYSIS

Stability measurements were performed at the pilot laboratory throughout the duration of the intercomparisons. The measurements were made over the complete frequency range, but at exact mid-band third-octave frequencies, rather than the full set of frequencies measured by the participants. The following analysis of the stability data was carried out to determine if the sensitivities of the microphones changed by a statistically significant amount during the intercomparison. Each frequency was analysed separately.

Ideally, the behaviour of an individual microphone's sensitivity throughout the intercomparison would be describable by a constant value, allowing for some random variability within the type A allowances of the pilot laboratory's uncertainty budget (type B components are expected to act systematically). A microphone conforming to this ideal would be said to have been stable throughout the period of measurements. To evaluate the stability of each microphone a statistical test was applied to evaluate the consistency of the fitting of the constant value to the original data, taking into account the expected variability of the data.

If the microphone's stability data could not be fitted successfully with a constant value, the next simplest description of its behaviour would be a straight line with a non-zero gradient. The validity of the straight-line behaviour model was also tested, by evaluating the consistency of the straight-line fitting to the original data.

If the straight line could be successfully fitted to the data, it was relatively simple to correct the data to compensate for the drift of the microphone sensitivity, but there were uncertainties associated with the corrections.

If the microphone's stability data could not be fitted successfully with a straight line, then we concluded that the behaviour of the microphone over the duration of the intercomparison was more complex. Any attempt to correct for this variation in sensitivity would be subject to large uncertainties. Any frequencies whose data fell into this category were ultimately excluded from the analysis.

For each frequency, a weighted least squares method was used to calculate the best fit constant function, of the form $y=C$, and a best fit straight line function, of the form $y=mx+C$, for the sensitivity (level and phase) of each microphone with time. The data was weighted according to the pilot laboratory's type A standard uncertainty. This uncertainty represents the expected variation between measurements made at a particular frequency. (It is a conservative estimate, usually applied as an acceptance limit on the actual standard deviation of three repeated measurements.)

Consistency data for straight line fitting for microphone 4160 2652754 has been provided in '*CCAUV-A-K5 Final Report Tables of Data.xls*'.

A.1 CONSISTENCY OF FITS

The consistency of each fit was assessed using a chi-squared test. A threshold based on the 95th percentile of a chi-squared distribution with degrees of freedom equal to the number of data points minus the number of parameters (i.e. one parameter for a constant fit or two parameters for a straight line fit) was used to determine if the test was passed. If the best fit constant was consistent according to the chi-squared test, the microphone sensitivity was considered to have been stable throughout the intercomparison. If the best fit constant was found to be an inconsistent fit and the best fit straight line a consistent fit, then the estimate of the slope parameter of the fit and its associated uncertainty was used to describe the drift of the microphone sensitivity and as the basis for correcting the data provided by the participating institutes to account for that drift.

Graphs of a subset of the frequencies (3.98 Hz, 125.9 Hz, 1 kHz, 3980 Hz and 10 kHz) are illustrated here as examples. In each case, the top graph shows the pilot laboratory's stability data (with $k = 2$

uncertainty bars) plotted against the number of days (where day 0 corresponds to 24 January 2011), the best-fit constant (dashed line) and the best-fit straight-line (solid line). The bottom graph shows the weighted residual deviations for the best-fit constant (circles) and the best-fit straight-line (pluses).

Weighted residual deviations are defined as the difference between the measured value, y_i , and the estimated (model) function value, $f(x_i)$, divided by the standard uncertainty associated with the measured value, σ_i .

$$(y_i - f(x_i))/\sigma_i$$

The colour blue is used to show a fit that is consistent according to a chi-squared test, and red when the fit is inconsistent. A microphone's behaviour at a frequency can be considered fitted correctly when there is a consistent fit, and weighted residual deviations that are random and take values (approximately) between -2 and +2.

It can be seen from Figures A.1(a) to A.1(e) and Figures A.1(f) to A.1(j), that the sensitivity level and phase of microphone 4160 811012 with time can be fitted consistently with a constant value at all frequencies and the microphone can therefore be considered stable.

It can be seen from Figures A.1(k) to A.1(o) that the sensitivity level of microphone 4160 2652754 with time cannot be fitted consistently using a constant value, except at very low frequencies where the uncertainty is large compared with the magnitude of the observed changes. The straight line does, however, provide a consistent fit for the lower part of the frequency range, but not above 5 kHz approximately. It is possible to apply a correction to the results to reliably account for drift for frequencies below 5 kHz. Above 5 kHz the drift in magnitude sensitivity shows more complicated characteristics, requiring modelling as, for example, a quadratic function with time, making correction of the results less reliable.

The sensitivity phase graphs (Figures A.1(p) to A.1(t)), for the same microphone, show that at most frequencies the sensitivity phase can be fitted consistently using a constant value, indicating no evidence of a drift, but at very high frequencies, such as 10 kHz (shown in Figure A.1(t)), it cannot be fitted consistently with either a constant or a straight line.

The observed behaviour for this microphone is consistent with predictions of the microphone lumped parameter model for a change in stiffness of a microphone's diaphragm. A change in diaphragm tension would be expected to result in a step change in the sensitivity level and an alteration in the resonance frequency of the microphone. A change in resonance frequency would result in a corresponding change in phase response at high frequencies (near and above resonance) and relatively little change at low frequencies, where the phase response is independent of the diaphragm stiffness.

One laboratory (DPLA) has noted that the (low frequency) sensitivity of 4160 2652754 seems to have changed considerably more during the first 100 to 200 days of the period of measurements as compared to the rest of the period. This may lead to an overestimation of the drift after the first 100 to 200 days. This may explain the apparent systematic development with time of the difference between DoEs for the two microphones (from -0.02 dB for GUM and NIM to +0.01 dB at VNIIFTRI and NMIJ).

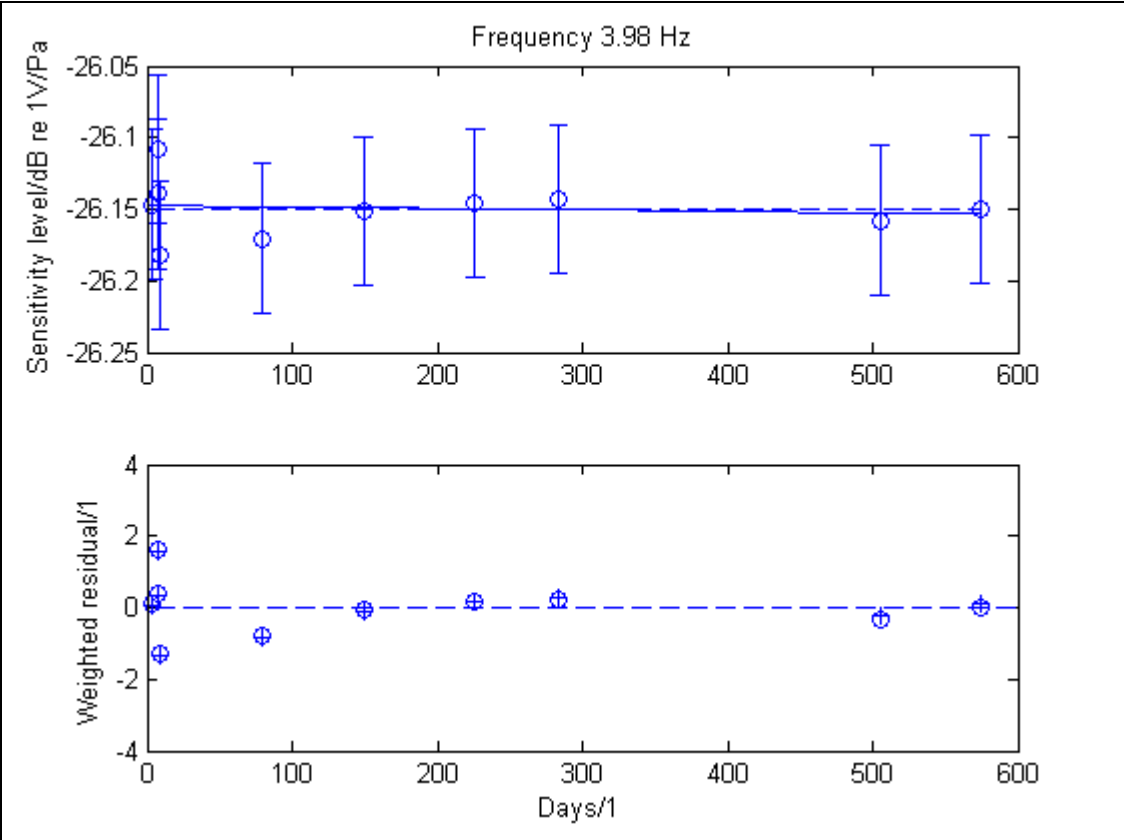


Figure A.1(a) Stability of 4160 811012 sensitivity level, at 3.98 Hz, fitted with a constant and a straight line – the top graph shows the pilot laboratory’s stability data plotted against the number of days (with $k = 2$ uncertainty bars), the best-fit constant (dashed line) and the best-fit straight-line (solid line). The bottom graph shows the weighted residual deviations for the best-fit constant (o) and the best-fit straight-line (+).

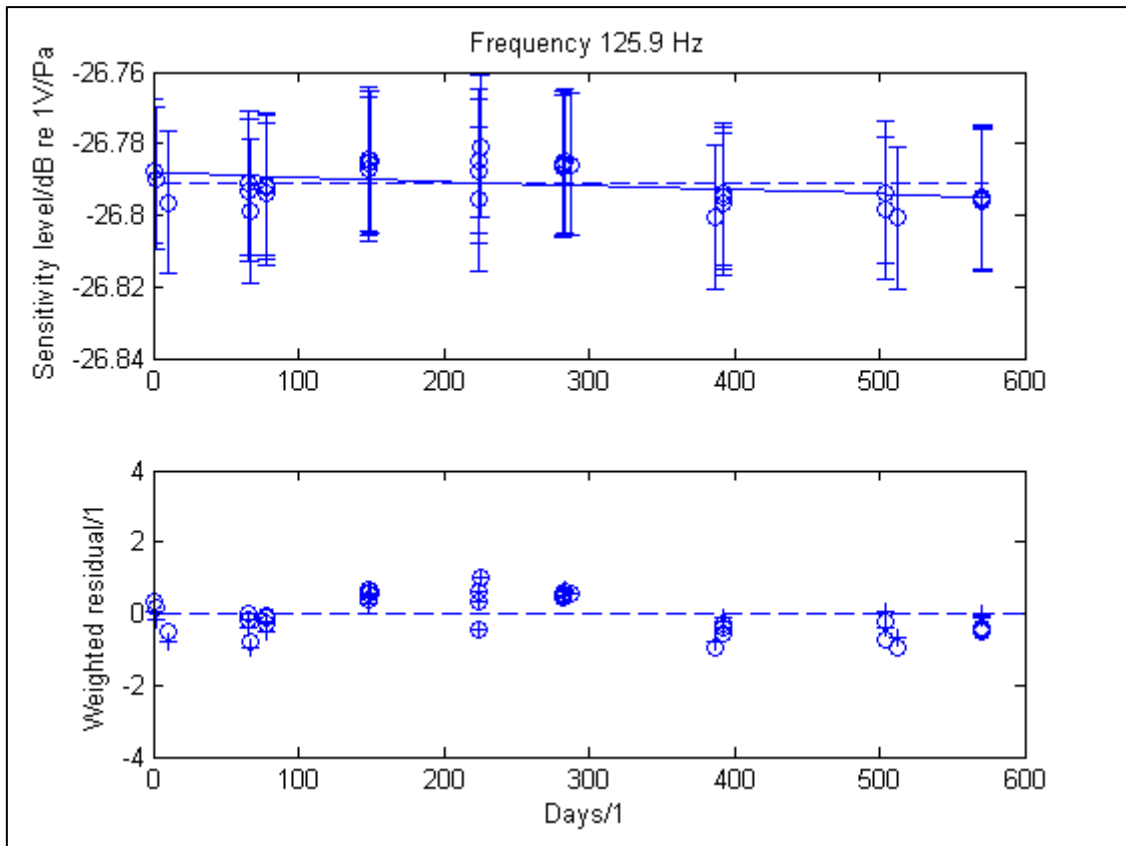


Figure A.1(b) Stability of 4160 811012 sensitivity level, at 125.9 Hz, fitted with a constant and a straight line – the top graph shows the pilot laboratory’s stability data plotted against the number of days (with $k = 2$ uncertainty bars), the best-fit constant (dashed line) and the best-fit straight-line (solid line). The bottom graph shows the weighted residual deviations for the best-fit constant (o) and the best-fit straight-line (+).

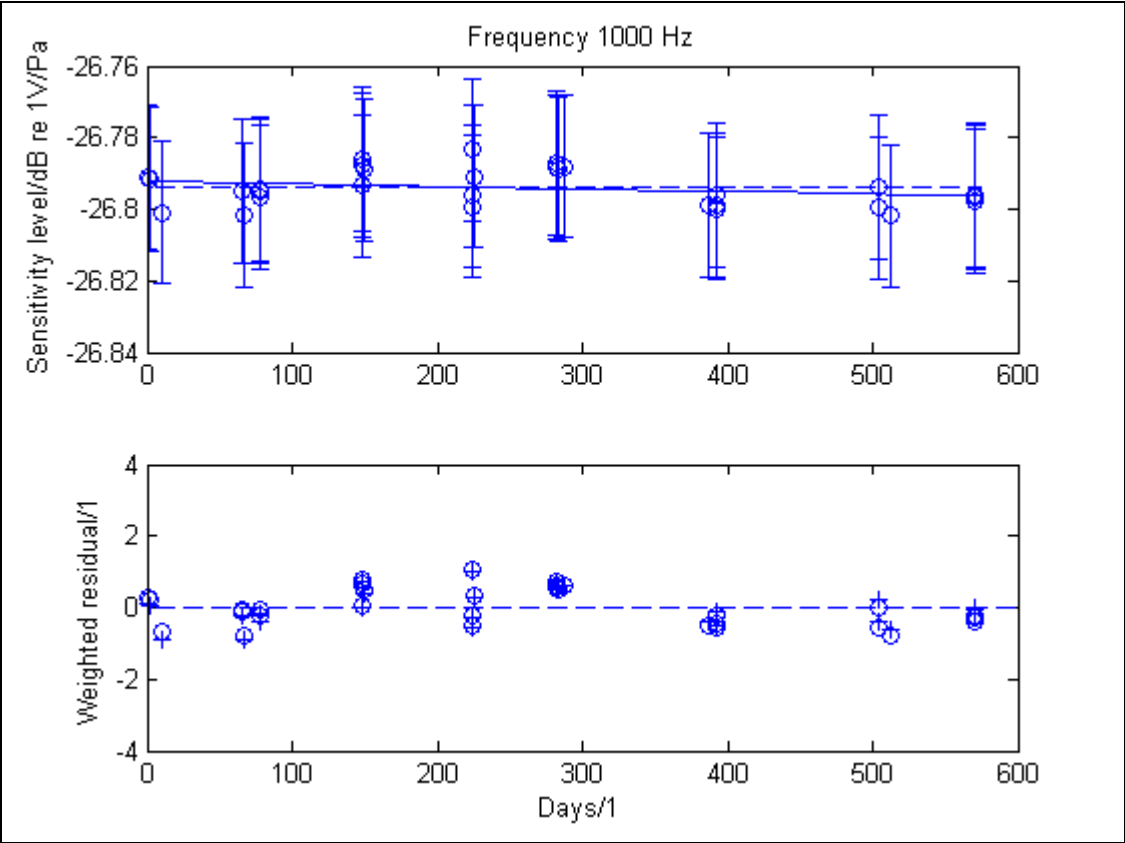


Figure A.1(c) Stability of 4160 811012 sensitivity level, at 1000 Hz, fitted with a constant and a straight line – the top graph shows the pilot laboratory’s stability data plotted against the number of days (with $k = 2$ uncertainty bars), the best-fit constant (dashed line) and the best-fit straight-line (solid line). The bottom graph shows the weighted residual deviations for the best-fit constant (o) and the best-fit straight-line (+).

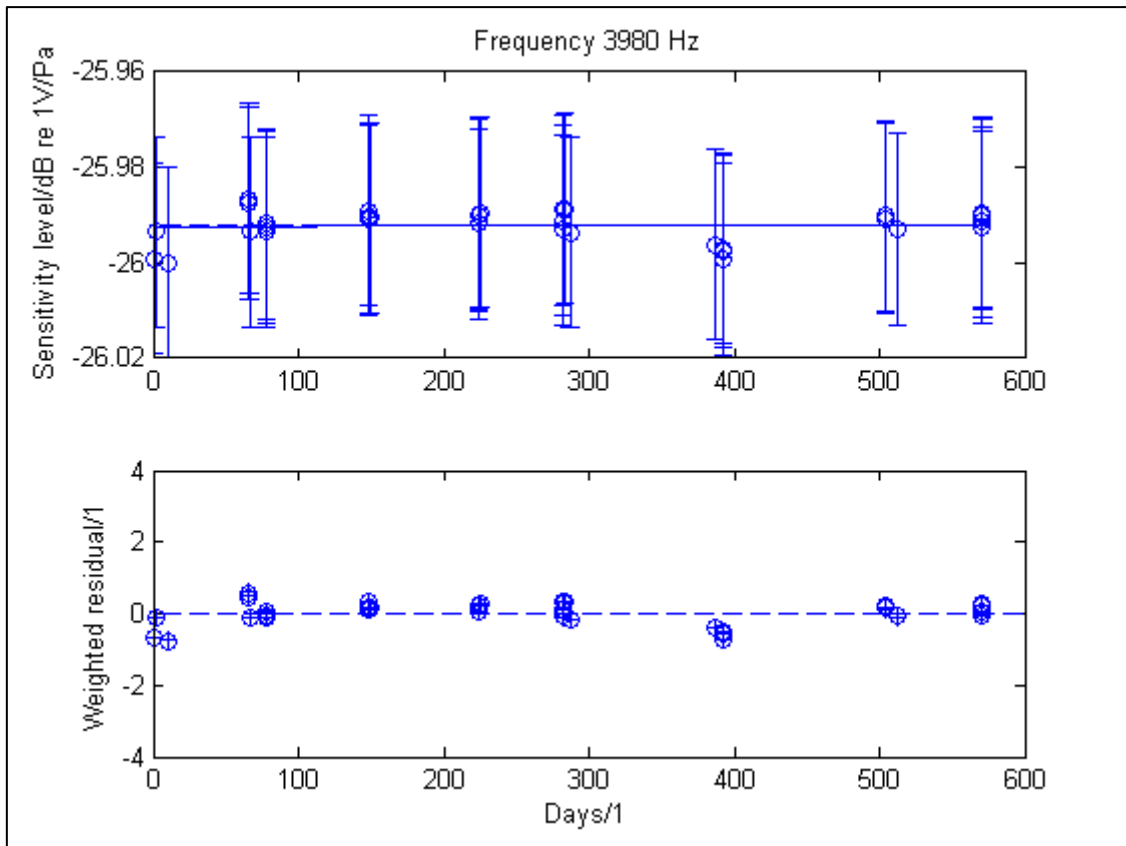


Figure A.1(d) Stability of 4160 811012 sensitivity level, at 3980 Hz, fitted with a constant and a straight line – the top graph shows the pilot laboratory’s stability data plotted against the number of days (with $k = 2$ uncertainty bars), the best-fit constant (dashed line) and the best-fit straight-line (solid line). The bottom graph shows the weighted residual deviations for the best-fit constant (o) and the best-fit straight-line (+).

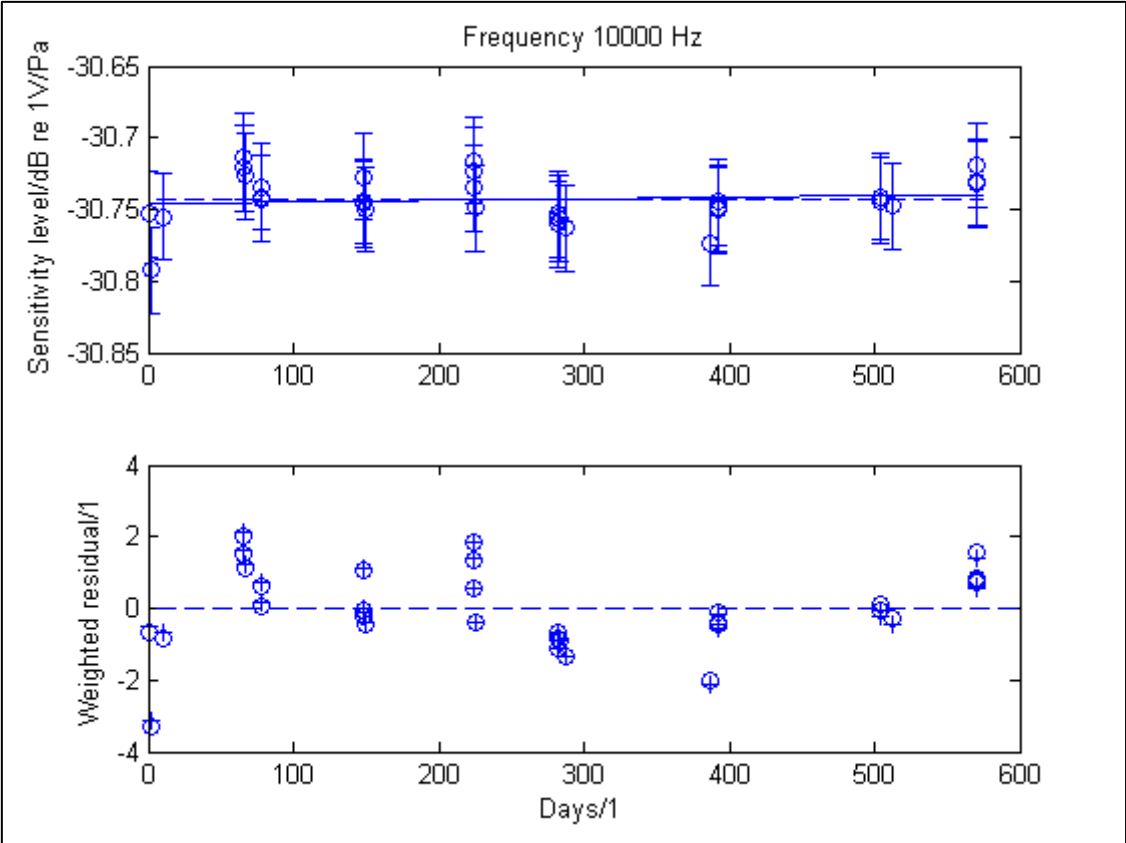


Figure A.1(e) Stability of 4160 811012 sensitivity level, at 10000 Hz, fitted with a constant and a straight line – the top graph shows the pilot laboratory’s stability data plotted against the number of days (with $k = 2$ uncertainty bars), the best-fit constant (dashed line) and the best-fit straight-line (solid line). The bottom graph shows the weighted residual deviations for the best-fit constant (o) and the best-fit straight-line (+).

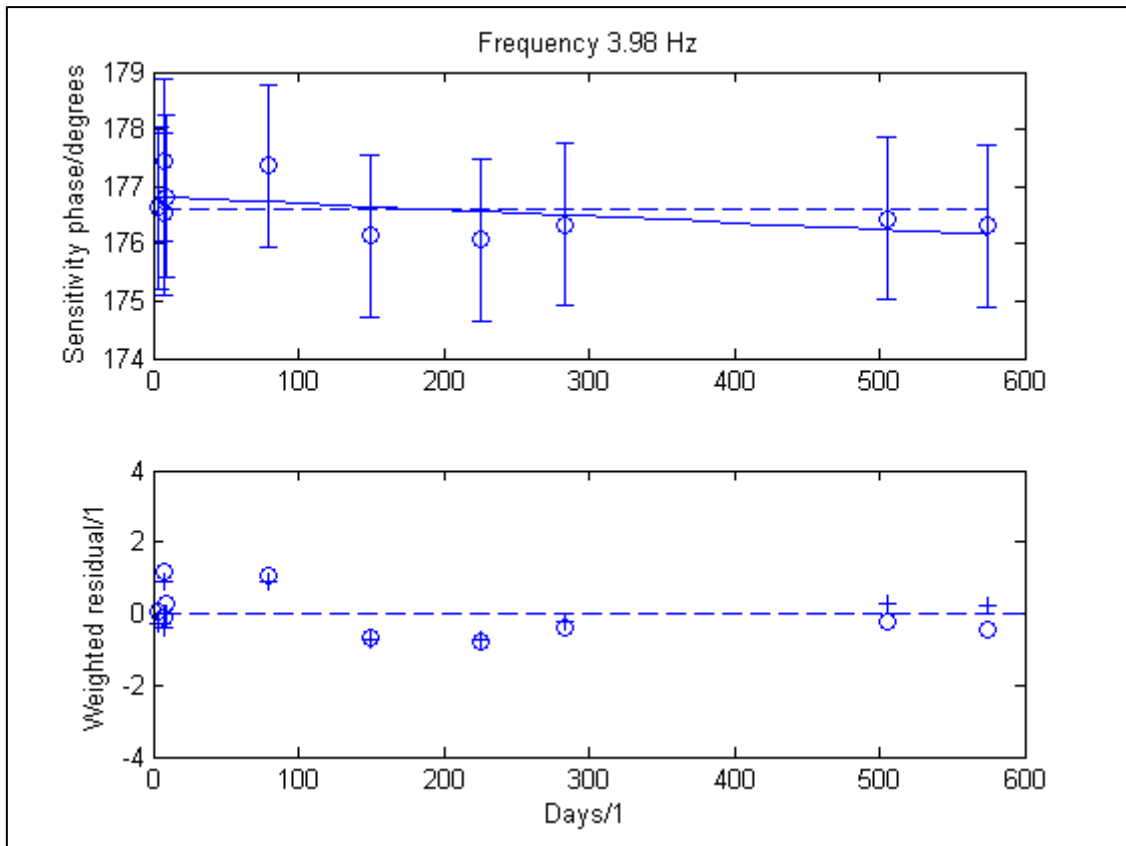


Figure A.1(f) Stability of 4160 811012 sensitivity phase, at 3.98 Hz, fitted with a constant and a straight line – the top graph shows the pilot laboratory’s stability data plotted against the number of days (with $k = 2$ uncertainty bars), the best-fit constant (dashed line) and the best-fit straight-line (solid line). The bottom graph shows the weighted residual deviations for the best-fit constant (o) and the best-fit straight-line (+).

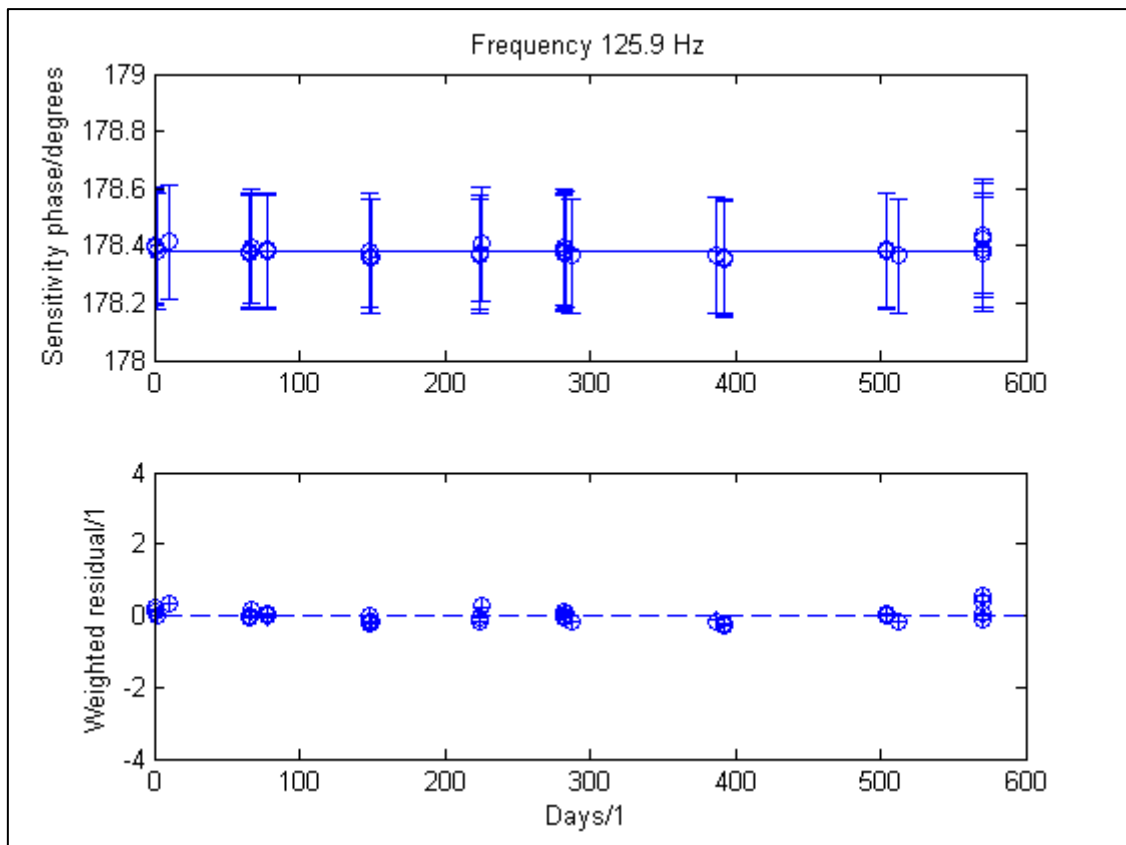


Figure A.1(g) Stability of 4160 811012 sensitivity phase, at 125.9 Hz, fitted with a constant and a straight line – the top graph shows the pilot laboratory’s stability data plotted against the number of days (with $k = 2$ uncertainty bars), the best-fit constant (dashed line) and the best-fit straight-line (solid line). The bottom graph shows the weighted residual deviations for the best-fit constant (o) and the best-fit straight-line (+).

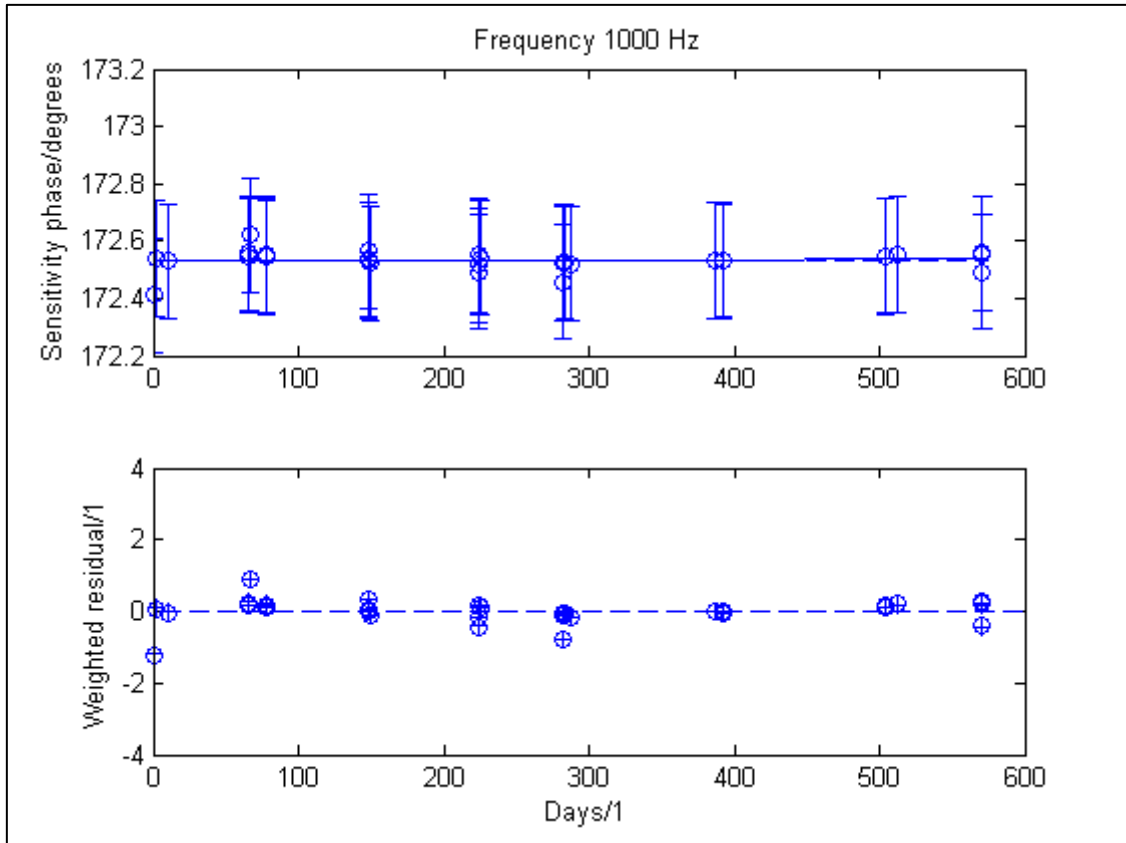


Figure A.1(h) Stability of 4160 811012 sensitivity phase, at 1000 Hz, fitted with a constant and a straight line – the top graph shows the pilot laboratory’s stability data plotted against the number of days (with $k = 2$ uncertainty bars), the best-fit constant (dashed line) and the best-fit straight-line (solid line). The bottom graph shows the weighted residual deviations for the best-fit constant (o) and the best-fit straight-line (+).

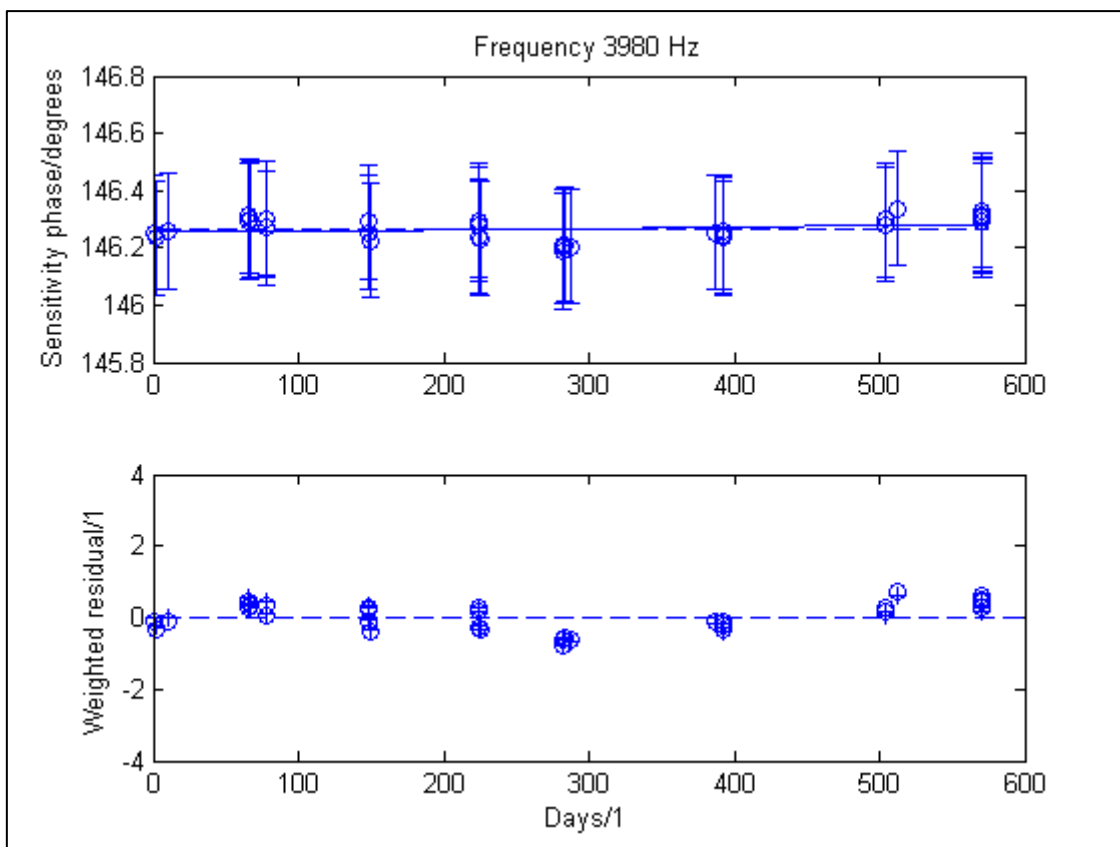


Figure A.1(i) Stability of 4160 811012 sensitivity phase, at 3980 Hz, fitted with a constant and a straight line – the top graph shows the pilot laboratory’s stability data plotted against the number of days (with $k = 2$ uncertainty bars), the best-fit constant (dashed line) and the best-fit straight-line (solid line). The bottom graph shows the weighted residual deviations for the best-fit constant (o) and the best-fit straight-line (+).

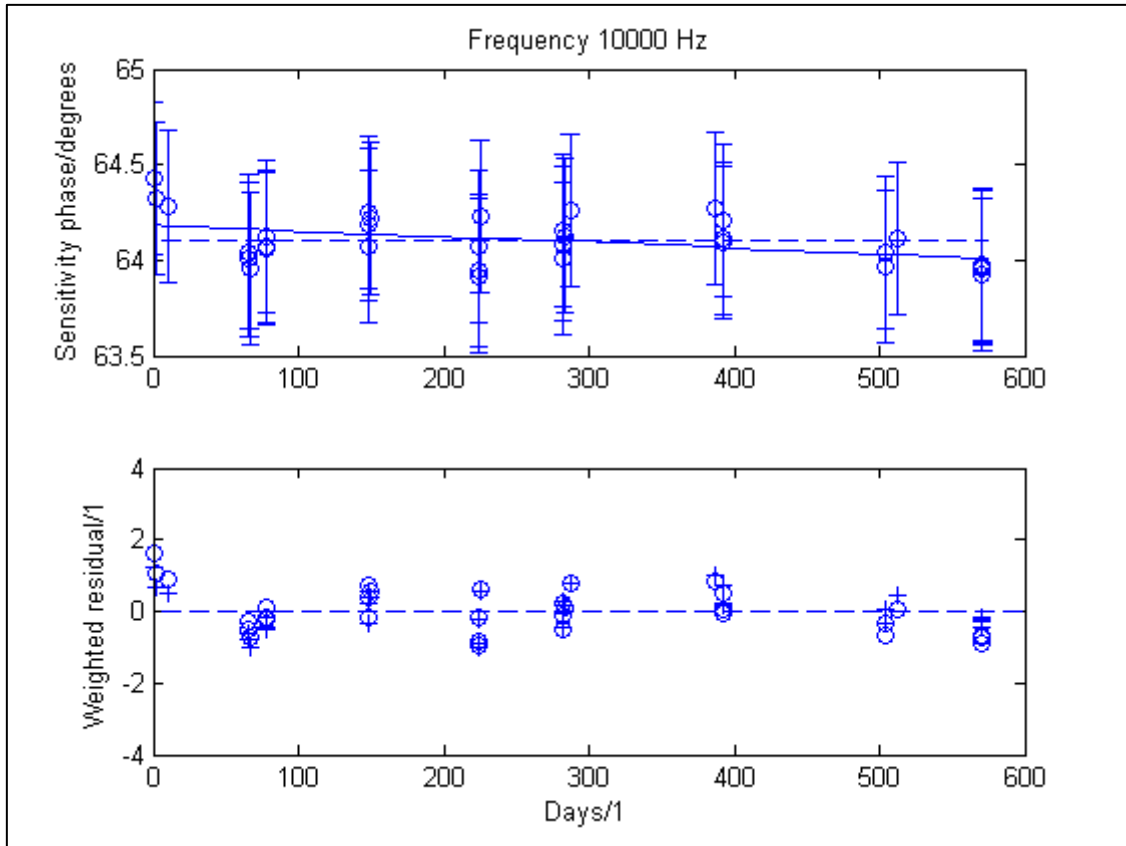


Figure A.1(j) Stability of 4160 811012 sensitivity phase, at 10000 Hz, fitted with a constant and a straight line – the top graph shows the pilot laboratory’s stability data plotted against the number of days (with $k = 2$ uncertainty bars), the best-fit constant (dashed line) and the best-fit straight-line (solid line). The bottom graph shows the weighted residual deviations for the best-fit constant (o) and the best-fit straight-line (+).

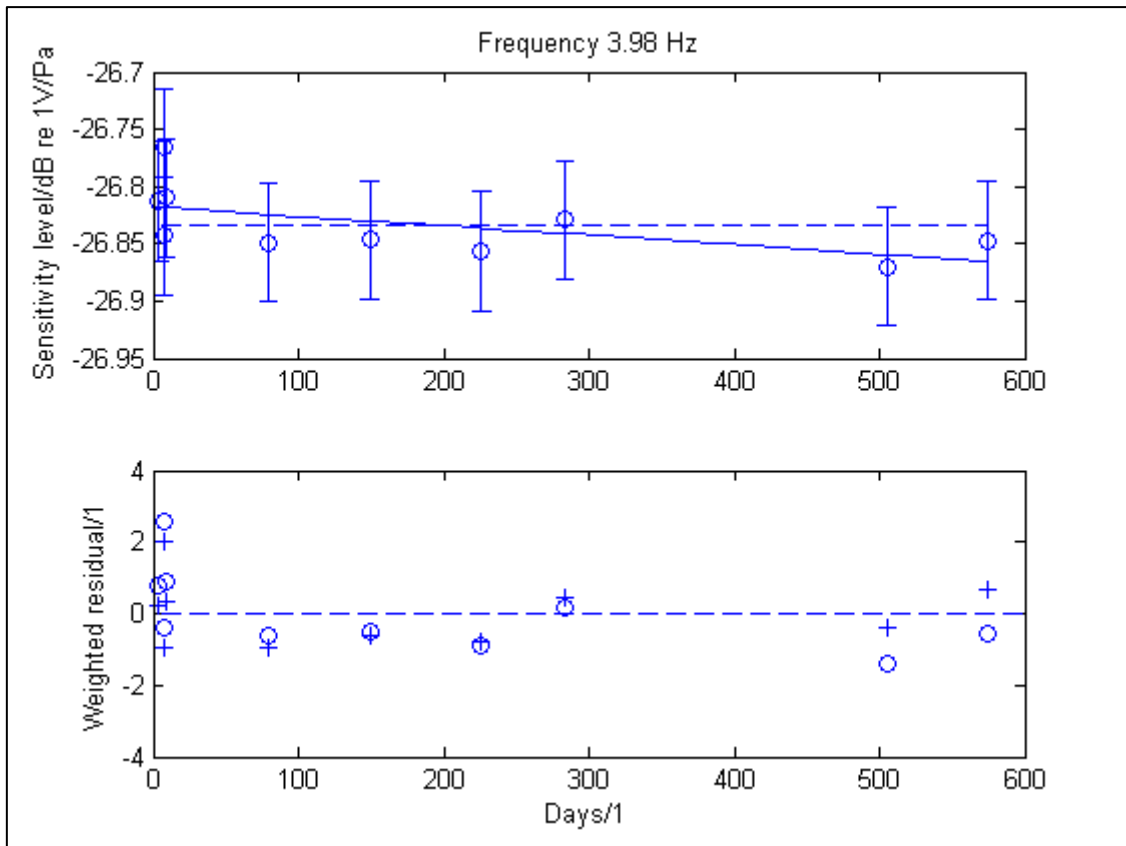


Figure A.1(k) Stability of 4160 2652754 sensitivity level, at 3.98 Hz, fitted with a constant and a straight line – the top graph shows the pilot laboratory’s stability data plotted against the number of days (with $k = 2$ uncertainty bars), the best-fit constant (dashed line) and the best-fit straight-line (solid line). The bottom graph shows the weighted residual deviations for the best-fit constant (o) and the best-fit straight-line (+).

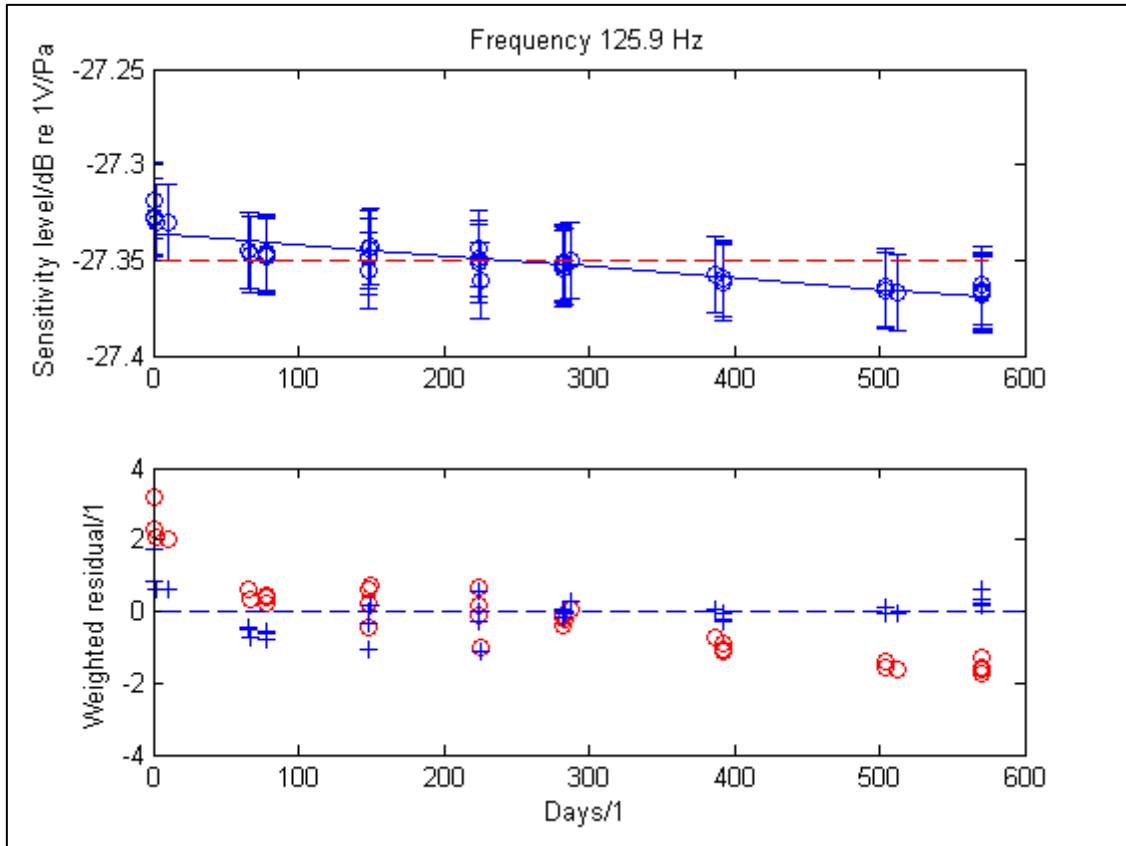


Figure A.1(i) Stability of 4160 2652754 sensitivity level, at 125.9 Hz, fitted with a constant and a straight line – the top graph shows the pilot laboratory’s stability data plotted against the number of days (with $k = 2$ uncertainty bars), the best-fit constant (dashed line) and the best-fit straight-line (solid line). The bottom graph shows the weighted residual deviations for the best-fit constant (o) and the best-fit straight-line (+).

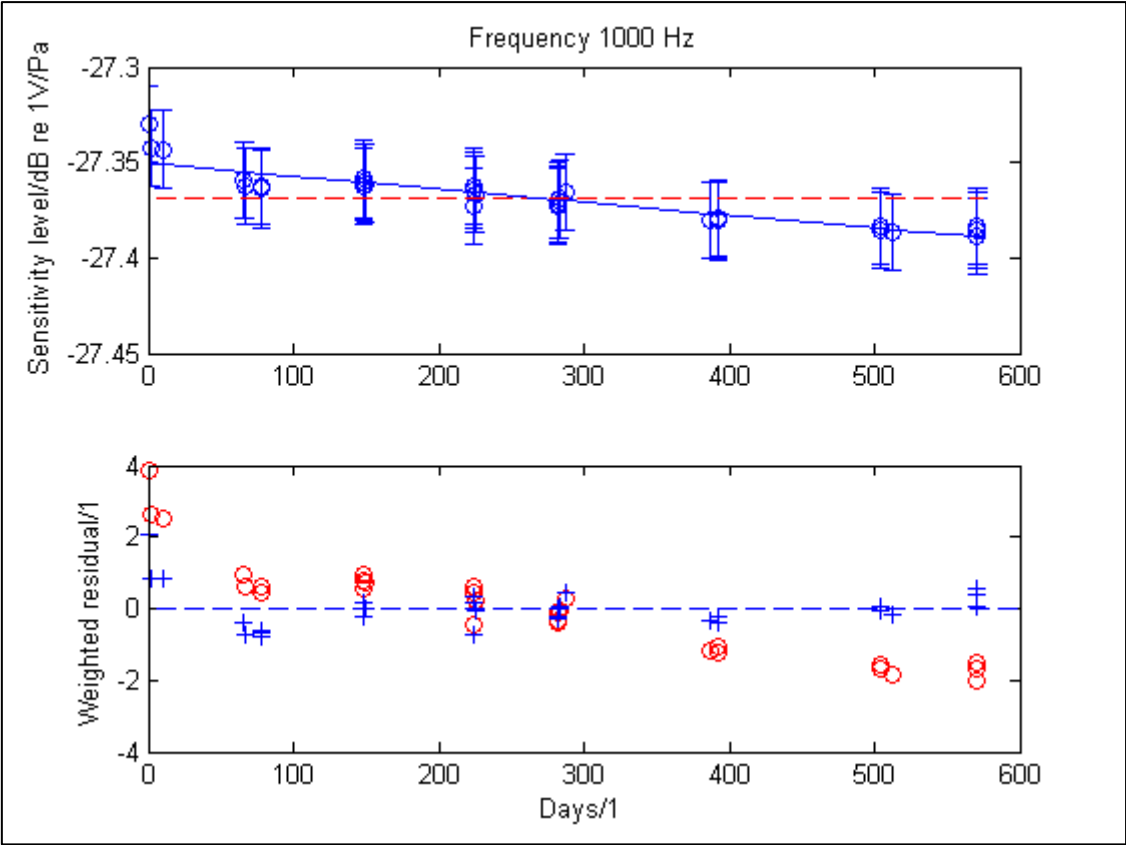


Figure A.1(m) Stability of 4160 2652754 sensitivity level, at 1000 Hz, fitted with a constant and a straight line – the top graph shows the pilot laboratory’s stability data plotted against the number of days (with $k = 2$ uncertainty bars), the best-fit constant (dashed line) and the best-fit straight-line (solid line). The bottom graph shows the weighted residual deviations for the best-fit constant (o) and the best-fit straight-line (+).

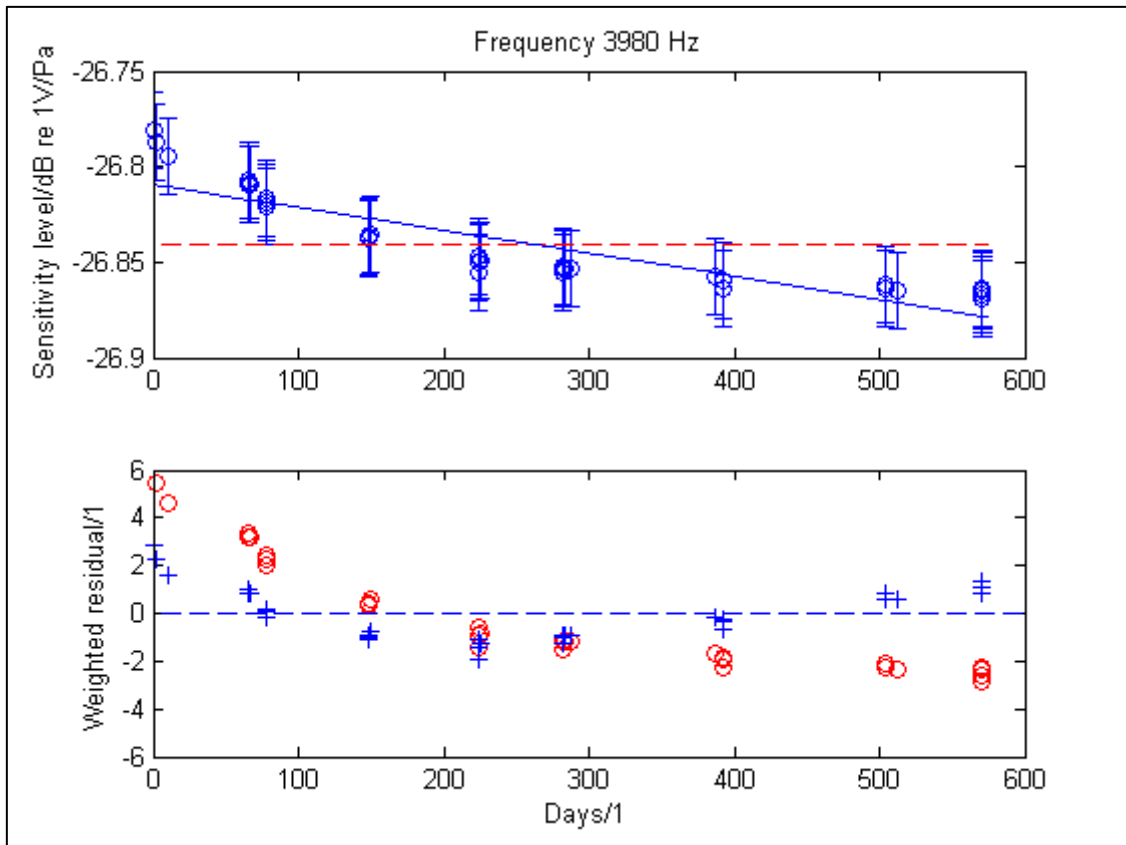


Figure A.1(n) Stability of 4160 2652754 sensitivity level, at 3980 Hz, fitted with a constant and a straight line – the top graph shows the pilot laboratory’s stability data plotted against the number of days (with $k = 2$ uncertainty bars), the best-fit constant (dashed line) and the best-fit straight-line (solid line). The bottom graph shows the weighted residual deviations for the best-fit constant (o) and the best-fit straight-line (+).

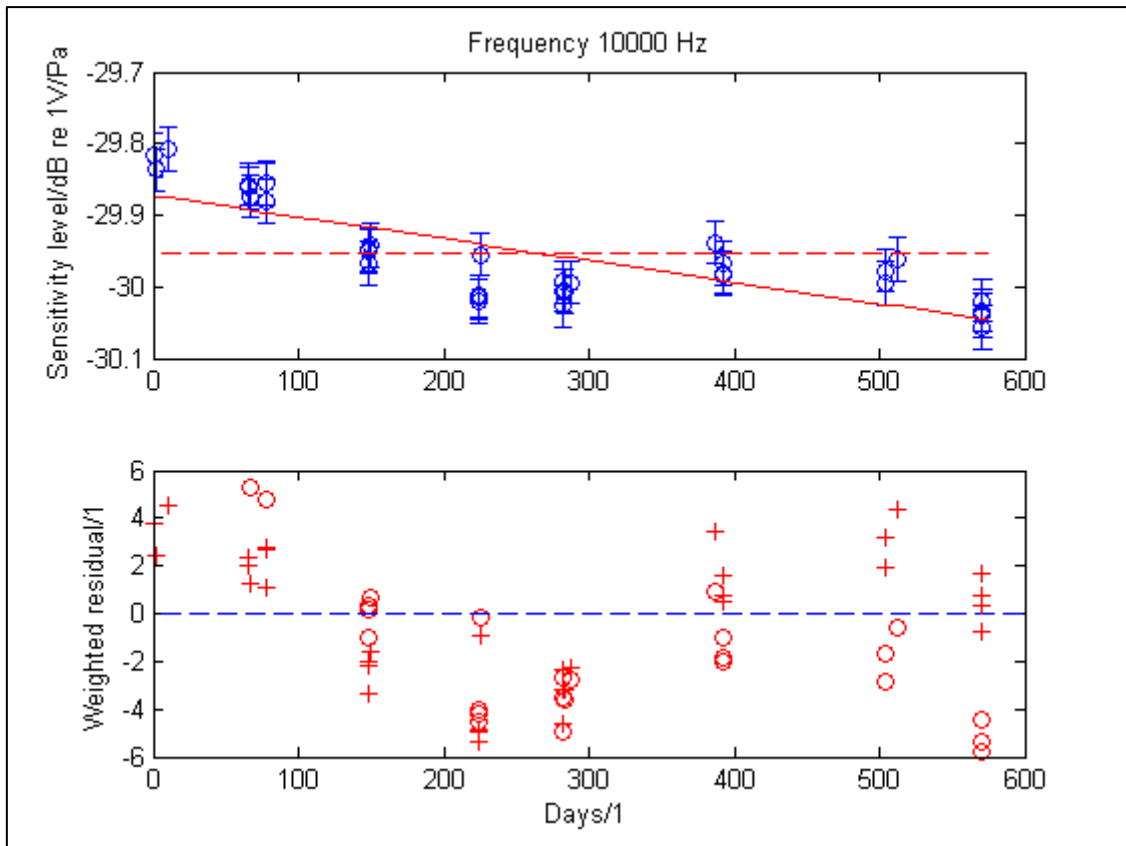


Figure A.1(o) Stability of 4160 2652754 sensitivity level, at 10000 Hz, fitted with a constant and a straight line – the top graph shows the pilot laboratory’s stability data plotted against the number of days (with $k = 2$ uncertainty bars), the best-fit constant (dashed line) and the best-fit straight-line (solid line). The bottom graph shows the weighted residual deviations for the best-fit constant (o) and the best-fit straight-line (+).

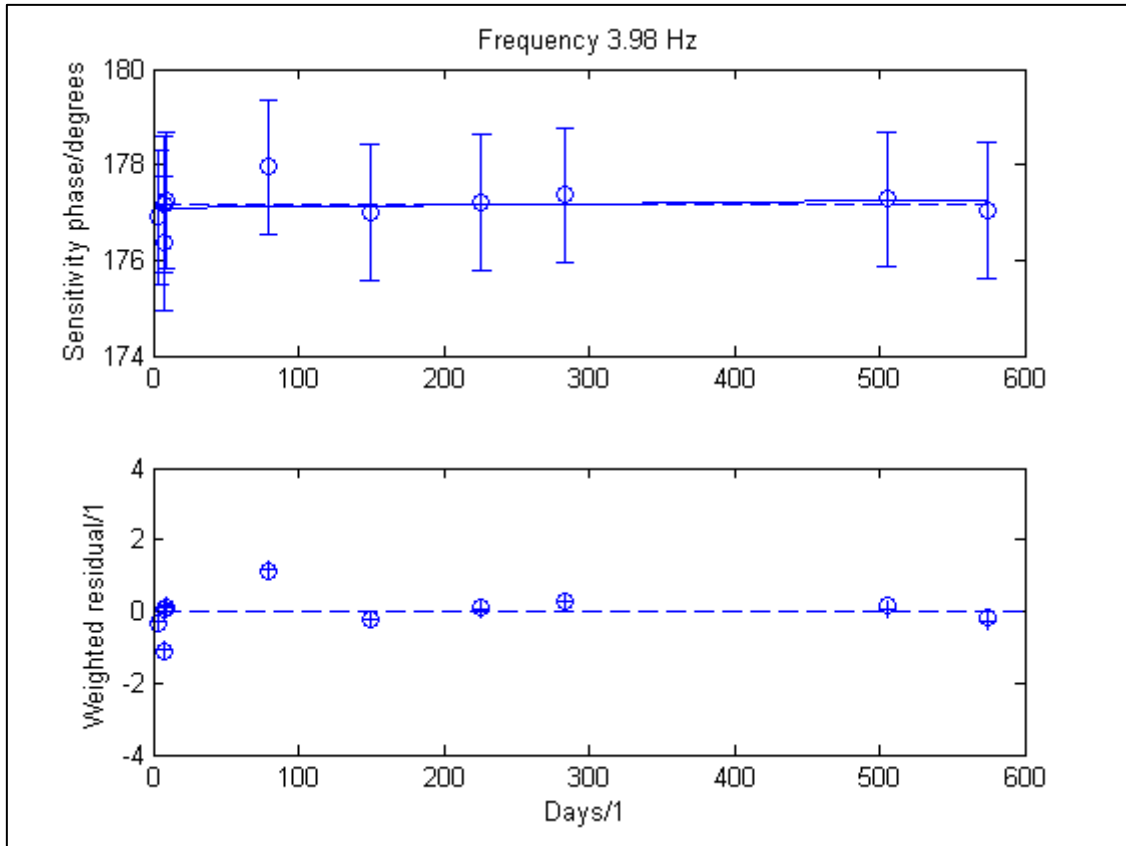


Figure A.1(p) Stability of 4160 2652754 sensitivity phase, at 3.98 Hz, fitted with a constant and a straight line – the top graph shows the pilot laboratory’s stability data plotted against the number of days (with $k = 2$ uncertainty bars), the best-fit constant (dashed line) and the best-fit straight-line (solid line). The bottom graph shows the weighted residual deviations for the best-fit constant (o) and the best-fit straight-line (+).

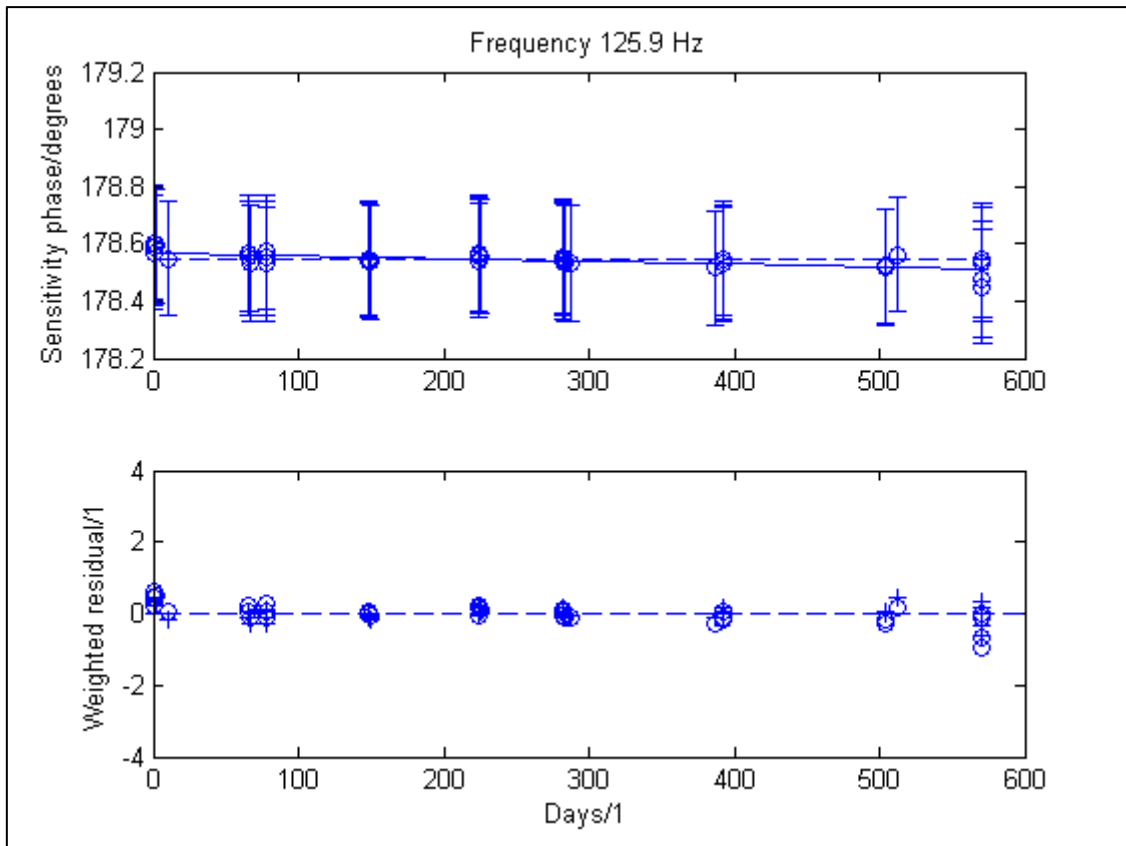


Figure A.1(q) Stability of 4160 2652754 sensitivity phase, at 125.9 Hz, fitted with a constant and a straight line – the top graph shows the pilot laboratory’s stability data plotted against the number of days (with $k = 2$ uncertainty bars), the best-fit constant (dashed line) and the best-fit straight-line (solid line). The bottom graph shows the weighted residual deviations for the best-fit constant (o) and the best-fit straight-line (+).

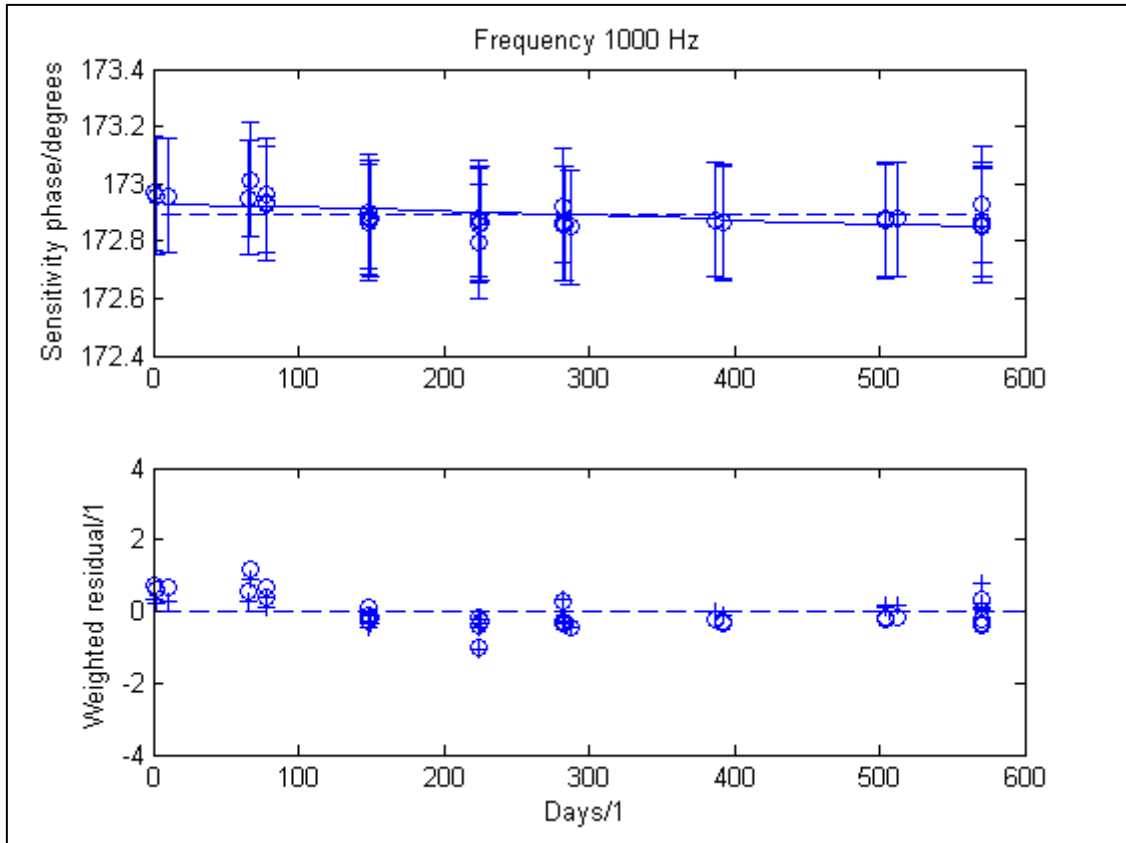


Figure A.1(r) Stability of 4160 2652754 sensitivity phase, at 1000 Hz, fitted with a constant and a straight line – the top graph shows the pilot laboratory’s stability data plotted against the number of days (with $k = 2$ uncertainty bars), the best-fit constant (dashed line) and the best-fit straight-line (solid line). The bottom graph shows the weighted residual deviations for the best-fit constant (o) and the best-fit straight-line (+).

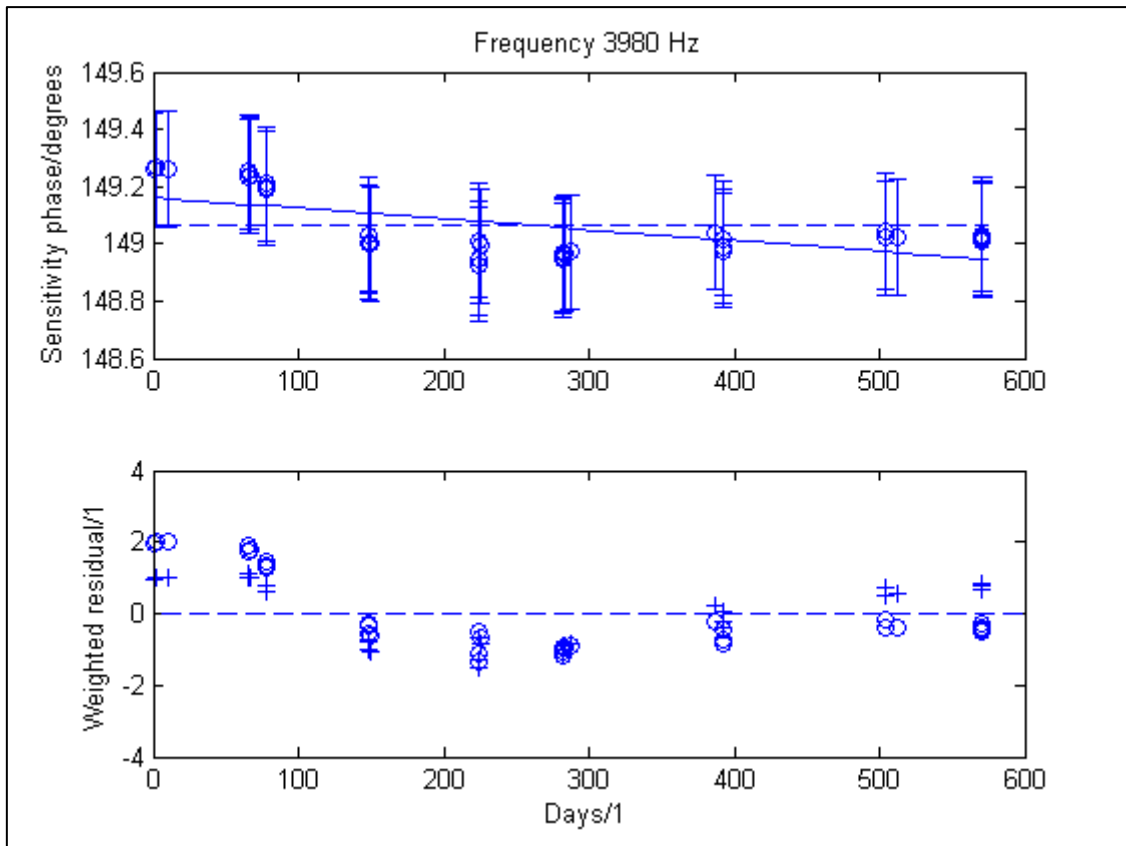


Figure A.1(s) Stability of 4160 2652754 sensitivity phase, at 3980 Hz, fitted with a constant and a straight line – the top graph shows the pilot laboratory’s stability data plotted against the number of days (with $k = 2$ uncertainty bars), the best-fit constant (dashed line) and the best-fit straight-line (solid line). The bottom graph shows the weighted residual deviations for the best-fit constant (o) and the best-fit straight-line (+).

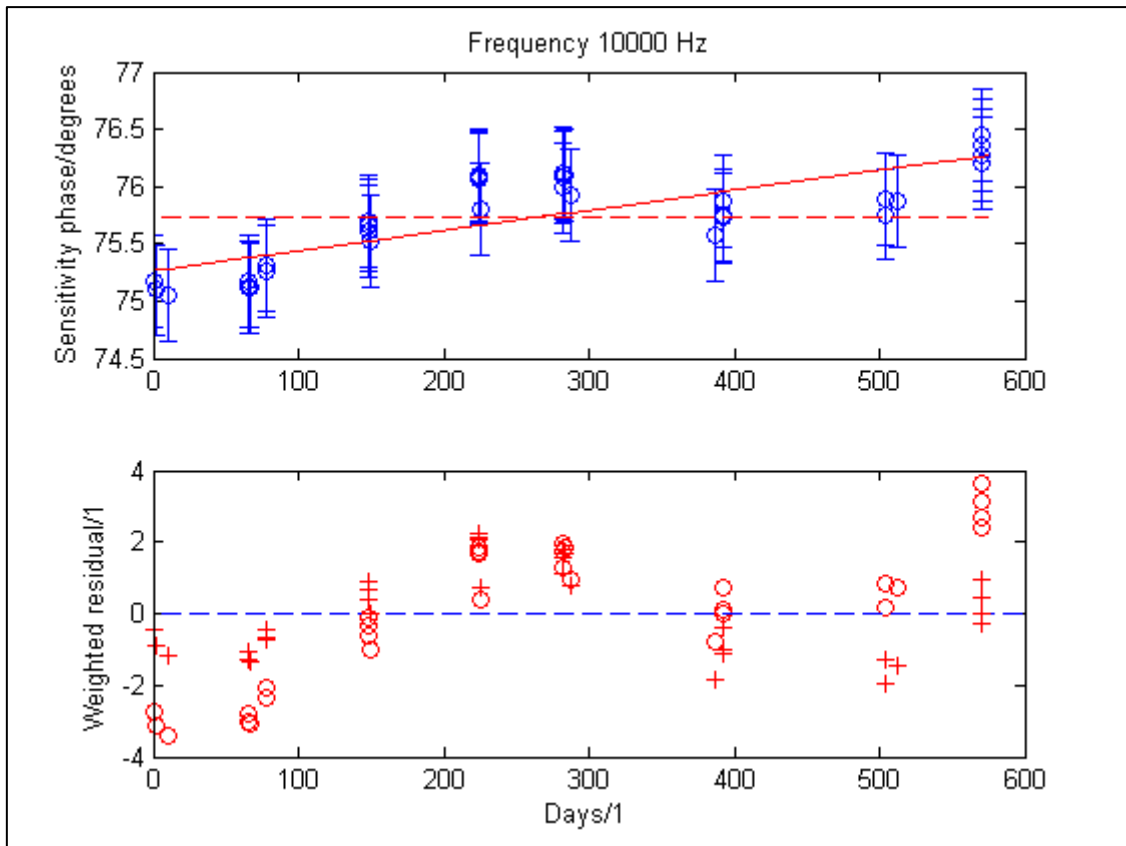


Figure A.1(t) Stability of 4160 2652754 sensitivity phase, at 10000 Hz, fitted with a constant and a straight line – the top graph shows the pilot laboratory’s stability data plotted against the number of days (with $k = 2$ uncertainty bars), the best-fit constant (dashed line) and the best-fit straight-line (solid line). The bottom graph shows the weighted residual deviations for the best-fit constant (o) and the best-fit straight-line (+).

A.2 DRIFT PARAMETERS FOR BEST-FIT STRAIGHT LINES

The following graphs provide information about the drift (slope) parameters in the best-fit straight-lines. Each graph shows the estimates and $k = 2$ uncertainty bars as a function of frequency.

At very low frequencies the uncertainties are large compared with the size of the drift. It is therefore difficult to make decisions about the presence, or absence, of a drift, based on measured data for these frequencies. It has been assumed that if a drift exists at higher frequencies, it also exists at the lowest frequencies, even if it cannot be shown to be statistically significant at these frequencies and corrections to the intercomparison data, where appropriate, have been applied accordingly.

Both sensitivity level and phase graphs for 4160 811012 (below) show uncertainty bars that include the value zero in their range at each frequency. This adds extra confidence to the assertion that the microphone was stable throughout the intercomparison. The 4160 2652754 sensitivity level graph shows uncertainty bars that do not include zero, through all but the lowest frequencies. This indicates that the microphone sensitivity level was subject to a statistically significant drift during the intercomparison. The sensitivity phase graph for the same microphone shows uncertainty bars that do not include zero at frequencies around the resonance frequency of the microphone. This indicates a shift in the resonance frequency of the microphone during the intercomparison. (Note, the phase response of the microphone is partly determined by phase of the acoustic impedance of the diaphragm, which itself is dominated by the diaphragm stiffness at low frequencies. In this stiffness controlled region the microphone phase response is therefore insensitive to changes in diaphragm tension that are suggested as the reason for the instabilities observed.)

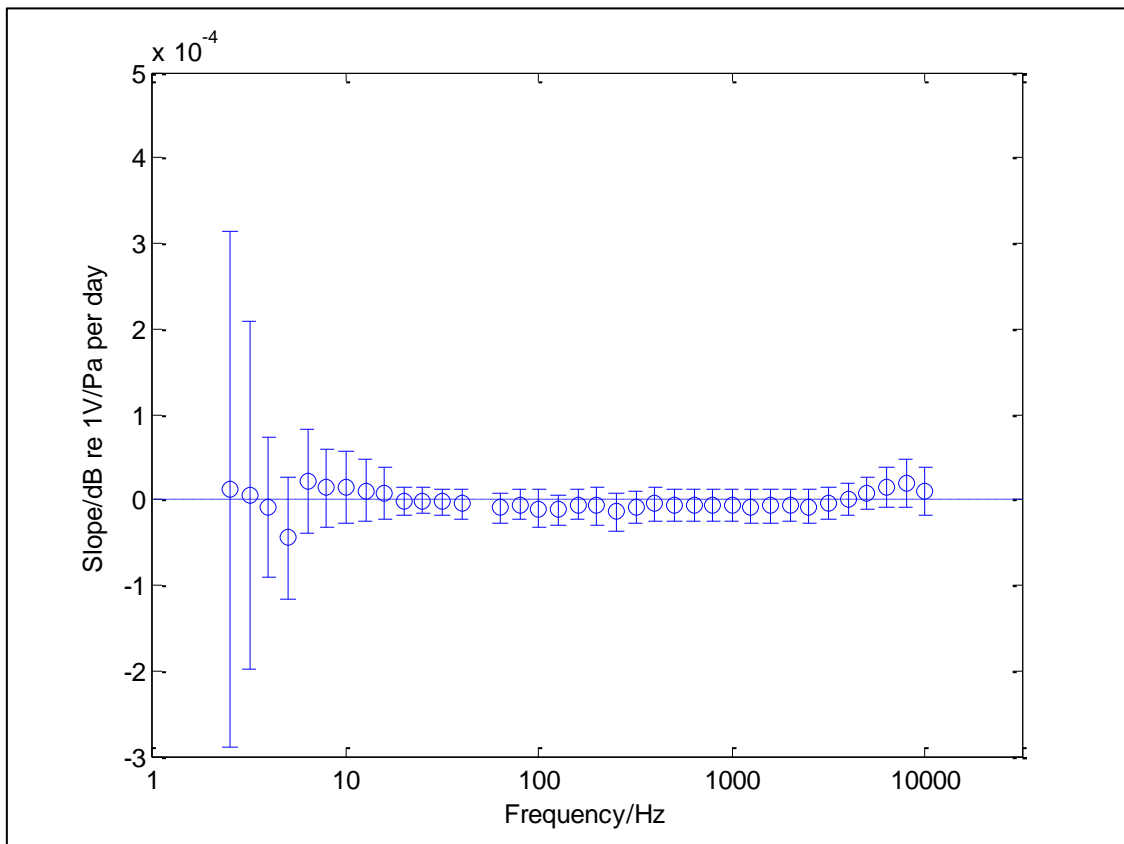


Figure A.2(a) Drift of 4160 811012: slope (m) of the best fit straight line ($y=mx+C$) that describes the drift in sensitivity level of the microphone, during the intercomparison, at each frequency, with $k=2$ uncertainty bars.

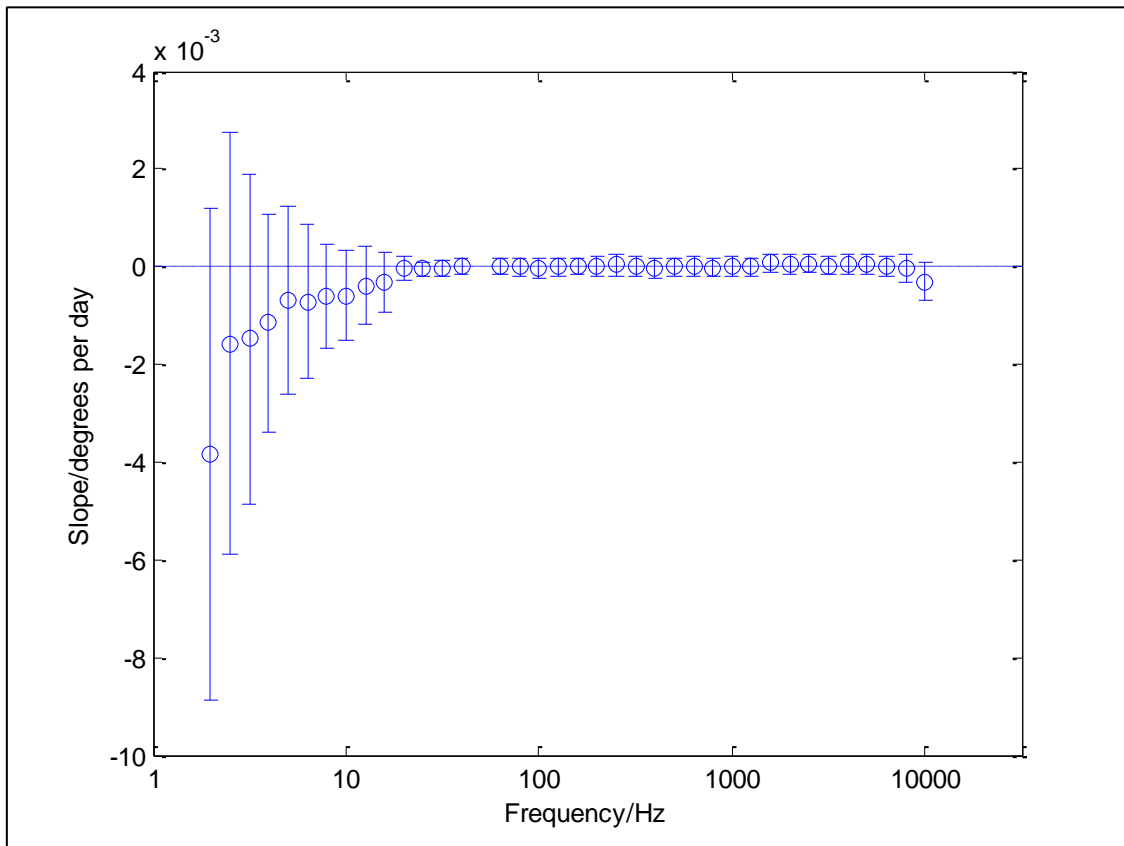


Figure A.2(b) Drift of 4160 811012: slope (m) of the best fit straight line ($y=mx+C$) that describes the drift in sensitivity phase of the microphone, during the intercomparison, at each frequency, with $k=2$ uncertainty bars.

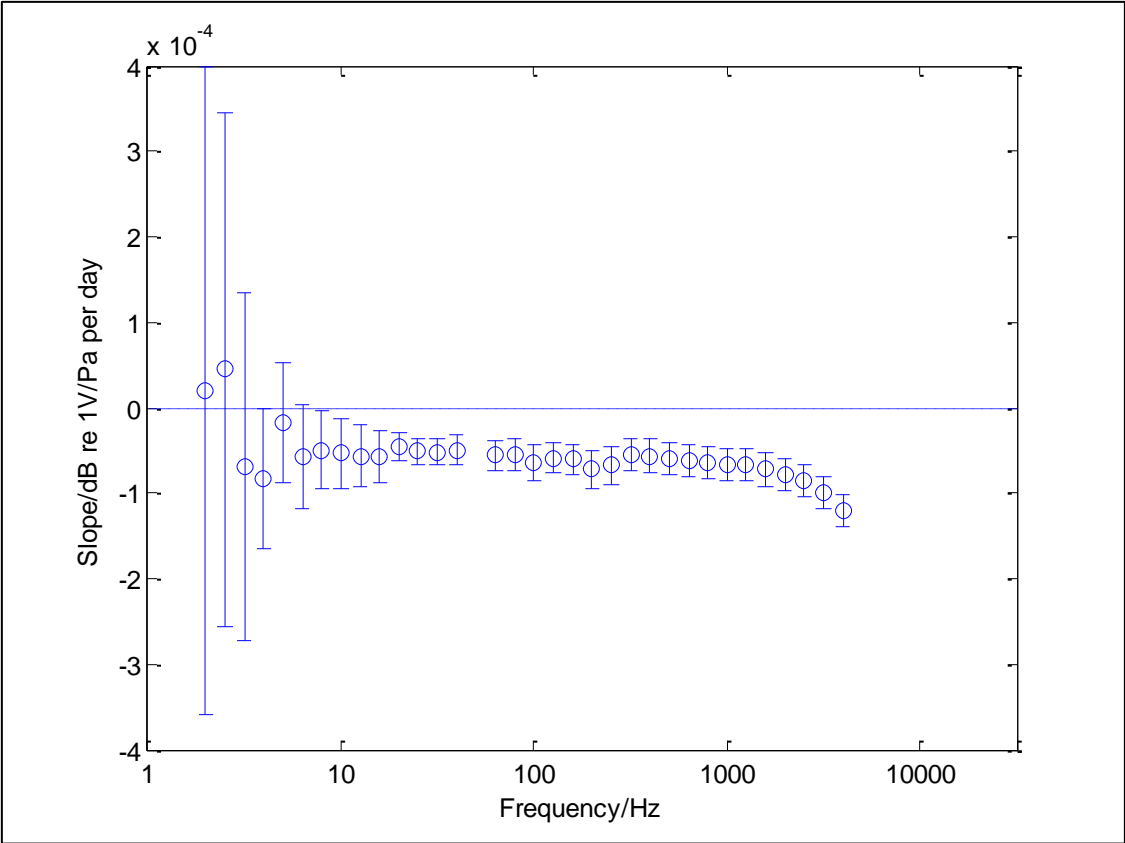


Figure A.2(c) Drift of 4160 2652754: slope (m) of the best fit straight line ($y=mx+C$) that describes the drift in sensitivity level of the microphone, during the intercomparison, at each frequency, with $k=2$ uncertainty bars.

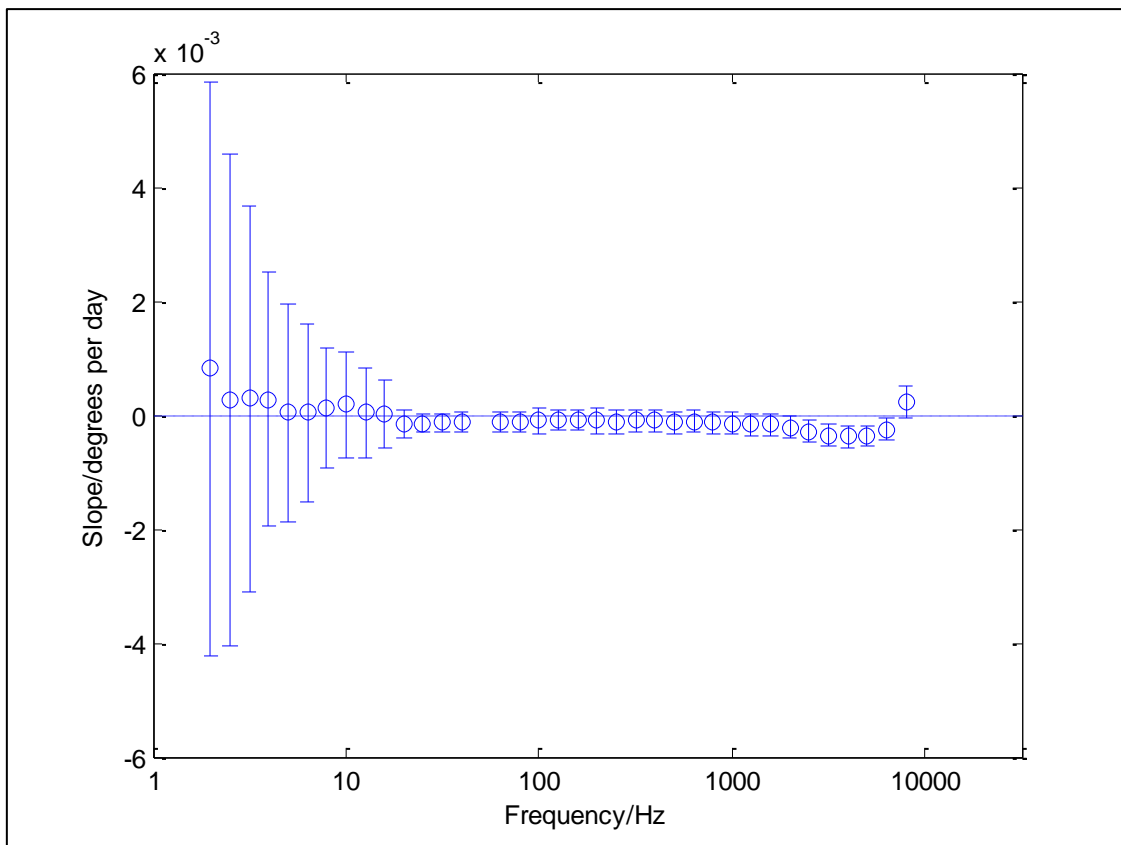


Figure A.2(d) Drift of 4160 2652754: slope (m) of the best fit straight line ($y=mx+C$) that describes the drift in sensitivity phase of the microphone, during the intercomparison, at each frequency, with $k=2$ uncertainty bars.

A.3 PARTICIPANTS' DATA DISPLAYED ALONGSIDE STABILITY DATA

As a supplement to the discussion above, Figures A.3(a), (b) and (c) show the trend with time in the sensitivity level measurements, along with the corresponding results declared by the participants. The results for microphone 4160 811012 are shown at 125.893 Hz, as a comparison with the weighted mean value calculated for the microphone. Similar results are obtained at other frequencies. The results for microphone 4160 2652754 are shown as a comparison with the un-weighted (and uncorrected) mean of the participants' measurements for that microphone. In this case the results are shown at 125.893 Hz and 3981.072 Hz to illustrate the contrast in performance across the frequency range. While a gradient is evident at 125.893 Hz, the change in sensitivity level is more pronounced and more complex at 3981.072 Hz.

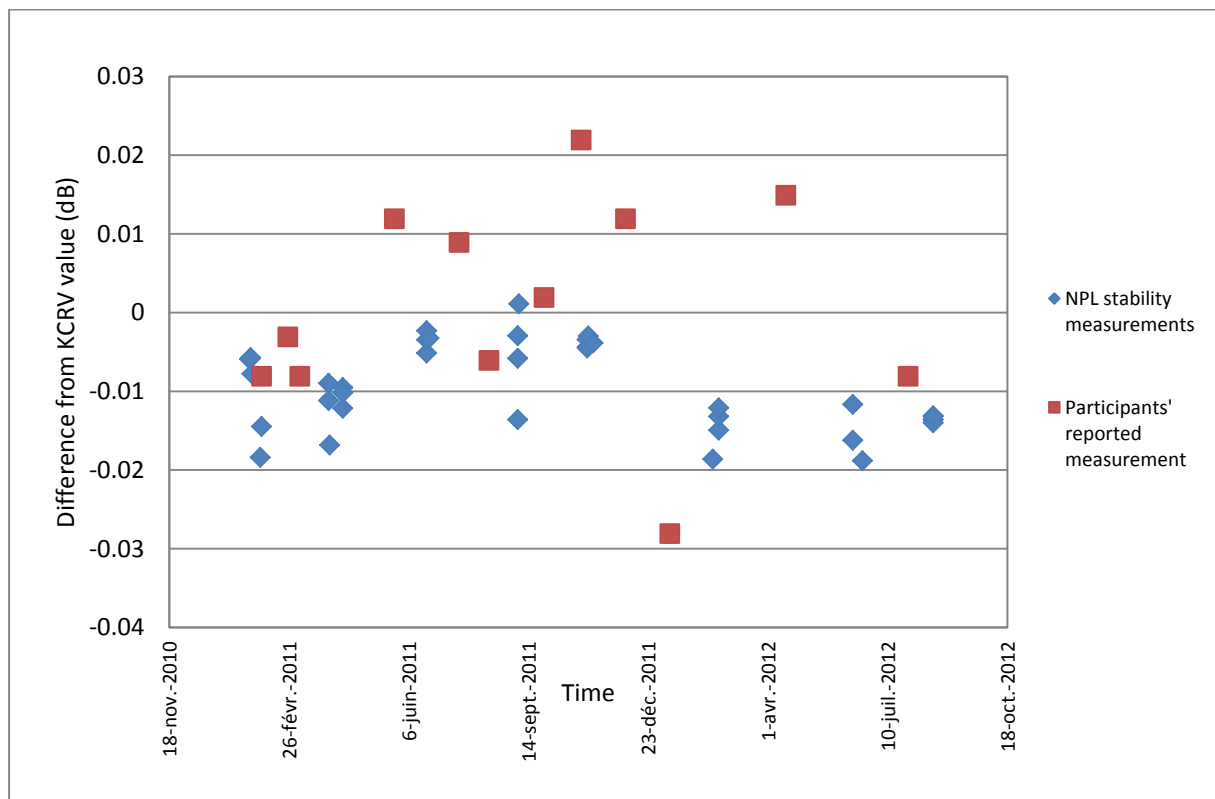


Figure A.3(a) Stability of 4160 811012 at 125.893 Hz during CCAUV.A-K5.

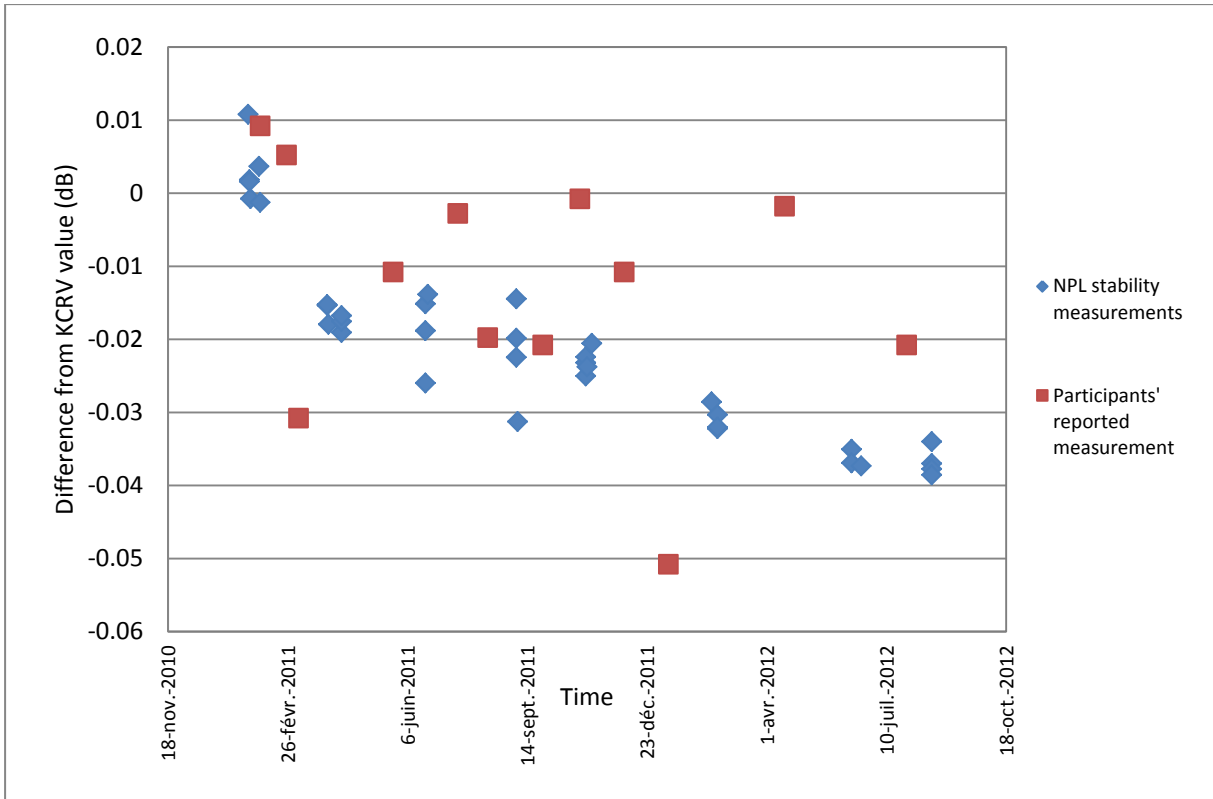


Figure A.3(b) Stability of 4160 2652754 at 125.893 Hz during CCAUV.A-K5.

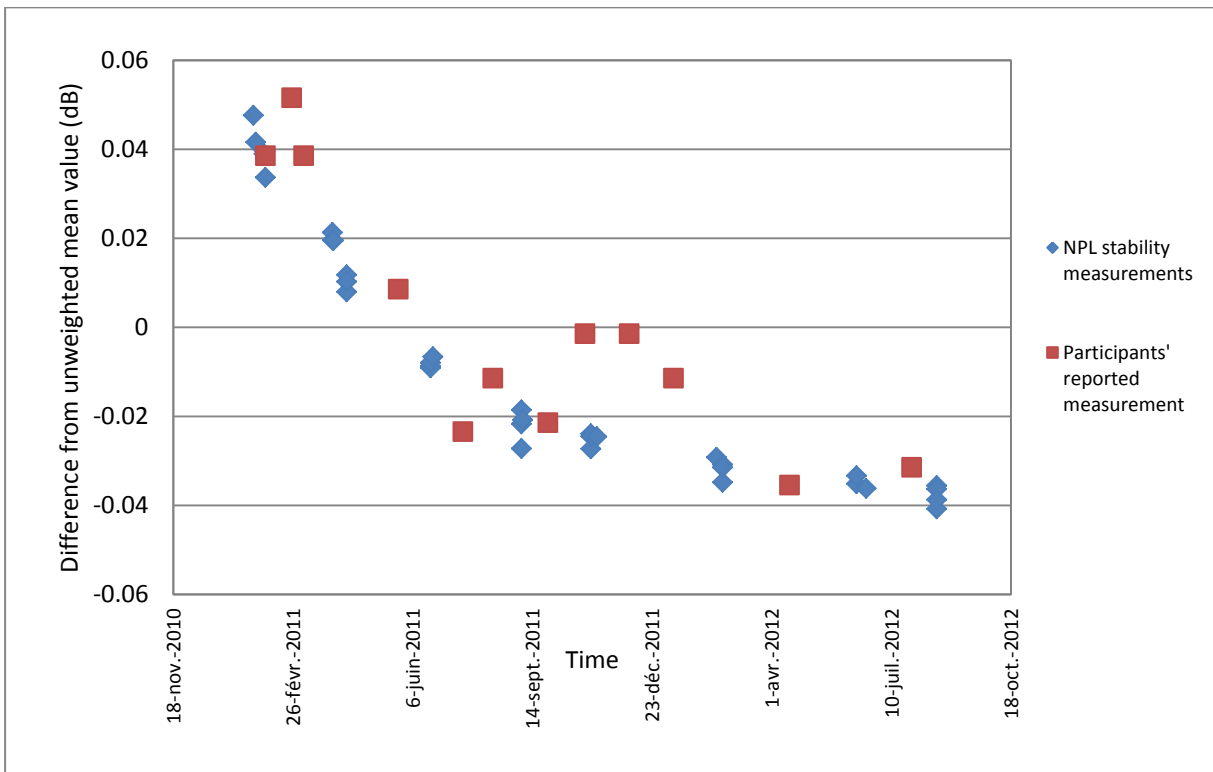


Figure A.3(c) Stability of 4160 2652754 at 3981.072 Hz during CCAUV.A-K5.

NOTE: ACCESS TO SPREADSHEETS

The accompanying Microsoft Excel spreadsheets '*CCAUV-A-K5 Final Report Tables of Data.xls*' and '*CCAUV_A-K5 Uncertainty Budgets Final Report.xlsx*' are available on request from NPL via an email to library@npl.co.uk.